

# **Polar Ordering of Guest Molecules in Host-Guest Inclusion Complexes**

deur  
Charl Xavier Bezuidenhout

*Tesis ingelewer ter gedeeltelike voldoening aan die vereistes vir die graad Magister in Chemie aan die Departement van Chemie en Polimeer Wetenskappe, Universiteit van Stellenbosch*



Studieleier: Prof. Leonard J. Barbour  
Fakulteit Natuurwetenskappe  
Departement Chemie en Polimeer Wetenskappe

December 2011

## Declaration

I, the undersigned , hereby declare that the work contained in this thesis is my own original work and that I have not preveously in its entirety or in part, submitted it at any university for a degree.

---

Signature

---

Name

## Opsomming

2,7-dimietielokta-3,5-diyne-2,7-diol vorm insluitingskomplekse met verskeie molekules as gaste, waar die gas-molekules polêr georden is. 'n Cambridge Struktuur Databasis (CSD) soektog lewer tien insluitings komplekse waarvan die gas-molekules polêr georden is. Deur gebruik te maak van Digtheidsfunksionele teorie (DFT) berekeninge (in die afwesigheid van die gasheer) het ons die inter-kanaal en wedersydse gas-gas interaksies tussen die gas molekules geëvalueer.

Twee polêr geordende insluitingskomplekse ((1,4,7-sikloheksaan-1,2,4,5,7,8-heksaoksonaan)- $\text{CHCl}_3$  en (2,4,6-(endolongifolyl)-1,3,5-trioksaan)- $\text{CDCl}_3$ ) is uitgesonder uit die CSD soektog vir verdere studies saam met 2,7-dimietielokta-3,5-diyne-2,7-diol. Aanslag was gemaak om enige 1,2,4,5,7,8-heksaoksonaan en 1,3,5-trioksaan derivate te sintetiseer en vas te stel of die polêre ordensvermoë oor die familie van verbindings strek. Ons het daarin geslaag om drie nuwe polêr geordende insluitingskomplekse op te lewer met 2,7-dimietielokta-3,5-diyne-2,7-diol ( $\text{Cl}(\text{CH}_3)_3$ ,  $\text{BrC}(\text{CH}_3)_3$  en  $\text{I}(\text{CH}_3)_3$ ), en sodoende die reeks uitgebrei na ses gaste wat polêr geordende insluitingskomplekse vorm. Net 1,4,7-sikloheksaan-1,2,4,5,7,8-heksaoksonaan kon gesintetiseer word en dit lewer twee polêr geordende insluitingskomplekse ( $\text{CHCl}_3$  en  $\text{CHBr}_3$  (nuut)). Drie 1,3,5-trioksane is gesintetiseer (die sikloheksiel, sikloheks-3-een-1-iel en siklopentiel derivate) en het nie enige oplosmiddels (gaste) ingesluit nie. Nietemin vorm hiedie 1,3,5-trioksane ook polêr geordende kristalle.

Hierdie verbindings en insluitingskomplekse is geanaliseer deur middel van enkelkristal X-straal diffraksie om hul kristalstrukture te bepaal. Alle kristalstrukture was opgelos en verwerk tot voldoende akkuraatheid (behalwe vir 2,4,6-tri(siklopentiel)-1,3,5-trioxane) met geen wanorde in die gas molekule posisies nie (waar van toepassing) en hul polêre ordensvermoë is ondersoek. As gevolg van groot verskille in hul molekulêre strukture, is hierdie verbindings afsonderlik bestudeer deur middel van molekulêre modellerings metodes (Digtheidsfunksionele teorie, molekulêre meganika, molekulêre dinamika en molekulêre stakings dinamika).

## Abstract

2,7-dimethylocta-3,5-diyne-2,7-diol forms inclusion complexes with various guests molecules, where the guest molecules are polar-ordered. A Cambridge Structural Database (CSD) search revealed ten inclusion complexes where the guest molecules were polar-ordered. Using Density Functional Theory (DFT) computational methods (in the absence of the host), we evaluated the intra-channel and lateral guest-guest interactions between the guest molecules.

Two polar-ordered inclusion complexes ((1,4,7-cyclohexane-1,2,4,5,7,8-hexaoxonane)·CHCl<sub>3</sub> and (2,4,6-(endolongifolyl)-1,3,5-trioxane)·CDCl<sub>3</sub>) were singled out in the CSD search for further studies along with 2,7-dimethylocta-3,5-diyne-2,7-diol. Synthesis of any 1,2,4,5,7,8-hexaoxonane and 1,3,5-trioxane derivatives was attempted to establish whether the polar-ordering ability extends into the family of compounds.

We managed to produce three new polar-ordered inclusion complexes with 2,7-dimethylocta-3,5-diyne-2,7-diol (ClC(CH<sub>3</sub>)<sub>3</sub>, BrC(CH<sub>3</sub>)<sub>3</sub> and IC(CH<sub>3</sub>)<sub>3</sub>), thus extending the series to six guest polar-ordered systems. We were only able to synthesise 1,4,7-cyclohexane-1,2,4,5,7,8-hexaoxonane and produce the CHCl<sub>3</sub> inclusion complex and one new polar-ordered inclusion complex (CHBr<sub>3</sub>). Three 1,3,5-trioxanes was synthesised (the cyclohexyl, cyclohex-3-en-1-yl and cyclopentyl derivatives), which did not include any solvents. However, these 1,3,5-trioxanes also form polar-ordered crystals.

These compounds and inclusion complexes were analysed by means of single crystal X-ray diffraction to determine their crystal structures. All the crystal structures could be solved and refined to adequate accuracy (except for 2,4,6-tri(cyclopentyl)-1,3,5-trioxane) with no disorder of the guest molecules (where applicable) and their polar-ordering property investigated. Due to their vast molecular differences, these compounds were studied separately by means of visual crystal structure analysis and computational modelling techniques (Density functional theory, molecular mechanics, molecular dynamics and molecular quench dynamics).

---

**TABLE OF CONTENTS**

<b>Declaration</b> .....	<b>i</b>
<b>Opsomming</b> .....	<b>ii</b>
<b>Abstract</b> .....	<b>iii</b>
<b>TABLE OF CONTENTS</b> .....	<b>iv</b>
<b>ABREVIATIONS</b> .....	<b>vii</b>
<b>ATOMIC COLOUR KEY</b> .....	<b>viii</b>
<b>LIST OF FIGURES</b> .....	<b>ix</b>
<b>LIST OF TABLES</b> .....	<b>xiii</b>
<b>CHAPTER 1</b> .....	<b>1</b>
<b>INTRODUCTION</b> .....	<b>1</b>
1.1 <i>Supramolecular chemistry</i> .....	3
1.2 <i>Crystal Engineering</i> .....	4
1.3 <i>Intermolecular interactions</i> .....	5
1.3.1 <i>Hydrogen bonds</i> .....	6
1.3.2 <i>Van der Waals interactions</i> .....	6
1.3.3 <i>Electrostatic interactions</i> .....	7
1.4 <i>Polar ordering in crystals</i> .....	7
1.5 <i>Related work</i> .....	8
1.6 <i>Aspects of this survey</i> .....	10
1.6.1 <i>Structural analysis of guest-guest interactions in polar-ordered systems</i> .....	10
1.6.2 <i>2,7-dimethylocta-3,5-diyne-2,7-diol (1)</i> .....	11
1.6.3 <i>3,3':6,6':9,9'-tris(pentamethylene)-1,2,4,5,7,8-hexaoxonane (2)</i> .....	11
1.6.4 <i>1,3,5-trioxanes (3, 4, 5 and 6)</i> .....	11
1.6.5 <i>Methods employed</i> .....	12
1.6.6 <i>Summary of objectives</i> .....	12
<b>CHAPTER 2</b> .....	<b>13</b>
<b>METHODOLOGY AND EXPERIMENTAL TECHNIQUES</b> .....	<b>13</b>
2.1 <i>Solution NMR</i> .....	14
2.2 <i>Crystallisations Methods</i> .....	14
2.3 <i>Single-Crystal Diffraction and data Analysis</i> .....	14
2.4 <i>Molecular Modelling</i> .....	14
2.4.1 <i>Density Functional Theory</i> .....	14
2.4.2 <i>Molecular Mechanics</i> .....	16
2.4.3 <i>Molecular Dynamics (MD)</i> .....	17
2.4.4 <i>Molecular Quench Dynamics (MQD)</i> .....	18
2.5 <i>Software packages</i> .....	18
2.5.1 <i>Cambridge structural database (CSD)</i> .....	18

## TABLE OF CONTENTS

2.5.2	<i>APEX II</i> <sup>56</sup> .....	18
2.5.3	<i>X-Seed</i> <sup>58</sup> .....	18
2.5.4	<i>SHELX-97</i> <sup>60</sup> .....	19
2.5.5	<i>Molden</i> <sup>62</sup> .....	19
2.5.6	<i>Gaussian03</i> .....	19
2.5.7	<i>Materials Studio</i> .....	20
2.6	<i>Compounds Studied</i> .....	22
2.6.1	<i>2,7-dimethylocta-3,5-diyne-2,7-diol (1)</i> .....	22
2.6.2	<i>1,2,4,5,7,8-Hexaoxonanes</i> .....	22
2.6.3	<i>1,3,5-trioxanes</i> .....	23
2.6.4	<i>Summary</i> .....	24
<b>CHAPTER 3</b> .....		<b>26</b>
<b>STRUCTURAL ANALYSIS OF GUEST-GUEST INTERACTIONS IN POLAR-ORDERED SYSTEMS</b> .....		<b>26</b>
3.1	<i>Introduction</i> .....	27
3.2	<i>CSD study</i> .....	27
3.3	<i>Molecular Modelling</i> .....	31
3.3.1	<i>Intra-channel guest-guest interactions</i> .....	31
3.3.2	<i>Lateral guest-guest interactions</i> .....	32
3.4	<i>Summary</i> .....	34
<b>CHAPTER 4</b> .....		<b>36</b>
<b>POLAR-ORDERED GUESTS IN 2,7-DIMETHYLOCTA-3,5-DIYNE-2,7-DIOL (1)</b> .....		<b>36</b>
4.1	<i>Introduction</i> .....	37
4.2	<i>Crystal structures</i> .....	37
4.2.1	<i>Through-channel interactions</i> .....	38
4.3	<i>Computational section</i> .....	40
4.3.1	<i>Potential energy profile of a guest moving inside the cavity of compound 1</i> .....	40
4.3.2	<i>Intra-channel guest alignment</i> .....	43
4.3.3	<i>Lateral guest alignment</i> .....	45
4.4	<i>Summary</i> .....	48
<b>CHAPTER 5</b> .....		<b>51</b>
<b>POLAR-ORDERED GUESTS IN 1,2,4,5,7,8-HEXAOXONANES</b> .....		<b>51</b>
5.1	<i>Introduction</i> .....	52
5.2	<i>1,4,7-cyclohexane-1,2,4,5,7,8-hexaoxonane (2)</i> .....	52
5.2.1	<i>Crystal structures</i> .....	53
5.2.2	<i>(1,4,7-Cyclohexane-1,2,4,5,7,8-hexaoxonane)-CHCl<sub>3</sub></i> .....	54
5.3	<i>Computational Section</i> .....	56
5.3.1	<i>Potential energy profile of a guest moving inside the cavity of compound 2</i> .....	56
5.3.2	<i>Molecular mechanics simulations of guest orientation changes within the cavity</i> .....	58
5.3.3	<i>Molecular quench dynamics simulations</i> .....	60

---

5.4	Summary.....	65
<b>CHAPTER 6</b>	.....	<b>67</b>
<b>POLAR-ORDERED GUEST MOLECULES IN 1,3,5-TRIOXANES</b>	.....	<b>67</b>
6.1	Introduction.....	68
6.2	Crystal Structures.....	68
6.2.1	2,4,6-(endolongifolyl)-1,3,5-trioxane·CDCl <sub>3</sub> (3-1).....	69
6.2.2	2,4,6-(cyclohexane)-1,3,5-trioxane (4).....	70
6.2.3	Brief summary.....	72
6.3	Molecular Modelling of 1,3,5-trioxanes.....	72
6.3.1	Role of R groups in 1,3,5-trioxanes.....	73
6.3.2	Guest stabilisation.....	74
6.3.3	Potential energy profile of guest moving inside cavity of 3-1.....	77
6.3.4	Investigation of polar alignment by means of MQD simulations.....	79
6.4	Summary.....	82
<b>CHAPTER 7</b>	.....	<b>85</b>
<b>CONCLUSION</b>	.....	<b>85</b>
7.1	Concluding remarks.....	86
7.2	Future work.....	88
<b>REFERENCES</b>	.....	<b>90</b>
<b>APPENDICES</b>	.....	Error! Bookmark not defined.

**ABBREVIATIONS**

<sup>d</sup> benzene	deuterated benzene	DFT	Density Functional Theory
<sup>d</sup> CF	deuterated chloroform	MD	Molecular Dynamics
CF	chloroform	MM	Molecular Mechanics
BF	bromoform	MO	Molecular Orbital
CM	chloromethane	MQD	Molecular Quench Dynamics
BM	bromomethane	NMR	Nuclear Magnetic Resonance
IM	iodomethane	vdW	van der Waals
CMP	2-chloro-2-methylpropane		
BMP	2-bromo-2-methylpropane		
IMP	2-iodo-2-methylpropane		
ACN	acetonitrile		
BTCM	bromotrichloromethane		
Cl-TMS	chlorotrimethylsilane		
TCAN	trichloroacetonitrile		
TCMS	trichloromethylsilane		
DCM	dichloromethane		
THF	tetrahydrofuran		

CSD Cambridge Structural Database



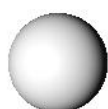
## ATOMIC COLOUR KEY



**Carbon**



**Chlorine**



**Hydrogen**



**Bromine**



**Oxygen**



**Iodine**



**Nitrogen**



**Silicon**

## LIST OF FIGURES

<b>Figure 1-1.</b>	TCAN solvate of 2,7-Dimethylocta-3,5-diyne-2,7-diol viewed along [010]. Only the guest is shown in space filled representation. <sup>5</sup> .....	3
<b>Figure 1-2.</b>	(a) No polar-ordering, (b) moderate polar-ordering and (c) perfect polar-ordering .....	8
<b>Figure 1-3.</b>	(a) Molecular design for the beloamphiphiles. (b) Polar stacking in (DecO,Cl)-azine. The R groups are mostly hydrogen atom or methyl groups, although other variations were attempted.....	9
<b>Figure 1-4.</b>	(a) Schematic of the guanidinium ( <b>G</b> ) and organodisulfonate ( <b>S</b> ) host framework. (b) The asymmetry in the organic fragment of the organodisulfonate ions. (c) Guest polar-ordered inclusion complex of the <b>GS</b> framework. <sup>4</sup> .....	10
<b>Figure 2-1.</b>	Model containing two molecules. (a) Percentage difference relative to MP2 for each method and basis set. (b) Calculation times for each method and basis set. ....	20
<b>Figure 3-1.</b>	Parameters used for the CSD search (CF used as an example). $r_{\text{guest}}$ = guest-guest distance along the channel or polar axis. Theta and phi are shown in red and blue, respectively. ....	27
<b>Figure 3-2.</b>	The lateral guest-guest distance ( $r_{\text{lateral}}$ ) is measured as indicated by the double-headed arrows. (a) The channel distance measured as viewed down the polar axis. (b) Viewed perpendicular to the polar axis with lines running through the guest molecules along the polar axis. The host molecules have been omitted for clarity. ....	29
<b>Figure 3-3.</b>	(a) Model used for head-to-tail guest-guest interactions, indicating the distance recorded. The bottom molecule was translated in the direction of the arrow. (b) Relative potential energy plots of results obtained from the calculations. ....	31
<b>Figure 3-4.</b>	Models used for DFT calculation to assess the guest-guest interactions. (a), (b) and (c) show the three optimised positions of the different relative orientations. ....	32
<b>Figure 3-5.</b>	(a) Potential energies relative to the head-to-tail orientation. (b) Boltzmann distributions at 298.0 K. (a), (b) and (c) on the abscissa correspond to the labels of the models in <b>Figure 3-4</b> .....	32
<b>Figure 3-6.</b>	a) Model used for determining lateral guest-guest interactions, indicating the distances recorded. The molecule on the right was translated in the direction of the arrows. b) Resultant relative potential energy surface obtained from the calculation. ....	33
<b>Figure 4-1.</b>	TCAN-included structure of <b>1</b> viewed along [010]. Only the guest is shown in space filled representation. ....	37
<b>Figure 4-2.</b>	CMP-included crystal structure of <b>1</b> (compounds <b>1-4</b> ). The BMP and IMP structures are isoskeletal to CMP. ....	38
<b>Figure 4-3.</b>	The two different hydroxyl groups, based on the O...O distances of the respective hydrogen bonded spirals. ....	38
<b>Figure 4-4.</b>	Space filled representation of all six polar guest molecules considered with their corresponding occupied molecular volume as determined by X-Seed.....	39
<b>Figure 4-5.</b>	Model used to determine the potential energy profile of the cavities of <b>1</b> . The green molecules represent the channel within which the guest will move and the blue molecules are included to account for any long-range dispersive host-guest interactions that might be present. ....	41

## LIST OF FIGURES

<b>Figure 4-6.</b>	The cavities are alternatively coloured and, for the sake of clarity, only the central channel is shown. The TCAN guest is translated in the direction of the arrow. a) <b>Scenario 1:</b> guest trapped in the cavity within the bulk of the crystal. b) <b>Scenario 2:</b> guest trapped in the cavity at the surface of the crystal. <b>A</b> and <b>B</b> denote the two orientations of the guest in both scenarios ( <b>A</b> - top, <b>B</b> - bottom). .....	41
<b>Figure 4-7.</b>	The two columns represent the energy profiles of the two scenarios as indicated by the headings. a) Total potential energy, b) electrostatic component of the total potential energy and c) vdW component of the total potential energy. The two series A and B represent the two orientations that were simulated.....	42
<b>Figure 4-8.</b>	Molecular mechanics model for calculating the guest-guest interactions within a channel. The sections highlighted in red in <b>1</b> and <b>2</b> shows the deviations from <b>0</b> (all guests aligned in the same direction).....	44
<b>Figure 4-9.</b>	Boltzmann distribution for guest-guest interactions within a channel. (a) Relative potential energies relative to <b>0</b> (head-to-tail orientation). (b) Corresponding Boltzmann distribution calculated at 298.0 K.....	44
<b>Figure 4-10.</b>	MM model used to investigate the polar alignment in inclusion complexes of <b>1</b> . <b>S1</b> , <b>S2</b> and <b>S3</b> represent the various simulations carried out within the central cavity. ....	45
<b>Figure 4-11.</b>	Potential energy of <b>A</b> relative to <b>B</b> ( <b>A</b> - congruent with crystal structure; and <b>B</b> 180° relative to crystal structure) obtained from the MM calculations based on the model in <b>Figure 4-10</b> for all guests studied. Negative values indicate that orientation <b>A</b> is more stable than <b>B</b> . The guest contribution was calculated as the difference between <b>GAC</b> and <b>EAC</b> . ....	47
<b>Figure 4-12.</b>	Relative vdW and electrostatic energies for the 6-guest-molecule model relative to orientation <b>B</b> (negative values indicate that <b>A</b> is favoured). a) With guests in surrounding channels. b) Absence of surrounding guests. ....	47
<b>Figure 5-1.</b>	(a) A single molecule of <b>2</b> and CF with the asymmetric unit highlighted in blue. (b) <b>2-1</b> viewed down the crystallographic c axis. The hydrogen atoms have been omitted for clarity. ....	54
<b>Figure 5-2.</b>	Inclusion complex <b>2-1</b> viewed down the crystallographic b-axis. The arrows indicate the alignment of the chloroform molecules (along the crystallographic c axis) and overall dipole moment vector. ....	55
<b>Figure 5-3.</b>	Space filled representation of a single cavity of <b>2-1</b> . (a) View down (001). (b) View down (100). The two different host orientations, with respect to the cavity, are shown in blue and yellow. The hydrogen atoms have been omitted for clarity. ....	55
<b>Figure 5-4.</b>	(a) Model used to determine the potential energy profile of CF moving in a cavity of <b>2</b> . The blue molecules form the side wall of the cavity with the green molecules on the ends. (b) Simulation <b>A</b> with CF orientation opposite to that in the crystal structure. (c) Simulation <b>B</b> with CF orientation the same as in the crystal structure; CF is translated in the direction of the arrows. <b>r</b> is the distance from the chlorine atoms to the peroxide ring (green host molecules).....	56
<b>Figure 5-5.</b>	(a) Total relative potential energy plot. (b) Electrostatic energy component of the total potential energy. (c) vdW energy component of the total potential energy. <b>r</b> is the distance from the chlorine atoms to the peroxide ring as shown in <b>Figure 5-4</b> . ....	57
<b>Figure 5-6.</b>	Open cavity model used to investigate the polar ordering. Red – host with cyclohexane group pointing towards the inside of the cavity. Blue – host with cyclohexane groups facing the cavity. Green - faces its peroxide ring towards the cavity. The calculation was divided into two: sides <b>A</b> and <b>B</b> as indicated and calculated one guest at a time.....	58
<b>Figure 5-7.</b>	Results from the molecular mechanics calculations of the model in <b>Figure 5-6</b> . (a) Boltzmann distribution calculated at 298.0 K. (b) Scenario produced by simulation results. (c) <b>A</b> : total potential energy divided into its components. (d) <b>B</b> : total potential energy divided into its components. 0° denotes the orientation that is congruent with the crystal structure and 180° the opposite orientation.....	59

## LIST OF FIGURES

<b>Figure 5-8.</b>	Left - closed cavity model used to determine polarity formation as viewed along an axis coinciding with the crystallographic <i>c</i> axis. Right – The simulation was divided into sides, <b>A</b> and <b>B</b> divided by the line dotted line. The green molecules on either end were translated in the direction of the arrows from an offset of 2 Å. Red – host with cyclohexane group pointing towards the inside of the cavity. Blue – host with cyclohexane groups facing the cavity. Green - faces its peroxide ring towards the cavity. ....	60
<b>Figure 5-9.</b>	Potential energy output produced by the MQD calculations for side <b>A</b> at different offset distances: (a) 2.0 Å, (b) 1.0 Å, (c) 0.7 Å, (d) 0.6 Å. Orientations of the conformations are indicated on each chart. <b>The two data sets in the 0.6 Å plot were obtained from two separate MQD calculations.</b> .....	62
<b>Figure 5-10.</b>	Boltzmann distribution at 298.0 K and relative electrostatic and vdW constituents of the potential energy (relative to the 0° conformation: negative values are in favour of the 0° conformation) generated by the quench dynamics simulations. 0° conformation is consistent with guest orientation as found in the crystal structure. ....	63
<b>Figure 5-11.</b>	Potential energy output produced by the MQD calculations for side <b>B</b> at different offset distances: (a) 2.0 Å, (b) 1.0 Å, (c) 0.7 Å, (d) 0.6 Å. Orientations of the conformations are indicated on each chart. <b>The two data sets in the 0.6 Å plot were obtained from two separate MQD calculations.</b> .....	64
<b>Figure 5-12.</b>	(a) Boltzmann distribution at 298.0 K. (b) The relative electrostatic and vdW components of the total potential energy (relative to the 0° conformation: negative values are in favour of the 0° conformation). The 0° conformation is consistent with guest orientation as found in the crystal structure. ....	64
<b>Figure 5-13.</b>	Overlay of the simulated CF positions at the 0.0 Å host offset of both models ( <b>A</b> and <b>B</b> ) on the CF position in crystal structure. The blue molecules represent the crystal structure positions, red - simulation <b>A</b> and green - simulation <b>B</b> . ....	65
<b>Figure 6-1.</b>	(a) A molecule of the host-guest complex <b>3-1</b> with the asymmetric unit shown in blue below. (b) The packing diagram of <b>3-1</b> viewed down [001]. The hydrogen atoms were omitted for clarity. ....	69
<b>Figure 6-2.</b>	Polar-ordered host-guest packing arrangement of <b>3-1</b> viewed along [100]. $\mu$ is the dipole moment vector as indicated by the arrow. The hydrogen atoms are omitted for clarity. ....	69
<b>Figure 6-3.</b>	Compound <b>3-1</b> viewed along [100] (the trioxane ring and CF guest molecules are rendered in space fill). Partial charges are indicated in the diagram. <sup>40</sup> $\mu_1$ and $\mu_2$ indicate the dipole moment vectors of the host and guest, respectively ( $\mu_{\text{total}} = \mu_1 + \mu_2$ ). ....	70
<b>Figure 6-4.</b>	(a) A single molecule of <b>4</b> with the asymmetric unit highlighted in blue (below). (b) Packing arrangement of <b>4</b> viewed down [001] in space filled representation. ....	71
<b>Figure 6-5.</b>	(a) Space filled representation of two host molecules (blue and green) of <b>4</b> viewed down [001]. (b) View of <b>4</b> along [100] (the trioxane ring is rendered in space fill). $\mu$ indicates the dipole moment vectors of the host molecules. ....	72
<b>Figure 6-6.</b>	(a) Model without steric-interfering surrounding host ( <b>A</b> ). (b) Model with surrounding steric-interfering host ( <b>B</b> ). (c) Aligned stacking. (d) Offset stacking. One molecule is shown in dark blue to differentiate between the two molecules. ....	73
<b>Figure 6-7.</b>	Results obtained from MM calculation of model described in Figure 6-6 plotted as (a) Boltzmann distribution at 298.0 K. (b) relative potential, vdW and electrostatic energy relative to the offset stacking. <b>A</b> denotes the model in Figure 6-6(a), without green molecules. <b>B</b> denotes the model in Figure 6-6b, with green molecules. ....	73
<b>Figure 6-8.</b>	Models used to determine the guest stabilisation of both <b>3</b> and <b>4</b> , demonstrated by the model of <b>3</b> . (a) Guest (CF) included. (b) Guest-omitted model. The same model was applied to the cyclohexyl derivative. ....	75

## LIST OF FIGURES

- 
- Figure 6-9.** (a) Relative total potential energy of CF included models of **3** and **4** with their electrostatic and vdW components relative to the guest-free models. A negative value favours CF guest inclusion and a positive value favours the guest-free structure. (b) Boltzmann distribution calculated from the relative total potential energies in (a). ..... 75
- Figure 6-10.** Overlays of (a) **3** and (b) **4**, CF included (blue molecules) and guest-free models (green molecules), after the geometry optimisation (for clarity, only the host molecules are shown). ..... 76
- Figure 6-11.** Model used for the potential energy profile of CF moving inside a cavity of **3-1**. Only the central host (green) and guest molecules are shown in models **A** and **B** with the surrounding blue host molecules omitted for clarity. The guest (CF) was translated in the direction of the arrow, as indicated.  $r$  is the distance between the CF and the trioxane rings..... 77
- Figure 6-12.** (a) Total relative potential energy plot. (b) The Boltzmann distribution calculated for the minima of **A** and **B** at 298.0 K. (c) Overlay of the CF molecules at the minima in **A** and **B**. (d) Electrostatic energy component of the total potential energy. (e) vdW energy component of the total potential energy. .... 78
- Figure 6-13.** (a) Model used for MQD simulations of **3-1**. (b), (c) and (d) shows only the central green column with the guests and trioxane rings in space filled representation. (b) Crystal structure positions. (c) The top host molecule was translated away as indicated by the arrow - simulation **A**. (d) The bottom host molecule was translated away as indicated by the arrow - simulation **B**. ..... 79
- Figure 6-14.** Simulation **A** results. (a), (b) and (c) are the energy profiles at 0, 3 and 4 Å translation respectively, which includes the total potential energy and its **vdW** and **electrostatic** constituents. (d) Structures of the minimum energy conformations. The surrounding molecules of the model were omitted for clarity in this figure. .... 80
- Figure 6-15.** Simulation **B** results. Left - energy profiles at (a) 0, (b) 3 and (c) 4 Å translations, respectively, which includes the total potential energy and its **vdW** and **electrostatic** constituents. Right - the structures of the conformations with labels corresponding to that of the energy profiles..... 81
-

---

**LIST OF TABLES**

<b>Table 1-1.</b>	Energy ranges associated with particular bonds and interactions. The numerical data are approximate values. <sup>20</sup> .....	5
<b>Table 1-2.</b>	List of a few types of hydrogen bonds and their associated energy ranges.....	6
<b>Table 2-1.</b>	Energy parameters used for molecular mechanics simulations and optimisations.....	20
<b>Table 2-2.</b>	Parameters used for molecular dynamics (including quench dynamics) and simulations. ....	21
<b>Table 2-3.</b>	All compounds and inclusion compounds synthesised. The guests in italics are those for inclusion compounds that have already been reported, but which have been studied further in this work. ....	25
<b>Table 3-1.</b>	Guests used to conduct the CSD search for polar-ordered crystals.....	28
<b>Table 3-2.</b>	Compounds that form polar-ordered crystals with CF and ACN. <sup>39-40, 69</sup> .....	30
<b>Table 4-1.</b>	Unit cell parameters of <b>1-1</b> - <b>1-6</b> . (All the inclusion complexes crystallise in the space group R3) .....	38
<b>Table 4-2.</b>	O...O distances of the two unique hydrogen-bonded spirals of <b>1</b> for all six polar inclusion complexes. The percentage difference in O...O distance is calculated relative to the O...O distance of the optimised guest-omitted structure.....	39
<b>Table 4-3.</b>	Percentage relative stabilisation of <b>S1</b> , <b>S2</b> and <b>S3</b> for all guests considered. A negative percentage is in favour of <b>A</b> (guest orientation in crystal structure) since the $\Delta E$ values were calculated relative to <b>B</b> .....	46
<b>Table 5-1.</b>	Crystallisations with 1,4,7-cyclohexane-1,2,4,5,7,8-hexaoxonane ( <b>2</b> ) and various polar solvents: .....	53
<b>Table 5-2.</b>	Unit cell parameters of <b>2</b> to <b>2-3</b> .....	54
<b>Table 5-3.</b>	DFT energies with calculated Boltzmann distribution.....	57
<b>Table 6-1.</b>	Unit cell parameters of <b>3-1</b> , <b>4</b> and <b>5</b> .....	68

# **CHAPTER 1**

## **INTRODUCTION**

Extensive studies of polar crystals have led to many applications in second harmonic generation (organic laser diodes),<sup>1</sup> optical parametric amplification and optical parametric oscillation in the infrared region,<sup>2</sup> pyro-electrics, organic light-emitting devices (OLED) materials and blue emitters.<sup>3</sup> Owing to the increased demand of modern society for improved telecommunications and data processing, the search for new materials with unique optical properties has increased exponentially. Areas such as photonics (the study and application of light) have become active fields of research, particularly with regard to organic nonlinear optical materials, thus increasing the demand for polar-ordered substances.

Polar-ordering of guest molecules in inclusion complexes has not been extensively investigated. In 2001 Holman and co-workers reported a host framework that induced polar-ordering of a variety of guests and they also demonstrated the non-linear optical properties of these materials (see Section 1.5).<sup>4</sup> Since the work by Holman *et al.* no significant progress has been made in discovering new guest polar-ordered inclusion complexes. Making polar crystals by design is difficult in general, and even more so, making guest polar-ordered crystals. However, guest polar-ordered crystals have an advantage over conventional organic polar crystals, i.e. the ability to tune the polar axis through the use of various polar guests, thus turning one polar crystal into a family of similar materials (provided that guest inclusion can be accomplished).

Our interest in guest polar-ordered systems began with work by Dr. Gareth Lloyd on inclusion compounds of 2,7-dimethylocta-3,5-diyne-2,7-diol, which crystallise in the polar and chiral space group  $R3$ . This compound yielded guest polar-ordered crystals with the following guests: bromotrichloromethane, trichloroacetonitrile and chlorotrimethylsilane.<sup>5</sup> These guests are not disordered in the crystal structure as they are compatible with the overall symmetry of the space group. The packing and morphology of this system has already been well described<sup>5</sup> and, as such, we will focus mainly on the explanation of its polar-ordering ability. Figure 1-1 illustrates the polar ordering of TCAN in 2,7-dimethylocta-3,5-diyne-2,7-diol along the crystallographic  $c$  axis (i.e. host-guest complex **1**).

The TCAN molecules are all aligned along the crystallographic  $c$  axis, thus maximising the dipole moment vector of the crystal in this direction. It can be argued that the alignment of these guests within a particular channel can be ascribed to dipole-dipole interactions between successive guest molecules. However, since the cavities of **1** appear to be symmetrical it is not obvious why the guest molecules in neighbouring channels should be aligned in the same direction parallel to the  $c$  axis (see Figure 1-1).



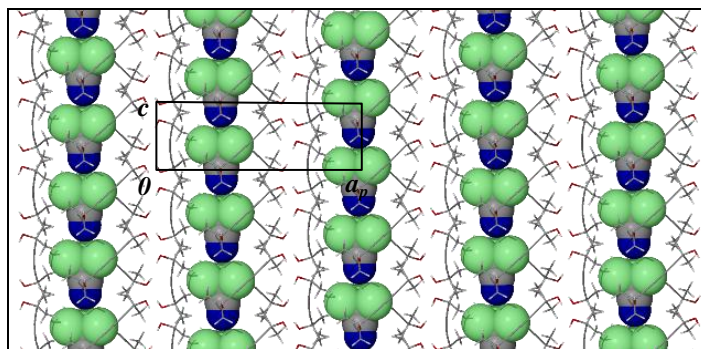


**Figure 1-1.** TCAN solvate of 2,7-Dimethylocta-3,5-diyne-2,7-diol viewed along [010]. Only the guest is shown in space filled representation.<sup>5</sup>

This result inspired us to search for other guest polar-ordered crystals and also to extend the series of polar-ordered inclusion complexes of 1. This host compound provides a means of altering (tuning) the dipole strength of the polar axis (and therefore the non-linear optical (NLO) properties) of these crystals by altering the included guest. 2,7-Dimethylocta-3,5-diyne-2,7-diol and two others compounds were investigated in this study.

## 1.1 SUPRAMOLECULAR CHEMISTRY

Over the centuries, crystals (derived from the Greek word “*krystallos*”, meaning “clear ice”) have attracted the interest of scientists as a result of the numerous variations in which they occur in nature. Robert Boyle (1627 - 1691) suggested that crystals were formed from molecules clustered together into geometrical shapes. This very crude way of viewing the formation of crystals was a ground breaking idea in its time. Boyle’s one-time assistant, Robert Hook, extended this idea when he proposed that different crystalline forms could be a result of different arrangements of the smaller entities of which they are composed.<sup>6</sup> This concept is the basic foundation for the study of crystalline materials. In the field of crystal engineering there is a need to gain control over the intermolecular interactions between molecules in an effort to manipulate and guide molecular motifs into a desired outcome, usually under controlled conditions (solvents, temperature, concentration, etc.).

The study of crystals entails, in part, the study of the intermolecular interactions between the molecules in the crystal structure, while the manipulation and control of these interactions represents a new era for molecular science. It was through the work of Jean-Marie Lehn that a new field in chemistry was born. He referred to it as “*supramolecular chemistry*” (from Latin *supra* “above, beyond”) (1978), which he later defined as “chemistry beyond the molecule”.<sup>6</sup> Supramolecular chemistry is the chemistry of molecular ensembles and intermolecular associations.<sup>7</sup> Similarly to covalent chemistry, where chemical bonds are used to produce a limitless assortment of molecules from a limited number of elements, supramolecular chemistry

uses non-covalent interactions to create various polymeric and oligomeric molecular entities (“supermolecules” and “supramolecular ensembles”) from individual molecules.<sup>8</sup> Jean-Marie Lehn summarised the importance of the intermolecular interaction in the field of supramolecular chemistry with the following statement: “*supermolecules are to molecules and the intermolecular bond what molecules are to atoms and the covalent bond*”.<sup>9</sup> This suggests that the primary objective in supramolecular chemistry is the understanding of these interactions, since they are the glue that holds supermolecules together.<sup>10</sup>

Generally, powerful techniques such as NMR spectroscopy, UV-visible and infrared spectrometry have been used successfully for the study of molecular aggregates in solution. However, none of these methods can provide accurate atomic positions for all the atoms in a particular system. The solution for this is provided by single-crystal X-ray diffraction (SCD), although a crystal of appropriate quality is required. Today supramolecular chemistry is a major interdisciplinary branch of science dealing with chemical, physical, biological and technological aspects of the preparation and study of complex chemical systems based on non-covalent interactions.

## 1.2 CRYSTAL ENGINEERING

Crystal engineering, or the design of crystalline solids with specific physical and chemical properties, continues to stimulate great interest.<sup>11</sup> This comprises a wide range of research activity from the understanding of crystal packing in organic molecular solids to the design of open network structures based on metal-ligand coordination bonds, the so-called coordination polymers. In 1894, E. Fischer introduced a principle that describes the notion of tailoring molecules using molecular functionality that would cause them to coordinate in predetermined fashion, thus forming the desired supramolecular assemblies.<sup>12</sup> However, the control of these assemblies is not clear cut; certain compounds can form several molecular assemblies known as polymorphs, depending on the conditions pertaining to the crystallisation of the compound.

In crystal engineering, the size, shape and geometric complementarity of molecules play a more critical role than their reactivity. It is possible to combine coordinatively unsaturated molecules, which do not interact chemically, into new chemical entities with their own unique set of physical and chemical properties.<sup>13</sup> Structural databases combined with computational studies provide the perfect platform to statistically analyse intermolecular interactions and molecular compatibility. Data retrieved from such studies may consequently be utilised in the synthesis of new compounds for the development of new crystalline materials.<sup>14</sup>

The choice of building blocks needed to yield the required structure and properties in a crystal still remains a fundamental problem of crystal engineering. However, a number of strategies that have proven to be useful in this regard do exist, such as Kitaigorodsky's principle of close packing for molecular crystals,<sup>15</sup> the concept of supramolecular synthons (a specific way of assembling crystals through functional groups of adjacent molecules - primarily for organic crystals),<sup>16</sup> M. C. Etter's rules (for crystals assembled *via* hydrogen bonding)<sup>17</sup> and the concept of a tecton (a molecule forming strong directed interactions in crystals - also mainly for organic crystals) as pointed out by G. R. Desiraju.<sup>18</sup>

### 1.3 INTERMOLECULAR INTERACTIONS

Intermolecular interactions occur between neighbouring molecules and are responsible for holding them together in an ordered arrangement, thus resulting in the formation of supermolecules or crystals. Consequently, the strength and directionality of short contacts and hydrogen bonds can be employed in suitable building blocks for the construction of supermolecules.<sup>19</sup> Table 1-1 contains a list of bonding and non-bonding interactions, along with their associated energy ranges.

Hydrogen bonding interactions are much lower in energy than (the) covalent bonds. However, they have profound structure directing capabilities in crystals and are often used in supramolecular synthons. Computational methods used in this study employ relative conformational interaction energies that can be compared to the energy ranges in Table 1-1 as a way of gauging the strength and impact of the computational energies on a particular molecular model. Interactions relevant to this study will be discussed further in this section.

**Table 1-1.** Energy ranges associated with particular bonds and interactions. The numerical data are approximate values.<sup>20</sup>

Bond/Interaction		Energy (kcal/mol)
<b>Covalent</b>	Single	24 - 136
	Double	120 - 147
	Triple	201 - 226
<b>Ion-ion</b>		24 - 120
<b>Hydrogen bond</b>	Very strong, involving (F-H-F)-	36 - 60
	Strong, charge-assisted	10 - 22
	Strong, involving neutral species	2 - 16
	Weak	<4

---

van der Waals	London (dispersion) forces	<1
---------------	----------------------------	----

---

### 1.3.1 Hydrogen bonds

The hydrogen bond is one of the most important structure-directing interactions used in crystal engineering.<sup>21</sup> Our concept of hydrogen bonding has been evolving over the last century, and it has become apparent that hydrogen bonds can be formed by a wide and varied range of chemical entities. The hydrogen bond is typically denoted by X-H...Y, where X and Y were originally identified as the electronegative elements N, O or F.<sup>22</sup> However, as described by Pimentel and McClellan in their book on the hydrogen bond, it has since been agreed that there should be no restriction on X or Y.<sup>23</sup>

**Table 1-2.** List of a few types of hydrogen bonds and their associated energy ranges.

H-bond type	Energy in (kcal/mol)
O—H...N	6.9
O—H...O	4 - 5
N—H...O	3.1
N—H...N	1.9
N,O—H... $\pi$	1.0 - 2.2

The application of hydrogen bonds as active design elements in the synthesis of novel materials and extended aggregates has made significant and very useful contributions to the field of crystal engineering.<sup>21</sup> Computational interaction energies obtained in this study often occur in the same range as the H-bonds listed in Table 1-2, indicating the significance of the computationally determined interaction energies.

### 1.3.2 Van der Waals interactions

The van der Waals force between two atoms is the sum of three different forces: (a) the Keesom force (angle-averaged dipole-dipole interaction), (b) the Debye force (angle-averaged dipole-induced dipole interaction) and (c) the dispersion force. The most important contribution to the van der Waals force is from the *dispersion force* also known as the *London force*, which acts between all molecules or atoms, at a distance that ranges from more than 100 Å down to 2 Å. The dispersion force arises from the formation of temporary fluctuating dipoles in atoms, which

cause instantaneous attractive or repulsive dipole-induced dipole interactions between molecules and atoms.<sup>24</sup> vdW potentials have a limited range, with a distance dependence of  $\frac{1}{r^6}$  ( $r$  is the distance between the atoms) described by the well-known Lennard-Jones Potential.<sup>25</sup> If we put this in computational chemistry terms, a model with ten molecules can have a higher vdW energy component than a model with only two molecules (provided that the molecules are within appropriate proximity of each other to interact).<sup>26</sup>

### 1.3.3 Electrostatic interactions

Electrostatic (Coulombic) interactions are most prominent in ionic crystals, since they occur between charged entities. Coulombic interaction potentials, as opposed to vdW interactions, fall off at a much slower rate than vdW interaction potentials with distance ( $\frac{1}{r}$ ), and are thus not negligible even at large distances. However, the precise nature of the variation in electrostatic interaction energy with distance depends on the structure of the species involved. Molecules not only have formally charged groups, but most molecules comprise neutral fragments with dipoles (partial positive and negative charges). As a result, in most computational molecular models the major component of the electrostatic interaction between molecules or fragments of molecules is a dipole-dipole interaction, which decreases at a rate of  $\frac{1}{r^3}$ .<sup>24b, 25b</sup>

Understanding how these interactions (vdW and electrostatic energy components) operate directly influences one's ability to interpret molecular modelling results. In the computational modelling suite Materials Studio (Section 2.4), vdW and electrostatic energies can be determined during molecular mechanics calculations (using the Forcite Plus module) and can be systematically studied for a particular model or system. This allows us to break down the interactions involved in a system, which could improve our ability to evaluate the significance of the interactions (vdW or electrostatic) in the system.

## 1.4 POLAR ORDERING IN CRYSTALS

Polar ordering can be described as the alignment of the molecules within a system (not necessarily a crystal) in such a way as to produce a net dipole moment, and thus inducing a polar axis within the material. In most cases polar ordering arises from the molecules aligning in a fixed orientation as the crystal grows. These types of materials are well described in the literature.<sup>3b, 27</sup> Perfect polar ordering maximises the optical (and other) properties of the

---

material, especially non-linear optical susceptibility. Figure 1-2 illustrates the concept of polar ordering (polar alignment).

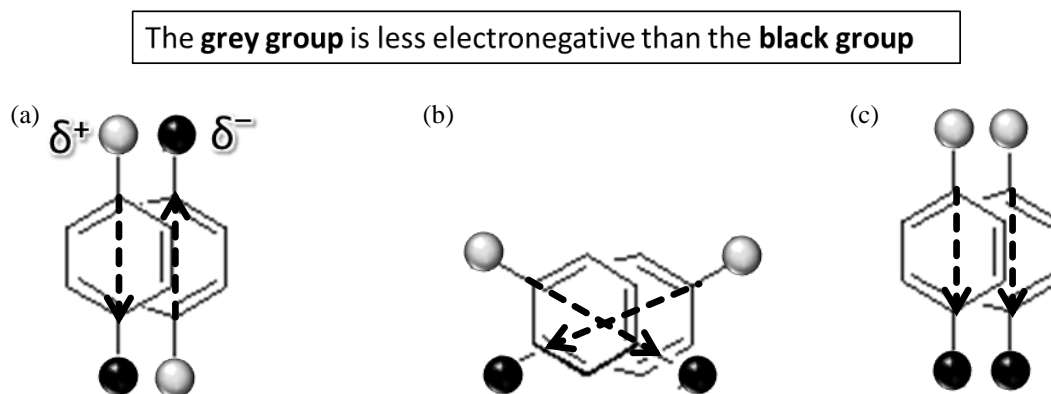
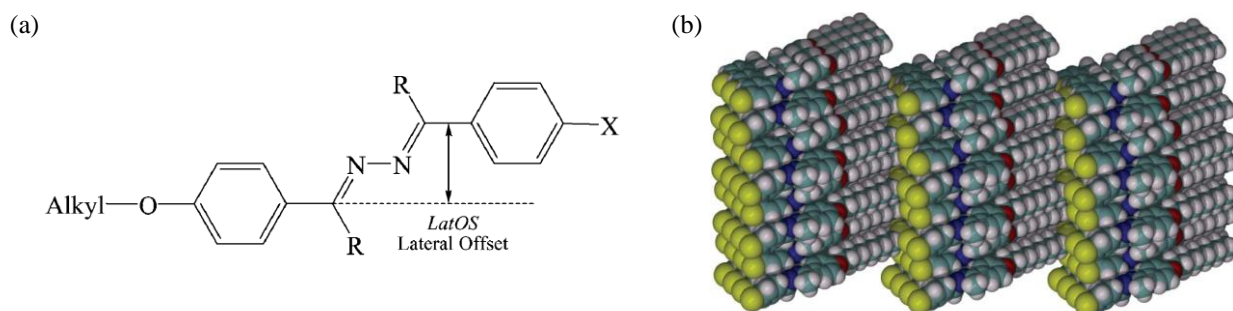


**Figure 1-2.** (a) No polar-ordering, (b) moderate polar-ordering and (c) perfect polar-ordering

Crystals with a polar axis are formed by many organic and inorganic materials and have mostly been studied in the context of optical inorganic materials, colloid and polymer science (polar-ordering in polymer films) as well as liquid crystal polymers where there are many applications for such materials.<sup>28</sup> Polar axes in single-component molecular crystals have been investigated extensively and these studies have led to many applications in second harmonic generation.<sup>1, 29</sup> However, polar ordering of guest molecules in inclusion complexes has been studied to a much lesser extent. There are several approaches in the literature towards achieving acentric (or polar) crystal packing; for example, acentric hydrogen bonded aggregates,<sup>30</sup> acentric metal-ligand coordination networks,<sup>31</sup> antiparallel alignment of ionic sheets,<sup>32</sup> and head-to-tail alignment of dipolar guests confined in channels of organic host lattices.<sup>27a, 33</sup> The modification of physical properties simply by varying the included guest in the same host framework could be studied systematically to investigate any differences in physical properties that may exist.

## 1.5 RELATED WORK

One topic that stands out in particular is the work by Glaser and co-workers on “*polar stacking of parallel beloamphiphile layers*”. Beloamphiphiles are polar and conjugated bolaamphiphiles (amphiphilic molecules that have hydrophilic groups at both ends of a sufficiently long hydrophobic hydrocarbon chain) and they also have lipophilic (fat-loving) properties.<sup>3b, 34</sup>



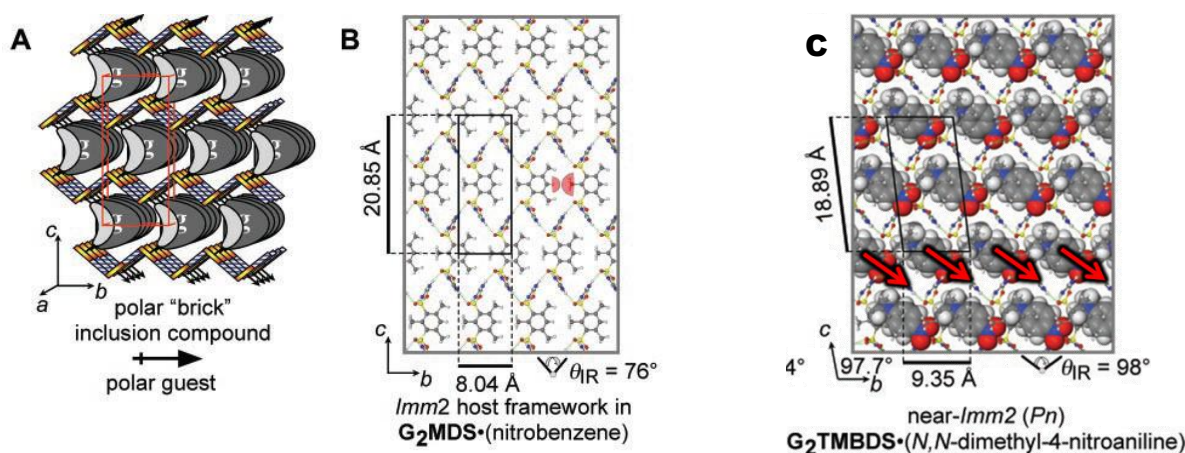
**Figure 1-3.** (a) Molecular design for the beloamphiphiles. (b) Polar stacking in (DecO,Cl)-azine. The R groups are mostly hydrogen atom or methyl groups, although other variations were attempted.

Figure 1-3 shows the molecular design for the beloamphiphiles (a) along with the polar-ordered (DecO,Cl)-azine derivative (b), some of which are polar-ordered. Other work by Glaser *et al.* entails the parallel alignment in the crystal structure of a 4'-acetyl-4-methoxybiphenyl.<sup>27c</sup>

Hulliger and co-workers have also made a significant impact on the area of polar ordering through their work on perhydrotriphenylene (PHTP),<sup>35</sup> tris(o-phenylenedioxy)cyclotriphosphazene (TPP)<sup>36</sup> and the families of the 4-X-triazines, which are crystalline channel-type materials. These crystals were loaded with bipolar molecules such as *para*-nitroaniline in such a way as to induce alignment of the guest.<sup>27a</sup> Their innovation of mapping the polarity of these materials using a technique called “*scanning pyroelectric microscopy*”<sup>37</sup> has transformed the study of polar-ordered crystals. This method, combined with computational studies, allows for the investigation of polarity evolution in these materials.<sup>38</sup>

Another study that is more closely related to this project is the work carried out by Holman *et al.*<sup>4</sup> on polar-ordered inclusion in lamellar host frameworks constructed from guanidinium and organodisulfonate ions (Figure 1-4(a)). The framework is held together by flexible hydrogen bonded sheets with banana-shaped pillars and forms one-dimensional channels occupied by guest molecules aligned in polar arrays. In addition, the asymmetric cavity (Figure 1-4(b)) of this framework has the ability to induce the alignment of asymmetric guest molecules (Figure 1-4(c)). With properly chosen guests, this framework can afford inclusion complexes that exhibit second harmonic generation owing to this alignment.





**Figure 1-4.** (a) Schematic of the guanidinium (G) and organodisulfonate (S) host framework. (b) The asymmetry in the organic fragment of the organodisulfonate ions. (c) Guest polar-ordered inclusion complex of the GS framework.<sup>4</sup>

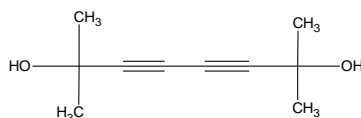
## 1.6 ASPECTS OF THIS SURVEY

### 1.6.1 Structural analysis of guest-guest interactions in polar-ordered systems

The first step was to conduct a Cambridge Structural Database (CSD) search to find more guest polar-ordered crystals (Section 3.2). The search was limited to relatively small polar guests (usually solvents) without disorder. The structural data retrieved were inspected visually using the graphical user interface X-Seed (Section 2.5). The role of guest-guest interactions was then studied computationally as discussed in Chapter 3. From the database search it was apparent that these types of crystals are not common in the literature and this spurred our pursuit of new guest polar-ordered crystalline materials. Two compounds (3,3:6,6:9,9-tris(pentamethylene)-1,2,4,5,7,8-hexaoxonane (**2**) and 2,4,6-endolongifolyl-1,3,5-trioxane (**3**)) appeared to be suitable for further study. The focus turned to the synthesis of new inclusion complexes containing polar-ordered guests, with the hosts (**1**), (**2**) and (**3**).

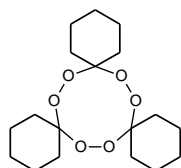


### 1.6.2 2,7-dimethylocta-3,5-diyne-2,7-diol (**1**)



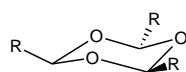
Three new polar-ordered inclusion complexes of **1** were produced. They grow in the same morphology to those previously described (rod-shaped needles): the CMP (**1-4**), BMP (**1-5**) and IMP (**1-6**) inclusion complexes of **1**. SCD analysis confirmed the polar ordering with no disorder of the guests. These new inclusion complexes were used, along with the previously described structures (see Chapter 3), to study the trends and commonalities of these polar-ordered crystals, with particular focus on the structural behaviour of the host and possible implications thereof on the orientation of the guest molecules trapped within the cavities. This work is the focus of Chapter 4.

### 1.6.3 3,3:6,6:9,9-tris(pentamethylene)-1,2,4,5,7,8-hexaoxonane (**2**)



3,3:6,6:9,9-tris(pentamethylene)-1,2,4,5,7,8-hexaoxonane (**2**) was identified from the CSD as forming a structure with a polar-ordered guest and was therefore studied further. After failed attempts to synthesise analogues of **2**, the study was continued by crystallising **2** from a variety of solvents. This yielded crystals of **2-1** (chloroform inclusion complex) which was confirmed to be identical to that reported in the literature, with polar-ordered guests that are not disordered.<sup>39</sup> We also obtained two new inclusion complexes of **2** with bromoform (**2-2**: polar-ordered) and benzene (**2-3**). Only **2-1** is described in detail since it is isostructural to **2-2**. Details of this work are given in Chapter 5.

### 1.6.4 1,3,5-trioxanes (**3**, **4**, **5** and **6**)



1,3,5-Trioxanes are commonly-used compounds that have been investigated extensively. However, no reference (in the literature) is made to the polar-ordering behaviour of these trioxanes.<sup>40</sup> We therefore undertook to synthesise a range of 1,3,5-trioxanes with different R

groups that form polar-ordered inclusion complexes similar to **3-1** and succeeded in obtaining the cyclohexyl (**4**), cyclohex-3-en-1-yl (**5**) and cyclopentyl (**6**) 1,3,5-trioxane derivatives (structural data of **4** are those found in the literature<sup>40</sup>). These compounds pack in a similar manner along the same projections. Therefore we only investigated one of the compounds in more detail, as described in Chapter 6.

### **1.6.5 Methods employed**

These new compounds were studied structurally using SCD analysis and computational methods, namely molecular mechanics (MM), molecular dynamics (MD) and density functional theory (DFT). Information regarding the experimental and computational methods used is given in Chapter 2.

### **1.6.6 Summary of objectives**

The main objectives of this study were to identify compounds that form guest polar-ordered inclusion complexes with simple polar guests such as CF, BF, TCAN, etc. and to elucidate their polar-ordering ability with respect to specific design features of the host compound. This involved identifying suitable compounds from the CSD and attempting to extend the number of known guest polar-ordered structures of inclusion complexes. Following on these results we employed computational methods, using the crystal structure data to construct the models, in order to explain the polar alignment of the guests.

# **CHAPTER 2**

## **METHODOLOGY AND EXPERIMENTAL TECHNIQUES**

## 2.1 SOLUTION NMR

Synthesised compounds were characterised using  $^1\text{H}$  and  $^{13}\text{C}$  NMR spectroscopy. Deuterated benzene ( $^d_6$ benzene) was used as solvent as one series of compounds (1,3,5-trioxanes - Section 2.6) dissociates in deuterated chloroform ( $^d_2\text{CF}$ ) and is insoluble in the other available solvents. All experiments were conducted on either a 400 MHz Varian Unity Inova NMR spectrometer or a 300 MHz Varian VNMRS NMR spectrometer at room temperature employing standard procedures.

## 2.2 CRYSTALLISATION METHODS

Crystallisations were carried out *via* slow evaporation at room temperature with 10 - 20 mg of sample. Samples were dissolved in the minimum amount of solvent and several required slight heating with either a heat gun or hot plate while subjected to gentle stirring to ensure complete dissolution. In some cases, ca. 100  $\mu\text{L}$  of the intended polar guest was used with the appropriate non-including solvent (toluene) to effect the crystallisation. This produced higher quality crystals compared to crystallisation from the polar solvents themselves. Various polar solvents were used in an attempt to obtain a variety of host-guest systems.

## 2.3 SINGLE-CRYSTAL DIFFRACTION AND DATA ANALYSIS

Suitable crystals with appropriate morphology and that uniformly extinguished plane-polarised light were cut when larger than the X-ray beam diameter (0.5 mm). In each case the crystal was placed on a MiTeGen mount using paratone oil. The crystal data were collected using a Bruker-Nonius Smart Apex diffractometer equipped with an Oxford Cryosystems cryostat operating at 100 K. Suitable parameters were chosen to obtain the best possible data sets for the available crystals.

## 2.4 MOLECULAR MODELLING

### 2.4.1 Density Functional Theory

Density Functional Theory (DFT)<sup>41</sup> is a computational method that derives properties of molecules by the determination of their electron density. Modern DFT expresses the energy of a system as a “*functional (defined as a function of a function)*” of the electron density of the

system; this is known as the Kohn-Sham (KS) non-interacting system (1965).<sup>42</sup> KS DFT has become one of the most popular tools in electronic-structure theory owing to its excellent performance-to-cost ratio as compared with correlated wave function theory (WFT), which uses the electron wave functions (complete description of how the electron behaves) to solve the Schrödinger equation for the determination of the energy.<sup>43</sup> As the number of electrons increases, the wave function becomes substantially more complicated (thus sharply decreasing the performance-to-cost ratio of WFT), whereas the determination of the electron density is not as dependent on the number of electrons; as a result DFT performs much faster (DFT suffers a loss in performance-to-cost ratio to a much lesser extent than WFT).<sup>44</sup>

The KS theory is shown here in its simplest form, which describes the mathematics of electron densities and their resulting correlations to molecular energies:

$$\text{Electron density} = \rho(x, y, z). \quad (1)$$

$$E_{\text{DFT}}(\rho) = T(\rho) + E_{\text{NE}}(\rho) + J(\rho) + E_{\text{XC}}(\rho) \quad (2)$$

where  $E_{\text{DFT}}$  is the energy,  $T$  is the kinetic energy of the electrons,  $E_{\text{NE}}$  is the nuclear-electron attraction (Coulombic) energy,  $J$  is the electron-electron repulsive (Coulombic) energy, and  $E_{\text{XC}}$  is the electron-electron exchange-correlation energy.<sup>45</sup> Note that each of these terms is a function of the function  $\rho$ , the electron density, which is itself a function of the three positional coordinates ( $x$ ,  $y$ , and  $z$ ) of the electrons.

*Ab initio* methods ('from first principles of quantum mechanics' and 100% mathematical) scale as  $N^4$  (i.e. the length of a calculation increases to the fourth power of the number of electrons), whereas DFT scales as  $N^3$  with better accuracy.<sup>46</sup> However, hybrid methods employed in DFT attempt to integrate some of the more useful features from *ab initio* methods (specifically Hartree-Fock methods) with some of the improvements of DFT mathematics and perform much faster as a result, with better accuracy.<sup>47</sup> Hybrid methods, such as B3LYP (Becke 3-term correlation functional; Lee, Yang, and Parr exchange functional), tend to be the most commonly used methods among computational chemists.<sup>48</sup> DFT is a general-purpose computational method, and can be applied to most systems. Like all computational methods, a specific DFT method is more useful for certain types of calculations than others.

DFT methods, unlike *ab initio* methods (computationally expensive), can be used for calculations involving transition metals. Hybrid methods, such as B3LYP, are often the method of choice for reaction calculations and can give sensible results in a relatively short period of time.<sup>49</sup>

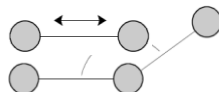
### 2.4.2 Molecular Mechanics

Molecular mechanics (MM, also known as force field methods) describes molecules by eliminating electronic motions and calculates the energy of a system as a function of the nuclear positions only. This is made possible due to the validity of several approximations such as the Born-Oppenheimer approximation. As a result, MM cannot provide properties that depend on electronic distribution in a molecule.<sup>50</sup> The nucleus and electrons of atoms are seen as virtual atomic particles using spherical representations and specific atomic charges and mass which depend on the elements.<sup>51</sup>

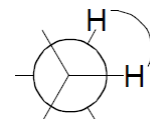
In molecular mechanics vibrations of complex molecules are treated by methods of classical mechanics derived from Hooke's law and Newton's second law.<sup>52</sup> These atomic particles are connected with springs which represent chemical bonds whose stiffness depends on which elements are bound together, and the bond order (single, double, or triple bond: stronger bond, higher force constant) and force constant.<sup>52</sup> All these parameters are determined using experimental and theoretical methods. The "force field" is a collection of all the equations and associated parameters used to calculate each energy term.

Some of the energy terms that need to be taken into account are:

Bond stretching ( $E_{stretch}$ ):



Bond angle bending ( $E_{\theta}$ ):



Dihedral angle rotation ( $E_{torsion}$ ):

van der Waals (vdW) forces ( $E_{vdW}$ ), hydrogen bonding ( $E_{HB}$ ) and electrostatic interactions ( $E_{electro}$ ). Electrostatic interactions within a molecule are handled using equations from classical physics, such as Coulomb's Law. What is known as the total potential energy (or steric energy) of the system is given by a summation of all the energy terms:<sup>53</sup>

$$E_{total} = E_{stretch} + E_{\theta} + E_{torsion} + E_{vdW} + E_{HB} + E_{electro} \quad (3)$$

Since molecular mechanics does not deal directly with electrons and orbitals, we cannot study chemical reactions or predict the reactivity of molecules with this technique.<sup>53</sup> In order to achieve good results from a molecular mechanics calculation, the molecule of interest should be similar to those used in the parameterisation procedure. Some force fields were developed for small organic molecules, while others are better applied to proteins, or solid-state oxides, or

inorganic molecules. This emphasises the importance of the choice of force field on the outcome of a molecular mechanics calculation.

In computational terms, molecular mechanics is the least costly (fastest) method. It is especially well suited to providing excellent structural parameters in terms of bond distances, angles, etc., for the most stable conformation of a molecule. This so-called “geometry optimisation” is often used as the first step before a calculation of another type is performed.<sup>54</sup> This is done to ensure that the molecule is in its lowest energy state so that calculated results can be compared to those obtained experimentally. Molecular mechanics is computationally inexpensive and is often the only method available for use with large molecules or clusters of molecules, provided the molecules in question are similar to those used in training sets.<sup>55</sup>

### 2.4.3 Molecular Dynamics (MD)

MD probes the relationship between molecular structure, movement and function. Molecular dynamics is a multidisciplinary method. Its laws and theories stem from mathematics, physics, and chemistry, and it employs algorithms from computer science and information theory. In its simplest form, molecular dynamics solves Newton's familiar equation of motion:

$$\mathbf{F}_i(t) = m_i \mathbf{a}_i(t) \quad (4)$$

where  $\mathbf{F}_i$  is the force exerted on particle  $i$ ,  $m_i$  is the mass, and  $\mathbf{a}_i$  is the acceleration of atom  $i$ . The force on atom  $i$  can be computed directly from the derivative of the potential energy  $V$  with respect to the coordinate  $\mathbf{r}_i$  (coordinates of atom  $i$ ):<sup>52</sup>

$$-\frac{\partial V}{\partial \mathbf{r}_i} = m_i \frac{\partial^2 \mathbf{r}_i}{\partial t^2} \quad (5)$$

There are three general approaches to carrying out molecular dynamics at constant temperature rather than constant energy. One method that is simple to implement and reliable is to periodically reselect atomic velocities at random from the Maxwell-Boltzmann distribution:<sup>50</sup>

$$f(v) = \left(\frac{m}{2\pi k_B T}\right)^{3/2} \exp\left(-\frac{mv^2}{2k_B T}\right) 4\pi v^2 \quad (6)$$

In Canonical ensemble (NVT - used in this study), moles ( $N$ ), volume ( $V$ ) and temperature ( $T$ ) are conserved (as opposed to energy). It is also sometimes called constant temperature molecular dynamics (CTMD). This is the appropriate choice when conformational searches of models are carried out in vacuum without periodic boundary conditions.<sup>24b</sup> The reader should be aware that analogous approaches exist for other ensembles, particularly to simulate at constant pressure or stress.<sup>56</sup> Popular techniques to control temperature include velocity rescaling, the

Nosé-Hoover thermostat, Nosé-Hoover chains, the Berendsen thermostat and Langevin dynamics.<sup>57</sup> MD Simulation runs are generally short: typically  $t = 10^3$ - $10^6$  MD steps, which correspond to perhaps a few nanoseconds of real time and, in special cases, extending to the microsecond regime.<sup>58</sup>

#### **2.4.4 Molecular Quench Dynamics (MQD)**

Quench dynamics (QD) is similar to standard dynamics, except that each structure produced by the dynamics calculation is also minimised. QD calculations provide a means of searching conformational space for low energy structures by alternating the phases of dynamics simulation, along a classical trajectory, with a quench period in which the structure is minimised (optimised). A standard dynamics simulation continues between quenches with intervals specified when the job is set up. After the quench process has been completed, the dynamics simulation continues from the unquenched structure to prevent disturbing the dynamics simulation. MD and MQD calculations explored in this work employ MM methods.

### **2.5 SOFTWARE PACKAGES**

#### **2.5.1 Cambridge structural database (CSD)**

The CSD (version 5.31 November 2009 + 4 updates) is a structural database that contains published single-crystal and powder, data. The user can conduct searches with specific constraints to obtain a refined set of structural data consistent with the imposed constraints. This makes it possible to study systems with similar traits, synthons etc. to further understand the nature of bonds and long range interactions and their role in the formation of crystals.<sup>59</sup>

#### **2.5.2 APEX II<sup>60</sup>**

Apex II is a software package using a graphical user interface (GUI) to manage SCD experiments, data collections, intensity corrections of X-ray reflections and crystal system and space group determination. It generates two output files (.ins and .hkl) that can be used by SHELX-97 *via* X-Seed to solve and refine the crystal structure.<sup>61</sup>

#### **2.5.3 X-Seed<sup>62</sup>**

X-Seed is a graphical software package used as an interface for the SHELX-97 software suite to solve and refine the single-crystal structure from the .ins and reflection (.hkl) files generated by

---



APEX II. X-Seed can also generate structural images using POV-Ray<sup>63</sup> as a rendering tool.

X-Seed is also used to visualise crystal structures extracted from the CSD.

#### 2.5.4 SHELX-97<sup>64</sup>

SHELX-97 is a software suite containing programs such as SHELX-S (for structure solution from crystallographic data) and SHELX-L (for refinement of the solution obtained from SHELX-S using intensity data)<sup>65</sup> and is employed within X-Seed.

#### 2.5.5 Molden<sup>66</sup>

This application is used to build molecules using internal coordinates (Z-matrix). The user can modify connectivity of the atoms in the molecule very easily and also has the option of saving the coordinates file as a Z-matrix or in xyz format. The results of Gaussian calculations can be displayed, allowing the user to confirm geometry and connectivity by visual inspection, and to rotate the molecule in three dimensions.

#### 2.5.6 Gaussian03<sup>48</sup>

Gaussian03 is an associated system of quantum chemistry programs aimed at performing a variety of semi-empirical, *ab initio* MO calculations, DFT, self-consistent field calculations and much more. It is controlled by an input file which contains all the instructions for the calculation, including calculation type, methods, basis-sets, level of convergence and the structure of the molecules to be calculated. All DFT type calculations were performed using Gaussian03.<sup>48</sup>

For this study the MPW1PW91 (Barone's Modified Perdew-Wang 1991 exchange functional and Perdew and Wang's 1991 correlation functional) hybrid method, coupled with a triple-zeta quality Pople basis set with two diffuse and polarisation functions (6-311++G(p,d)),<sup>67</sup> was found to be the most suitable for all potential energy scans and geometry optimisations of simple guest molecules such as: TCAN, Cl-TMS and BTCM. This was determined by modelling ACN (models containing one and two molecules) using a number of methods (B3LYP, B971, MPW1PW91, MP2 and CCSD) and various basis sets and comparing them to MP2 and CCSD. However, we were unable to calculate the two-molecule model with the CCSD method (owing to technical restrictions), and since MP2 compared well to CCSD in the one-molecule model (% difference relative to CCSD < -0.03%), it was decided to compare the remaining methods to

MP2. All energies were converted from Hartree to kcal/mol. Figure 2-1 shows the results of the two-molecule model.

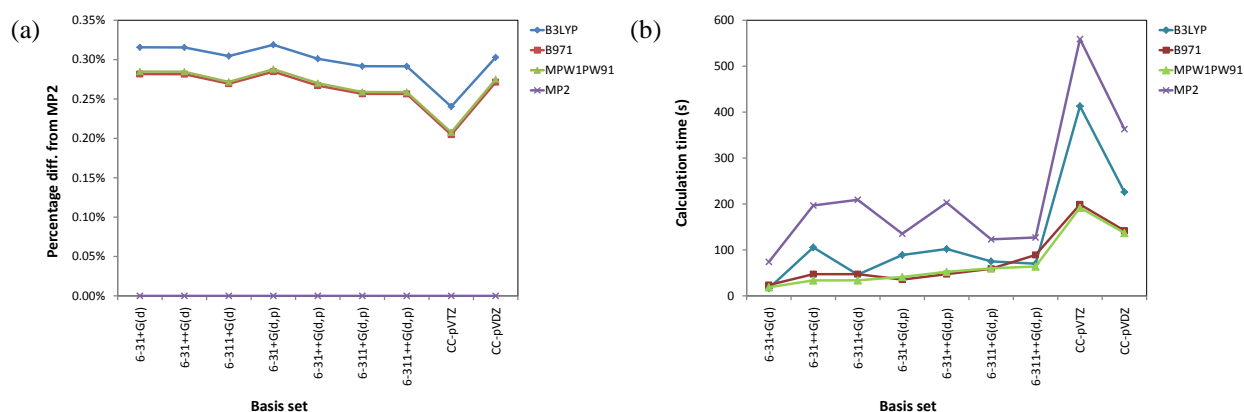


**Figure 2-1.** Model containing two molecules. (a) Percentage difference relative to MP2 for each method and basis set. (b) Calculation times for each method and basis set.

Methods MPW1PW91 and B971 performed similarly and better than B3LYP in terms of accuracy (Figure 2-1(a)). However, MPW1PW91 performs slightly better than both in calculation time. Since the models for this study are much larger, we opted for the MPW1PW91 method with an appropriate basis set.

### 2.5.7 Materials Studio

Although the program suite can run various computational methods such as DFT and molecular mechanics/dynamics, we only have access to the Forcite Plus and Discover modules, which are both based on molecular mechanics, allowing us to perform optimisations and molecular dynamics calculations. We made use of the Forcite Plus module to run molecular mechanics, molecular dynamics and quench molecular dynamics calculations.<sup>24b</sup> The parameters used for optimisations and molecular dynamics are given in Table 2-1 and Table 2-2 respectively.

**Table 2-1.** Energy parameters used for molecular mechanics simulations and optimisations.

Geometry optimisation parameters	
<b>Energy</b>	
Force field	CVFF
Charges	Force field assigned
Quality	$2 \times 10^{-5}$ kcal/mol
Summation method - electrostatic	Group based
Summation method - van der Waals (vdW)	Group based
<b>Geometry optimisation</b>	
Algorithm	Smart

---

<b>Quality</b>	$2 \times 10^{-5}$ kcal/mol
<b>Max iterations</b>	500

---

The Smart algorithm is a cascade of the steepest descent, ABNR (Adjusted basis set Newton-Raphson), and quasi-Newton methods.

**Table 2-2.** Parameters used for molecular dynamics (including quench dynamics) and simulations.

---

<b>Dynamics parameters</b>	
<b>Temperature</b>	298.0 K
<b>Time step</b>	1 fs
<b>Tot. sim. time</b>	500 ps
<b>Number of steps</b>	500 000
<b>Frame output</b>	1000 steps
<b>Ensemble</b>	NVT
<b>Thermostat</b>	Velocity scale
<b>Temp. difference</b>	2.0 K
<b>Quench dynamics</b>	
<b>Quench period</b>	5000 steps
<b>Geometry optimisation</b>	See Table 2-1 Table 2-1

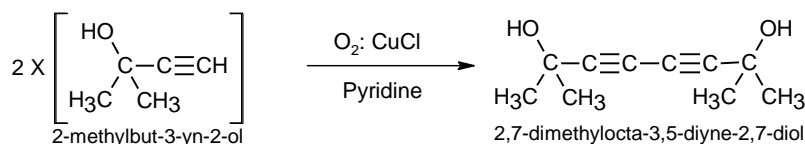
---

## 2.6 COMPOUNDS STUDIED

The syntheses of all compounds were carried out using methods as described in the literature. Modifications to synthetic procedures were made where necessary and are indicated. Verification of products was achieved by  $^1\text{H}$  and  $^{13}\text{C}$  NMR spectroscopy.

### 2.6.1 2,7-dimethylocta-3,5-diyne-2,7-diol (1)

This reaction was carried out on half the scale stipulated in the literature.<sup>68</sup> Instead of bubbling oxygen through the solution, the reaction mixture was kept under a constant oxygen pressure while shaken for 6 hours. The reaction mixture became slightly warm, which indicated that the coupling reaction was occurring.

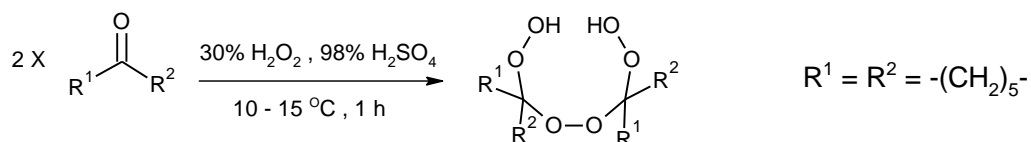
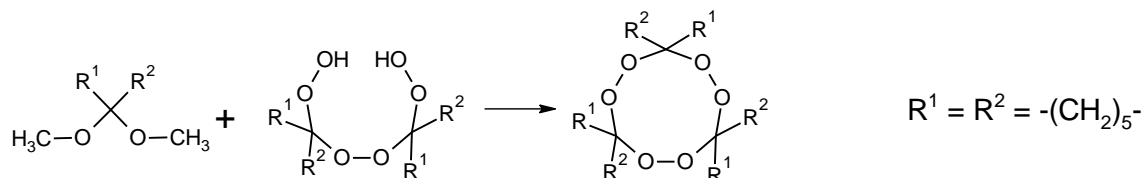
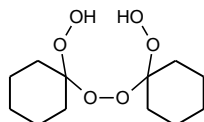


**Scheme 2-1:** Synthesis of **1**

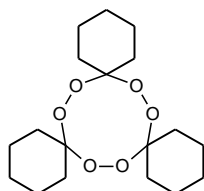
**Preparation of 2,7-dimethylocta-3,5-diyne-2,7-diol (1):** 17.4 g (20 mL) 2-methylbut-3-yn-2-ol was added to 20 mL methanol and 6 mL dry pyridine. 1 g of the CuCl catalyst was added to the mixture which was then shaken under an oxygen atmosphere for 6 hours. 10 mL conc. HCl was added to the mixture, which was then filtered. The solid was washed with a 50 mL saturated NaCl solution and then dried under vacuum. Recrystallisation from toluene yielded a pure white product (**1**) in 54% yield (3.65 g). The product was characterised using NMR spectroscopy.

### 2.6.2 1,2,4,5,7,8-Hexaoxonanes

These compounds first require the synthesis of a precursor under the general name, 1,1'-dihydroperoxydi(cyclohexane)peroxide. Caution was required when working with peroxides and 1,2,4,5,7,8-hexaoxonane as they might be explosive (a blast shield should always be used). General reactions for both the precursor and final product are given below, according to the synthetic procedure of Terent'ev *et al.*<sup>39</sup>

**Scheme 2-2:** Synthesis of the peroxides**Scheme 2-3:** Synthesis of the 1,2,4,5,7,8-hexaoxonanes**1,1'-dihydroperoxydi(cyclohexane)peroxide (Scheme 2-2)**

Water (5 mL) and cyclohexane (5.3 mL) were simultaneously added drop wise (using two dropping funnels) to a mixture of 16 mL 30%  $\text{H}_2\text{O}_2$  and 2.4 mL 98%  $\text{H}_2\text{SO}_4$  over 10 min. The reaction mixture was stirred for 1 h while maintaining the temperature between 10-15  $^\circ\text{C}$ .

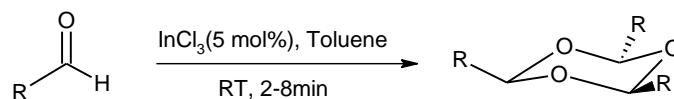
**3,3:6,6:9,9-tris(pentamethylene)-1,2,4,5,7,8-hexaoxonane (Scheme 2-3)**

1,1-dimethoxycyclohexane (acetal) (0.396 mL) was added to a solution of 1,1'-dihydroperoxydi(cyclohexyl)peroxide (540.72 mg) in 1.5 mL  $\text{Et}_2\text{O}$ . A solution of  $\text{BF}_3 \cdot \text{Et}_2\text{O}$  (0.309 mL) in  $\text{Et}_2\text{O}$  was added at 0-5  $^\circ\text{C}$  and then stirred at 20-25  $^\circ\text{C}$  for 3-8 h. After purification only 112 mg (26.6%) pure compound was isolated and characterised by NMR spectroscopy.

**2.6.3 1,3,5-trioxanes**

A modified procedure for the solvent-free trimerisation of aldehydes as described in the literature was used to synthesise the 1,3,5-trioxanes<sup>69</sup> (see Scheme 2-4). A mixture of the aliphatic aldehydes (2 mL) and 5 mol% of indium (III) chloride was diluted with 10 mL toluene and allowed to react under stirring for 2-8 min (see Scheme 2-4) to yield a solid product. 10 mL

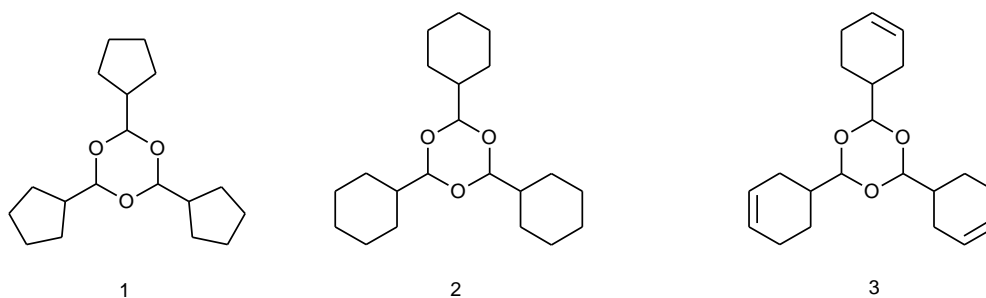
water was added while stirring and heating to dissolve the  $\text{InCl}_3$  in the aqueous phase, which was then separated from the organic layer. Recrystallisation of the product from toluene resulted in yields between 64% and 77%. The product was characterised with  $^1\text{H}$  and  $^{13}\text{C}$  NMR using  $d_6$ benzene as solvent.  $^1\text{H}$  and  $^{13}\text{C}$  NMR spectra of the 1,3,5-trioxanes showed peaks corresponding to the CH proton at 4.5 ppm and a carbon resonance at 110 ppm, which are indicative of the cyclic trimer.



**Scheme 2-4:** Synthesis of the 1,3,5-trioxanes

The following trioxanes were successfully synthesised using this method:

1. 2,4,6-tri(cyclopentyl)-1,3,5-trioxane
2. 2,4,6-tri(cyclohexyl)-1,3,5-trioxane
3. 2,4,6-tri(cyclohex-3-en-1-yl)-1,3,5-trioxane



Attempts were made to synthesise trioxanes with bulkier alkyl or aryl groups in an effort to obtain polar-ordered inclusion compounds. However, all the known methods for synthesising 1,3,5-trioxane proved unsuccessful.

#### 2.6.4 Summary

All compounds that were successfully synthesised are listed in Table 2-3 (below), along with the solvents used to obtain inclusion compounds.

## Chapter 2 - Methodology and Experimental Techniques

**Table 2-3.** All compounds and inclusion compounds synthesised. The guests in italics are those for inclusion compounds that have already been reported, but which have been studied further in this work.

Compound	Guest	Inclusion compound	Compound number
			<b>1</b>
2,7-dimethylocta-3,5-diyne-2,7-diol	<i>bromotrichloromethane (BTCM)</i>	Yes	<b>1-1</b>
	<i>trichloroacetonitrile (TCAN)</i>	Yes	<b>1-2</b>
	<i>chlorotrimethylsilane (Cl-TMS)</i>	Yes	<b>1-3</b>
	2-chloro-2-methylpropane (CMP)	Yes	<b>1-4</b>
	2-bromo-2-methylpropan (BMP)	Yes	<b>1-5</b>
	2-iodo-2-methylpropane (IMP)	Yes	<b>1-6</b>
			<b>2</b>
1,4,7-cyclohexane-1,2,4,5,7,8-hexaoxonane	<i>chloroform (CF)</i>	Yes	<b>2-1</b>
	bromoform (BF)	Yes	<b>2-2</b>
	benzene (C <sub>6</sub> H <sub>6</sub> )	Yes	<b>2-3</b>
	<i>R = endolongifolyl</i>	<i>chloroform (CF)</i>	Yes
2,4,6- <i>R</i> -1,3,5-trioxane	cyclohexyl	No	<b>4</b>
	cyclohex-3-en-1-yl	No	<b>5</b>
	cyclopentyl	No	<b>6</b>

All compounds and inclusion complexes will hereafter be referred to by their **Compound numbers**.

# **CHAPTER 3**

## **STRUCTURAL ANALYSIS OF GUEST-GUEST INTERACTIONS IN POLAR-ORDERED SYSTEMS**



### 3.1 INTRODUCTION

Work carried out by Dr. Gareth Lloyd on the inclusion complexes of **1** showed that guests such as BTCM (**1-1**), TCAN (**1-2**) and Cl-TMS (**1-3**) are polar ordered.<sup>5</sup> The ordered inclusion of these simple polar guests (solvents) in **1** inspired us to discover similar systems. We therefore conducted a CSD (version 5.31 November 2009 + 4 updates) search containing simple polar guests to identify additional polar-ordered crystal structures. The similarities and/or differences between the systems will thus be examined in order to establish the parameters required for polar-ordered inclusion of these small guests. Properties such as guest and host symmetry, crystal system and space group and size of the host constituents etc. were investigated to determine their role, if any, on polar-ordered inclusion. The setup and results of this CSD study will be discussed in this chapter. This study could promote our understanding of the requirements for the formation of guest polar-ordered crystals and establish inherent trends within these systems. Our results show that some of the common factors are the guest-guest distance within a particular channel and between neighbouring channels. Hence the guest-guest interactions were modelled using DFT calculations.

### 3.2 CSD STUDY

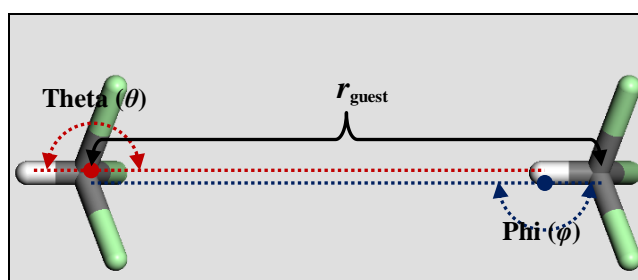


**Figure 3-1.** Parameters used for the CSD search (CF used as an example).  $r_{\text{guest}}$  = guest-guest distance along the channel or polar axis. Theta and phi are shown in red and blue, respectively.

A survey was conducted to find all crystal structures deposited in the CSD that contain polar-ordered guests. The search parameters are shown in Figure 3-1. The guests used and the number of structures identified are given in Table 3-1. The CSD search was conducted with a guest-guest distance ( $r_{\text{guest}}$  - measured between the central atoms of the guests, Figure 3-1) of 4 - 15 Å. The lower bound of 4 Å corresponds to the sum of the vdW radii, while the upper bound of 15 Å was chosen to account for any long-range polar alignment. Two angles were defined ( $\theta$  and  $\phi$ , Figure 3-1) with limits of 160° - 180° relative to each other to refine the search even further by

constraining the molecules to be aligned in the same general direction with a 20° tolerance on the angle for both molecules. The results were limited to structures without disorder. All structures thus obtained were inspected visually using X-Seed (Section 2.5.3) to confirm that the guests were indeed polar-ordered. Only a small, yet diverse set of crystal structures was identified that contain polar-ordered guests. Most of them have CF, and the rest ACN, as the polar guest. The results of this search are presented in Table 3-1.

**Table 3-1.** Guests used to conduct the CSD search for polar-ordered crystals.

Guest	No. polar-ordered structures	Guest dipole moment (D - Debye)
CF	6	1.07
ACN	4	3.97
BF	0	1.0
BMP	0	2.21
BTCM	0	0.21
Cl-TMS	0	1.93(2)
CMP	0	2.15
DCM	0	1.54 - 1.63
DMF	0	3.86(1)
DMSO	0	3.90(1)
IMP	0	2.13
TCAN	0	2.00
THF	0	1.69(1)

The distance between vectors running through the guests along the polar axis was defined as indicated by the double-headed arrow in Figure 3-2. This lateral distance between the guests in different “channels” (not all guests are situated in open channels) is particularly important as it can indicate whether the guests in neighbouring channels are close enough to interact with one another, thus indicating whether the guest alignment in these systems is driven by guest-guest, host-guest or both types of interactions.

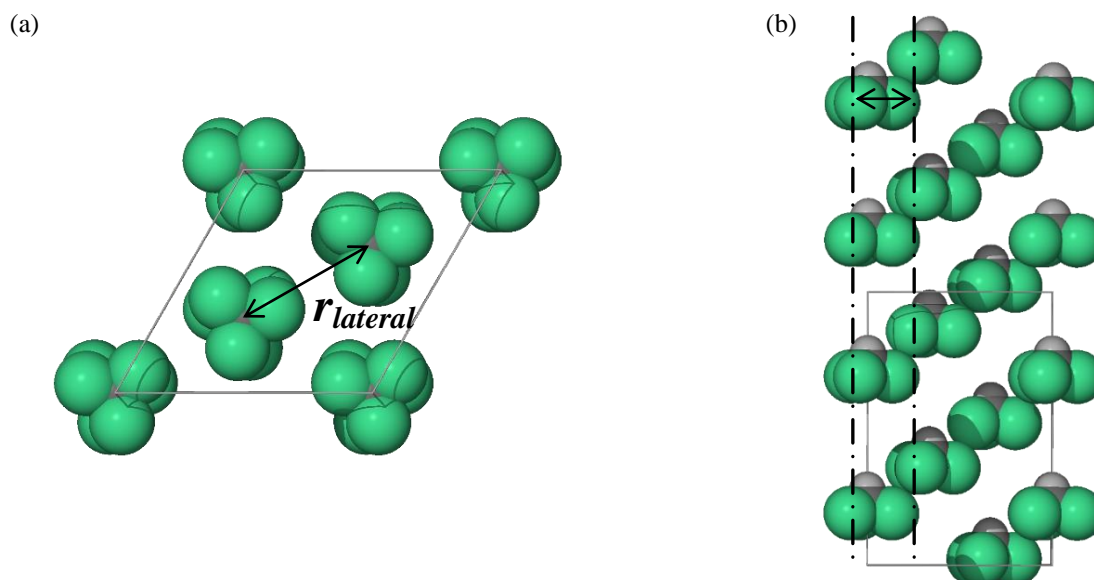


**Figure 3-2.** The lateral guest-guest distance ( $r_{lateral}$ ) is measured as indicated by the double-headed arrows. (a) The channel distance measured as viewed down the polar axis. (b) Viewed perpendicular to the polar axis with lines running through the guest molecules along the polar axis. The host molecules have been omitted for clarity.

The host compounds located in the CSD search are quite diverse (Table 3-2). Most crystallise in the trigonal ( $R3c$  or  $R3$ ) and monoclinic ( $Cc$ ) crystal systems, while only two crystallise in the hexagonal ( $P6_3$ ) or orthorhombic ( $Pnn2$ ) crystal systems.

A variety of lateral guest-guest distances were found for the different structures, ranging between 8.2 and 17.7 Å. These are relatively large distances, which raises the question of whether the guest molecules can interact with one another at such distances in order to facilitate the formation of guest polar-ordered crystals. The other plausible and intuitive alternative would be that host-guest interactions are responsible for this phenomenon. In the next section this question will be addressed using DFT methods to investigate guest-guest interactions in the absence of surrounding host molecules.

## Chapter 3 - Structural analysis of guest-guest interactions in polar-ordered systems

**Table 3-2.** Compounds that form polar-ordered crystals with CF and ACN. <sup>39-40, 70</sup>

	Compound	Lateral distance (Å)	Crystal system	Space group	Guest	CSD refcode
<b>i</b>	2,4,6-(endolongifolyl)-1,3,5-trioxane•CDCl <sub>3</sub>	12.16	Trigonal	<i>R3</i>	CHCl <sub>3</sub>	MUTYAB
<b>ii</b>	3,3:6,6:9,9- <i>tris</i> (pentamethylene)-1,2,4,5,7,8-hexaoxonane	8.20	Trigonal	<i>R3c</i>	CHCl <sub>3</sub>	LIRREK
<b>iii</b>	<i>trans,trans,trans</i> -(1.1.1)(3,3')-azobenzophane	14.56	Trigonal	<i>R3c</i>	CHCl <sub>3</sub>	ALUSOP
<b>iv</b>	((1a,2b,3a,4a,5a,6a,7b,8a)-4,5-dichloro-tetracyclo(6.2.1.02,7.03,6) undec-9-ene-3,6-diyl)bismethanol (natural compound)	14.04	Trigonal	<i>R3c</i>	CHCl <sub>3</sub>	NAHZOL
<b>v</b>	dibenzyl-dichloro-(1,10-phenanthroline)-tin(iv) chloroform solvate	9.11	Monoclinic	<i>Cc</i>	CHCl <sub>3</sub>	FILZOG
<b>vi</b>	dichloro-( $\eta^2$ , $\eta^2$ -9,10-dihydro-9,10-ethenoanthracene)-platinum(ii)chloroform solvate	11.51	Monoclinic	<i>Cc</i>	CHCl <sub>3</sub>	QAVXEQ
<b>vii</b>	triethylammonium 26,27,28-trihydroxypentacyclo (19.3.1.13,7.19,13.115,19) octacos-1(25),3,5,7(28),9,11,13(27),15,17,19(26),21,23-dodecaen-25-olate	17.73	Monoclinic	<i>Cc</i>	CH <sub>3</sub> CN	AFEBIW
<b>viii</b>	dichloro-(tris(2-pyridylmethyl)amine)-iron(ii)	-	Orthorhombic	<i>Pnn2</i>	CH <sub>3</sub> CN	QALZUZ
<b>ix</b>	1-chloro-2,8,9-trioxa-5-aza-1-germatricyclo(3.3.3.0)undecane	8.48	Hexagonal	<i>P6<sub>3</sub></i>	CH <sub>3</sub> CN	XEBTUT
<b>x</b>	rac-(di-iodo-(N,N,N',N'-tetrakis(2-pyrazinylmethyl)-1,3-trimethylenediamine)-cerium(iii) iodide	15.60	Trigonal	<i>R3c</i>	CH <sub>3</sub> CN	OBPEV

### 3.3 MOLECULAR MODELLING

The molecular modelling described in this section was carried out to quantify guest-guest interactions in the absence of the host. The arrangement of polar guest molecules within a channel was first investigated in an effort to establish whether they will adopt the same polar alignment *via* dipole-dipole or vdW interactions. The second part involved ascertaining the minimum lateral guest-guest distance required for the existence of lateral guest-guest interactions and determining how this distance would affect the alignment of the guest molecules.

#### 3.3.1 Intra-channel guest-guest interactions

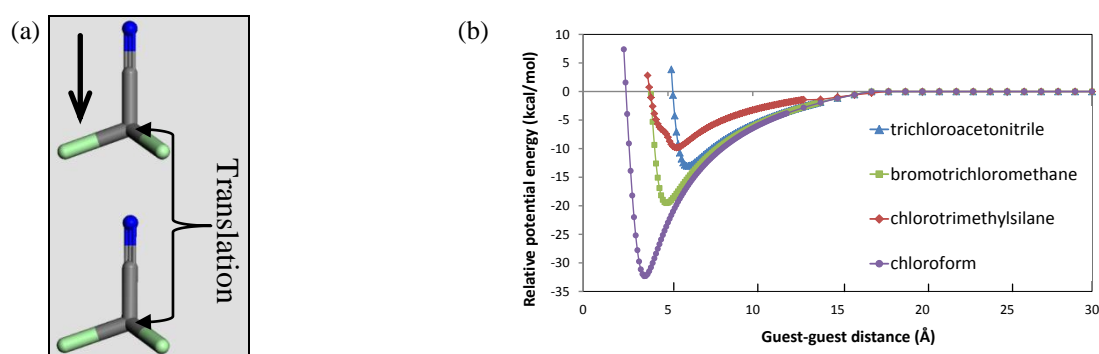


**Figure 3-3.** (a) Model used for head-to-tail guest-guest interactions, indicating the distance recorded. The bottom molecule was translated in the direction of the arrow. (b) Relative potential energy plots of results obtained from the calculations.

Figure 3-3(a) illustrates the model used to calculate the head-to-tail interactions of polar guests (TCAN, BTCM, Cl-TMS and CF) within a channel. The guest molecule at the bottom was translated in the direction indicated by the arrow in increments of 0.1 Å for 100 steps and then 1.0 Å for another 20 steps. Eventually the guests became separated by ca. 30 Å, at which point there should be negligible interaction between them. This final position was thus assigned a value of 0.0 kcal/mol, and all other energies were expressed relative to it (for each guest individually) to yield the stabilisation energy.

The results shown in Figure 3-3(b) clearly show significant stabilisation energy for all the guests, with the greatest stabilisation being more than 30 kcal/mol (CF). It was also possible to identify the guest-guest distances corresponding to their respective minima. The variation in guest-guest distance (C–C distance) of the potential minima for these guest molecules is a result of their respective geometries (CF (3.6 Å), BTCM (4.9 Å), Cl-TMS (5.4 Å) and TCAN (6.2 Å)). At distances greater than 17 Å the stabilisation of the system diminishes to zero for all the guests, indicating that the guest-guest interactions do not play a role at such distances.

To further explore the role of the head-to-tail alignment, a series of calculations that incorporates the different relative orientations of the guests was performed (see Figure 3-4).

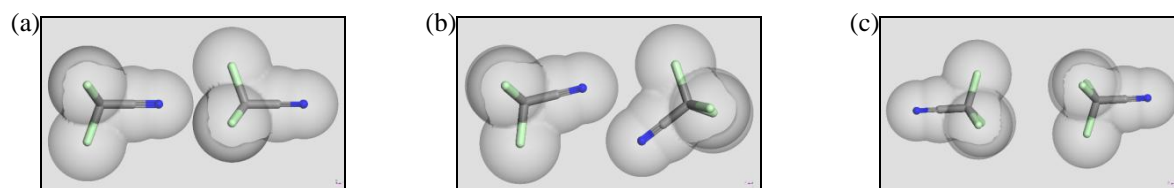


**Figure 3-4.** Models used for DFT calculation to assess the guest-guest interactions. (a), (b) and (c) show the three optimised positions of the different relative orientations.

Two guests were placed in three different relative orientations and their positions were allowed to optimise, thus yielding the structures shown in Figure 3-4. These conditions were applied to all the guests considered. The energies for each of the six guests were calculated relative to the head-to-tail orientation of each particular guest (Figure 3-5(a)), and these were used to determine the Boltzmann distribution at 298.0 K (Figure 3-5(b)).

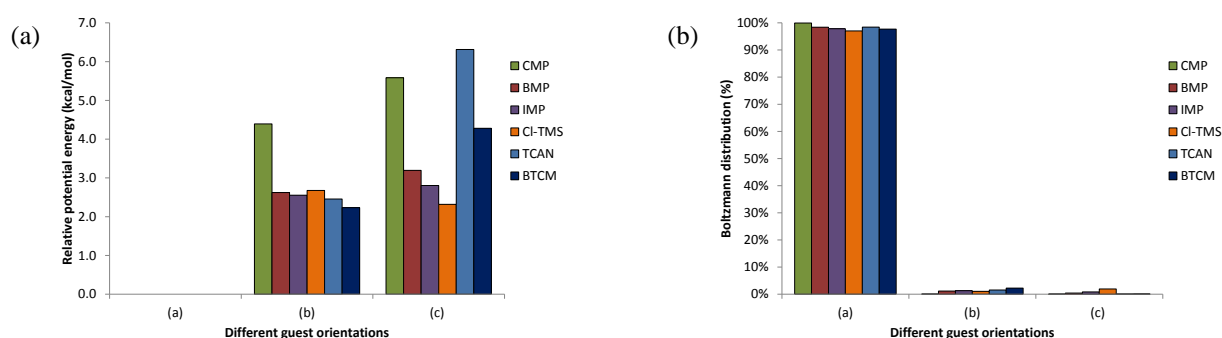


**Figure 3-5.** (a) Potential energies relative to the head-to-tail orientation. (b) Boltzmann distributions at 298.0 K. (a), (b) and (c) on the abscissa correspond to the labels of the models in **Figure 3-4**.

It is clear from Figure 3-5(a) that (b) and (c) are very unstable relative to the head-to-tail arrangement, as indicated by the positive relative energies. The resulting Boltzmann distributions (Figure 3-5(b)) show that (a) is favoured for all guests, confirming the relative stability of the head-to-tail alignment as observed in the crystal structures.

### 3.3.2 Lateral guest-guest interactions

In order to determine whether the observed lateral guest-guest distances are too large for the guests to interact, a DFT calculation was performed for two guests moving away from each other laterally, and translating relative to each other as shown in Figure 3-6a. TCAN was chosen for this simulation since it involves a time-consuming calculation due to the large number of data points required (Figure 3-6(b)). (TCAN forms polar inclusion complexes with **1**). The

lateral guest-guest distances in all the crystal structures obtained from the CSD study, as well as in **1** (12.381 Å) are larger than 8 Å.

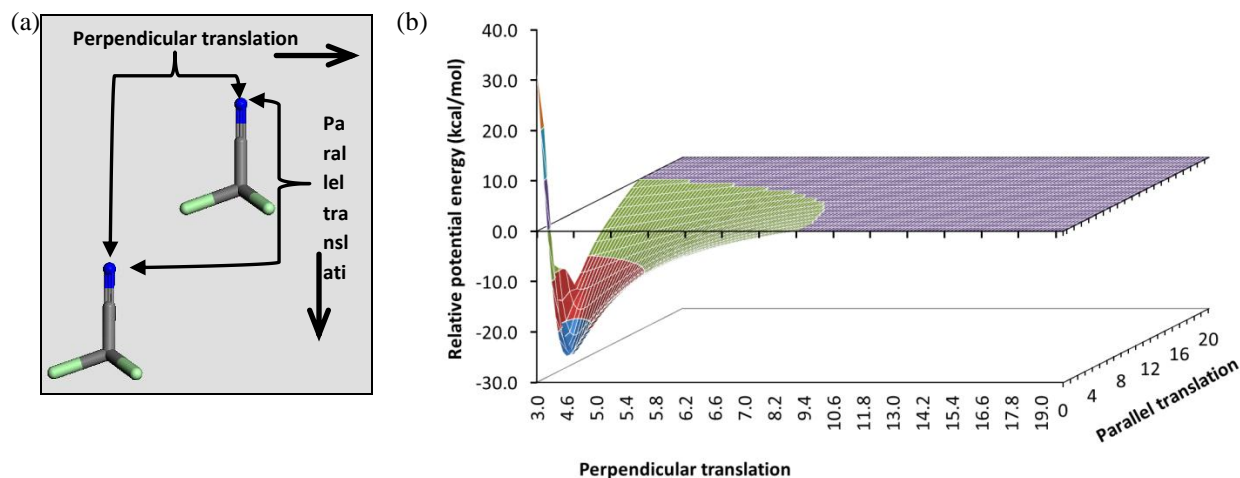


**Figure 3-6.** a) Model used for determining lateral guest-guest interactions, indicating the distances recorded. The molecule on the right was translated in the direction of the arrows. b) Resultant relative potential energy surface obtained from the calculation.

One TCAN molecule was placed in a fixed position, while a second molecule was translated relative to the stationary guest in two directions: a translation to move the guest perpendicular to the polar axis of the stationary guest and a translation to move the guest parallel to the polar axis of the stationary guest (as indicated by the arrows in Figure 3-6(a)).

The perpendicular translation shows whether and where a cut-off distance (area where no interaction is present between the guests) exists. A 0.0 Å parallel translation corresponds to a head-to-tail alignment. (Figure 3-6(b)) shows the results obtained from this simulation as a potential energy surface plot with the relative potential energy on the  $z$ -axis.

A clear minimum (-25.8 kcal/mol) can be seen on the potential energy surface plot (Figure 3-6(b)) at 4.0 Å perpendicular and 2.0 Å parallel translation. The plateau of the energy surface is the area of zero interaction and can be regarded as the cut-off area for the guest-guest interactions. The largest perpendicular distance at which 0 kcal/mol interaction is obtained at 9.1 Å for a 0.0 Å parallel translation and is considered as the cut-off for guest-guest interactions. This suggests that only when the host is **ii** or **ix** (Table 3-2), there might be sufficiently strong guest-guest interactions to induce guest polar ordering since their perpendicular guest-guest distance (Table 3-2) is within the cut-off area. It should be kept in mind that this simulation was carried out in the absence of the host, which could shield the guests from each other or enhance the interaction between them. The channels of the remaining polar-ordered structures in Table 3-2 are too far apart ( $\geq 12.2$  Å) for the guest to interact without the aid of the host. It is therefore

plausible that these systems have to rely on host-guest interactions and/or host-mediated guest-guest interactions through the channel or cavity.

### 3.4 SUMMARY

A CSD survey was conducted to identify crystal structures containing polar-ordered guests, where the targeted guests were usually small, simple solvents (Table 3-1) with different dipole moments. The search only yielded polar-ordered structures for two of the guests: CF (5 structures) and ACN (4 structures). The small number of guest polar-ordered crystal structures found is evidence of their rarity in the literature.

The host compounds identified were compared for similarities that might shed light on their ability to form polar-ordered crystal structures. Five of the compounds crystallise in a polar trigonal space group ( $R3c$  or  $R3$ ) and three in the monoclinic space group ( $Cc$ ). The two remaining compounds, which include ACN, crystallise in different polar space groups, hexagonal ( $P6_3$ ) and orthorhombic ( $Pnn2$ ). It was decided to further investigate compounds that crystallise in the trigonal system since there are more compounds of this type (including **1**).

The lateral guest-guest distances of all the structures range from 8.2 Å to 17.7 Å. The lateral guest-guest potential energy profile (using TCAN) indicates that a distance beyond 9.1 Å is outside the attractive interaction range of the guests. This either requires the host to mediate guest-guest interactions through its walls, or for the host itself to induce the polar-ordering of the guests. Both of these scenarios will be addressed in the subsequent chapters and resolved using computational methods. The simulation of head-to-tail guest-guest interactions revealed a strong dipole-dipole interaction between the guests that would drive all the guests in one channel to follow the same alignment, provided they are within close enough proximity to overcome any repulsive interactions.

The syntheses of most of the compounds in Table 3-2 are quite challenging, which limits the choice of compounds used for further study. On this basis it was decided to focus on the 1,2,4,5,7,8-hexaoxonanes (**2**, Chapter 5) and 1,3,5-trioxanes (**2 - 5**, Chapter 6), along with **1** by exploring their polar-ordering ability both computationally and experimentally.

Three compound types were selected for the rest of this study with a view to extending the range of known polar-ordered compounds and to understand the mechanisms and properties responsible for the formation of guest polar-ordered crystal structures:



- 2,7-dimethylocta-3,5-diyne-2,7-diol (**1**)
- 1,2,4,5,7,8-hexaoxonanes (**2**)
- 1,3,5-trioxanes (**3, 4 and 5**)

The 1,2,4,5,7,8-hexaoxonanes and 1,3,5-trioxanes were chosen due to their relatively simple syntheses and the fact that they form different asymmetrical cavities, thus inducing polar-ordering of the guests. The syntheses, crystal structures and properties of these compounds will be discussed in the following chapters, along with calculations used to investigate the different factors involved in their formation of guest polar-ordered crystal structures.

# CHAPTER 4

## POLAR-ORDERED GUESTS IN 2,7-DIMETHYLOCTA-3,5-DIYNE-2,7-DIOL (1)

## 4.1 INTRODUCTION

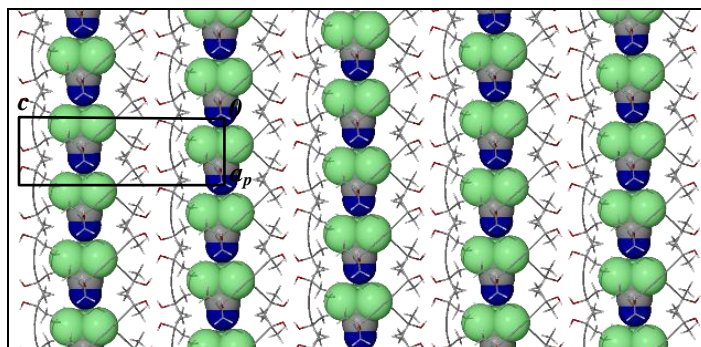


**Figure 4-1.** TCAN-included structure of **1** viewed along [010]. Only the guest is shown in space filled representation.

The polar ordering of the guests in inclusion complexes of **1** has sparked great interest,<sup>5</sup> and it was thus decided to further investigate the extent of this effect. The structure of **1** is held together by hydrogen bonded spirals (running parallel to the *c* axis), which bind the host molecules together in three dimensions: each host molecule can hydrogen bond to two spirals. The smaller nose of the polar molecule protrudes somewhat through the constrictions in the channel with the bulky tail resides in the wider regions. This allows the polar molecules to move closer to one another for stronger dipole-dipole electrostatic interactions, further stabilising the system and aligning the guests within a particular channel.

In order to explain why all the guest molecules assume the same orientation, the respective roles of the host-guest and guest-guest interactions within a channel, or through the wall of a channel, were investigated using DFT, MM and MD.

## 4.2 CRYSTAL STRUCTURES

To extend the range of known polar-ordered inclusion compounds of **1**, an array of crystallisations was carried out with the following solvents: CMP, BMP, IMP, THF, CF, BF, DCM and TCMS. Polar-ordered inclusion compounds were obtained with only three of these: CMP, BMP and IMP. They all formed needle-shaped crystals congruent with the previously obtained inclusion compounds of **1**. These three new inclusion compounds are polar ordered along the crystallographic *c* axis (see Figure 4-2) and assume a similar packing arrangement to the previously reported polar-ordered inclusion compounds of **1** (see Table 4-1).

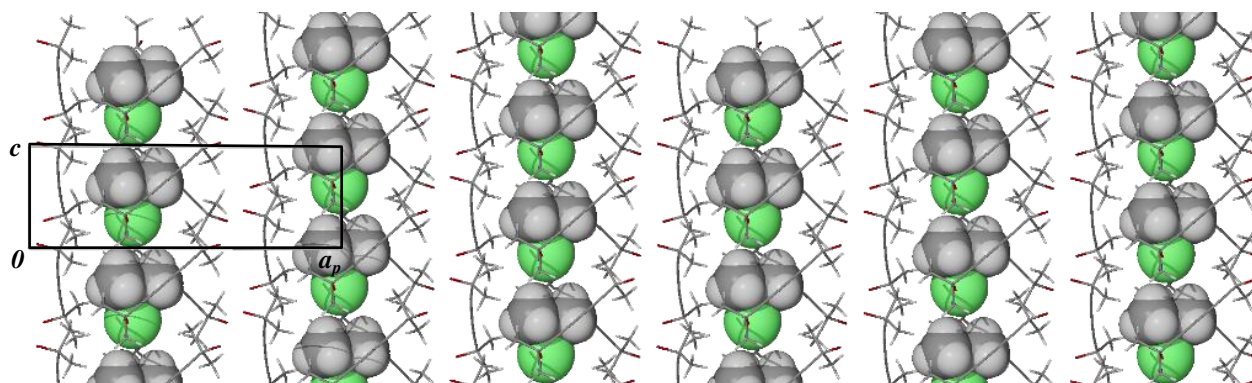


**Figure 4-2.** CMP-included crystal structure of **1** (compounds **1-4**). The BMP and IMP structures are isoskeletal to CMP.

**Table 4-1.** Unit cell parameters of **1-1** - **1-6**. (All the inclusion complexes crystallise in the space group R3)

Compound	$a$ (Å)	$b$ (Å)	$c$ (Å)	Volume (Å <sup>3</sup> )
<b>1-1</b>	22.398(6)	22.398(6)	6.222(2)	2703.1(1)
<b>1-2</b>	22.273(2)	22.273(2)	6.297(1)	2705.4(7)
<b>1-3</b>	22.432(2)	22.432(2)	6.235(1)	2716.9(6)
<b>1-4</b>	22.215(2)	22.215(2)	6.275(0)	2681.4(3)
<b>1-5</b>	22.174(2)	22.174(2)	6.301(1)	2686.5(3)
<b>1-6</b>	22.085(7)	22.085(7)	6.447(2)	2723.2(2)

#### 4.2.1 Through-channel interactions

It was noted that, for all the polar-ordered inclusion compounds of **1**, the six hydrogen bonded spirals around the cavities have two unique, but significantly different O $\cdots$ O distances that alternate around each column. This may have an affect on the polar inclusion of the guest during the crystal growth process, or it may be an artefact of the resulting structure.

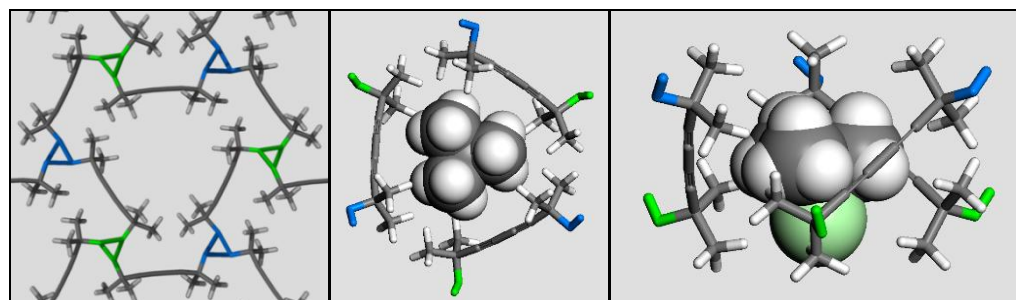


**Figure 4-3.** The two different hydroxyl groups, based on the O $\cdots$ O distances of the respective hydrogen bonded spirals.

The green hydrogen bonded spiral (GS) shown in Figure 4-3 has a shorter O···O hydrogen bond distance than the blue spiral (BS). This occurs in all the inclusion complexes of **1**. The O···O distances for all the polar-ordered inclusion complexes of **1** are given in Table 4-2, which also includes the percentage difference between the two different O···O distances, as well as the molecular volume of each guest. For comparison a guest-omitted structure was optimised over all the atomic positions using MM.

**Table 4-2.** O···O distances of the two unique hydrogen-bonded spirals of **1** for all six polar inclusion complexes. The percentage difference in O···O distance is calculated relative to the O···O distance of the optimised guest-omitted structure.

Guest	Blue spiral (BS), (Å)	Blue spiral % difference	Green spiral (GS), (Å)	Green spiral % difference	Guest molecular volume (Å <sup>3</sup> )
None, Optimised	2.802(2)		2.603(2)		
TCAN	2.741(3)	-2.18	2.660(3)	2.19	91
BTCM	2.737(4)	-2.32	2.651(4)	1.84	96
Cl-TMS	2.769(4)	-1.18	2.636(4)	1.27	101
IMP	2.766(3)	-1.28	2.642(3)	1.50	99
BMP	2.760(2)	-1.50	2.644(2)	1.58	95
CMP	2.754(2)	-1.71	2.645(2)	1.61	89

The optimised structure with guests omitted also has shorter (GS) and longer (BS) O···O distances, implying that the host is asymmetric even without the guest, and may be a possible cause for the polar alignment. The two types of H-bonded spiral would have two distinct dipole moments, thus resulting in a net dipole along the *c* axis. The greatest deviation from the guest-omitted structure was found for TCAN and BTCM, which contain electronegative chlorine atoms and could thus induce stronger electrostatic interactions than the other guests (Figure 4-4).

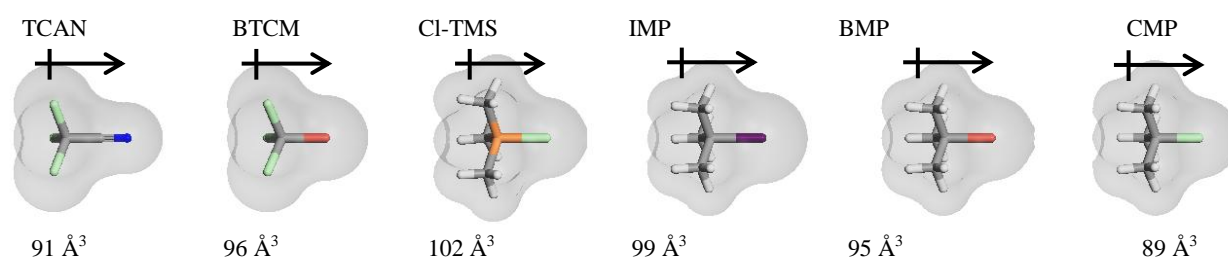


**Figure 4-4.** Space filled representation of all six polar guest molecules considered with their corresponding occupied molecular volume as determined by X-Seed.

Surprisingly, however, Cl-TMS has the largest molecular volume (Figure 4-4) and yet causes the least deformation of the cavity relative to the guest-omitted optimised structure. The chlorine atom in Cl-TMS is bonded to the central silicon atom, causing it to have a greater negative charge than the CMP chlorine, which is bonded to a carbon atom. It could thus simply be that Cl-TMS is a better fit for the cavity and that the host need not deform much to accommodate it.

The relationship between the structural distortions and the specific guest attributes is thus not entirely clear and warrants further investigation. To this end a series of MM calculations was carried out to determine the effect of the H-bond asymmetry on the alignment of the guests. Firstly, the asymmetry of the cavity was probed by investigating the potential experienced by the guest moving in opposite directions through the cavity (described in Section 4.3.1). The alignment of the guests within individual channels in the absence of surrounding host molecules was then studied in an attempt to explain the polar ordering through guest-guest interactions.

### 4.3 COMPUTATIONAL SECTION

#### 4.3.1 Potential energy profile of a guest moving inside the cavity of compound 1

Since the host-guest models involve substantially more atoms than those used for DFT calculations, molecular mechanics was used rather than DFT to reduce computation time. The model shown in Figure 4-5 was used to determine whether the cavities have an asymmetric energy profile along the polar *c* axis of the crystal. This may indicate whether or not the directionality of the guest is induced by the host, and at which stage this interaction would have to occur to induce the same alignment for all the guest molecules. It was decided to use TCAN to create a scenario as close as possible to the actual crystallisation process.

In the first calculation the guest was placed within the channel as shown in Figure 4-6(a) to determine the potential energy profile of the cavity when the guest can interact with the host in all three dimensions. All the host molecules (blue and green) are fixed whereas the guest is manually translated by increments of 0.1 Å as shown in Figure 4-6 and allowed to optimise its orientation at each point while fixing the carbon attached to the chlorine atoms. The second calculation addresses interactions involved in the interface between the (001) face of the crystal and a guest molecule in the mother liquor from which the crystal is grown.

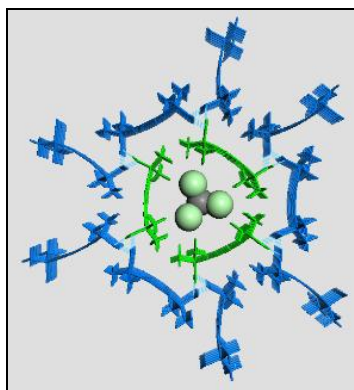


**Figure 4-5.** Model used to determine the potential energy profile of the cavities of **1**. The green molecules represent the channel within which the guest will move and the blue molecules are included to account for any long-range dispersive host-guest interactions that might be present.

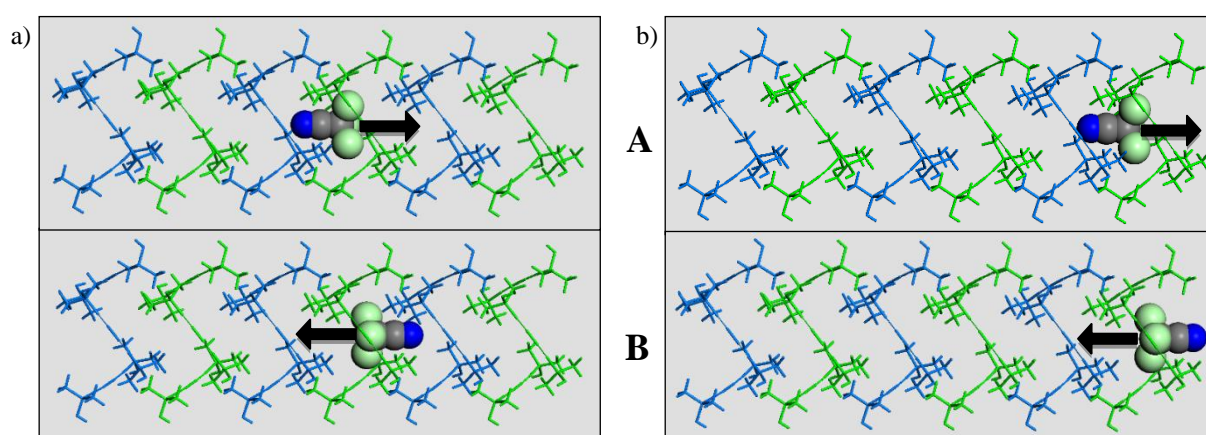


**Figure 4-6.** The cavities are alternatively coloured and, for the sake of clarity, only the central channel is shown. The TCAN guest is translated in the direction of the arrow. a) **Scenario 1**: guest trapped in the cavity within the bulk of the crystal. b) **Scenario 2**: guest trapped in the cavity at the surface of the crystal. **A** and **B** denote the two orientations of the guest in both scenarios (**A** - top, **B** - bottom).

From the energy plots for **Scenario 1** (Figure 4-7) we can see that the total potential energies for the two orientations are in good agreement, indicating a symmetrical energy profile of the cavity along the polar  $c$  axis. This means that a cavity within the bulk of the crystal cannot induce specific directionality of the guest along the  $c$  axis. The disparities in the electrostatic energy profile are quite small when considering the scale of the plot and they are compensated for by the slight differences in the vdW energies of the two orientations.



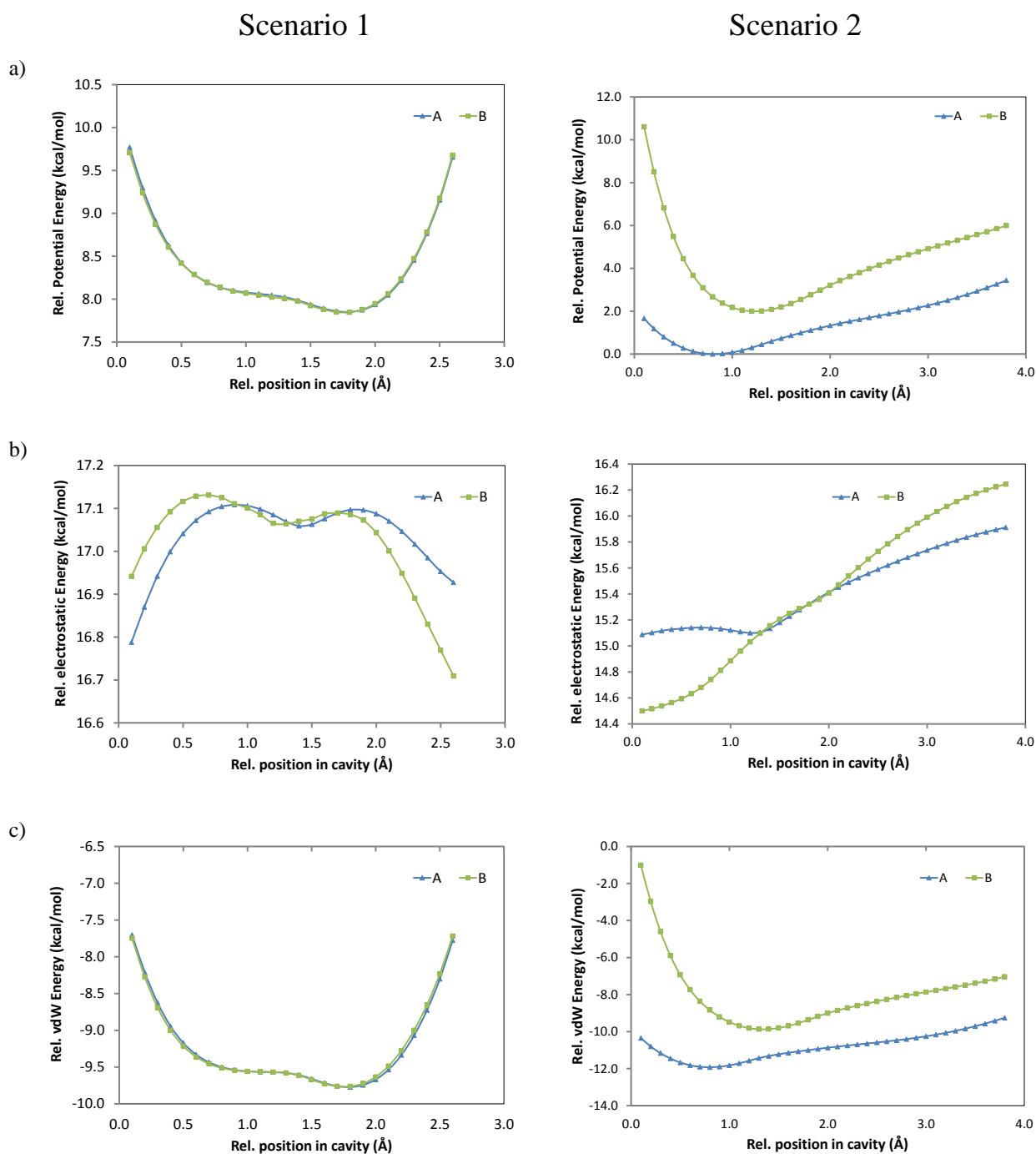


**Figure 4-7.** The two columns represent the energy profiles of the two scenarios as indicated by the headings. a) Total potential energy, b) electrostatic component of the total potential energy and c) vdW component of the total potential energy. The two series A and B represent the two orientations that were simulated. The bond, angle and torsion energies as well as the cross-term energies of the total potential energy are not shown here.

**Scenario 2** (Figure 4-7) yielded non-matching energy profiles for the two orientations, suggesting an asymmetric profile along the polar  $c$  axis. Upon closer inspection of the energy profiles it seems that **A** is relatively more stable throughout the cavity than **B** (2.1 kcal/mol more stable at the minimum positions). This could impose directionality on the guest as it enters the



cavity. It is also evident that the relative vdW energy contributes the most to the total potential energy throughout the cavity.

According to these results, polar alignment can only be imposed in the outer cavities, which should result in the formation of a bipolar crystal, which has two distinct domains with opposite polarity, if the crystal grows in both directions of the polar axis.<sup>38</sup> Since the crystals are polar there are two possibilities that could lead to this phenomenon: (i) the crystal grows from a polar seed which dictates the alignment for the rest of the crystal, (ii) the crystal grows in one direction, leading it to be polar ordered *via* the host-guest interactions (due to the asymmetric energy profile of outer cavities). The latter effect can also be regarded as surface recognition, whereby the orientation of a guest is dictated by its interaction with the surface of the crystal/material.<sup>33a</sup> It is possible that the interactions are so subtle that we cannot identify the mechanism with this model (i.e. the cavity appears symmetrical). A larger model with more guest molecules was considered in order to investigate the cumulative effect of the guest molecules on their alignment. This possibility will be discussed further in this chapter.

### 4.3.2 Intra-channel guest alignment

From the crystal structures, it is not difficult to comprehend why the guests within the same channel are aligned in the same direction. This alignment is due to the electrostatic dipole-dipole interactions between the polar guest molecules. The following molecular mechanics calculations were carried out to confirm these interactions and to determine their relative strengths by analysing the Boltzmann distribution (298.0 K) of the different conformations (relative orientations). Sufficient host molecules were included in the model to investigate the effect of the host on the intra-channel alignment of the guest molecules in **1**.

The MM model (see Figure 4-8) consists of a central channel filled with guest molecules, and empty surrounding channels. Two further models where the guest molecules at either end of the central channel (green) were flipped in the opposite orientation were also optimised, while the host molecules were kept in fixed positions. The relative energies and corresponding Boltzmann distributions of the three different models were calculated and are shown in Figure 4-9.

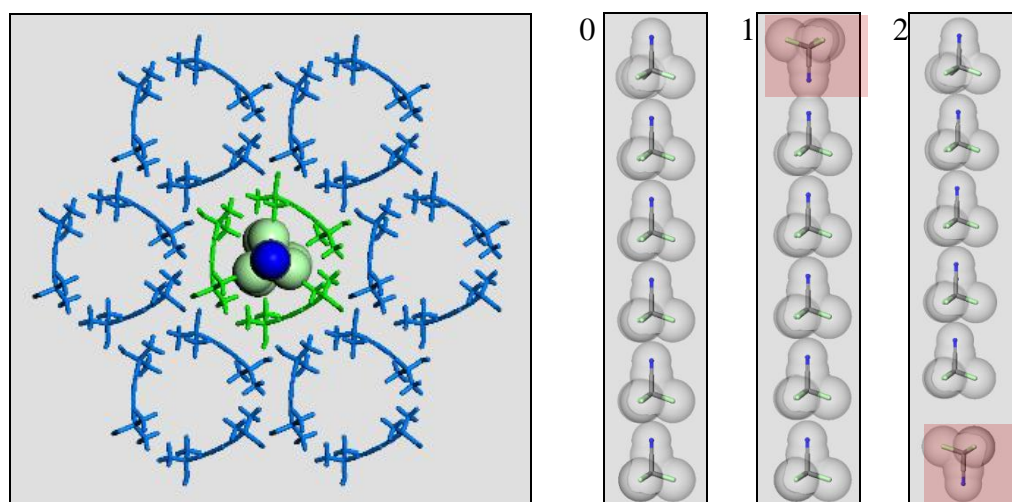


**Figure 4-8.** Molecular mechanics model for calculating the guest-guest interactions within a channel. The sections highlighted in red in **1** and **2** shows the deviations from **0** (all guests aligned in the same direction)

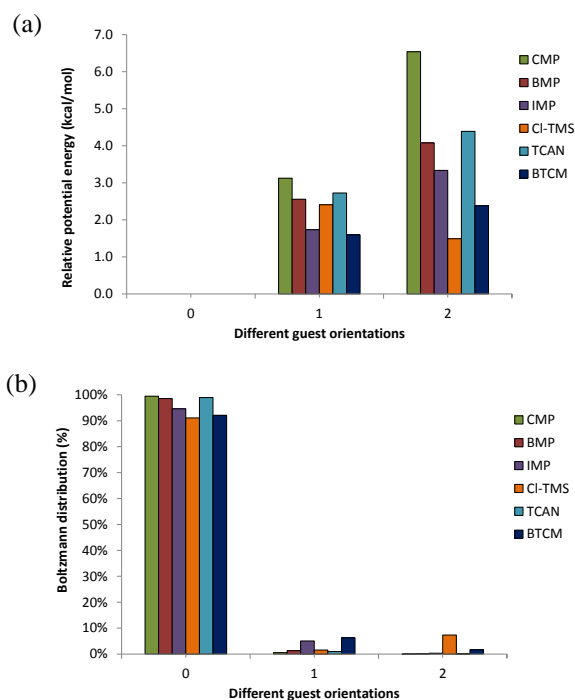


**Figure 4-9.** Boltzmann distribution for guest-guest interactions within a channel. (a) Relative potential energies relative to **0** (head-to-tail orientation). (b) Corresponding Boltzmann distribution calculated at 298.0 K.

The MM results show a percentage probability above 90% (according to the Boltzmann distribution at 298.0 K) for all six guest molecules, indicating that the head-to-tail alignment (**0**) is most favourable. The percentage Boltzmann distribution for the head-to-tail alignment decreases from CMP to Cl-TMS and from TCAN to BTCM (Figure 4-9(b)). This relates not only to the dipole moments of the guests, but also to their electrostatics. A larger dipole moment relates to a stronger dipole-dipole electrostatic interaction (for the head-to-tail alignment) between the guests, resulting in an increase in relative stability. The sizes and shapes of the

guest molecules could result in their being closer or further away from one another within a particular channel, causing differences in relative stabilisation for the different guest molecules. These results show two series, in which the major difference is between the bulky trimethyl (CMP, BMP, IMP and Cl-TMS) and trichloro (TCAN and BTCM) groups. Even though BTCM has the smallest dipole moment, its bulky trichloro moiety can increase electrostatic interactions with the host and guest molecules. These results are consistent with those described in Section 3.3.1.

### 4.3.3 Lateral guest alignment

Sections 4.2.1 and 4.3.1 above illustrate the use of one guest molecule might not be sufficient to identify the mechanisms involved in polar ordering of the guests. For further investigation, larger models were constructed and calculated using MM to establish whether the orientation of the guest molecules in one channel can be influenced by the orientation of guest molecules in the adjacent channels or by host-guest interactions (due to the slight asymmetric features of the host), or both.

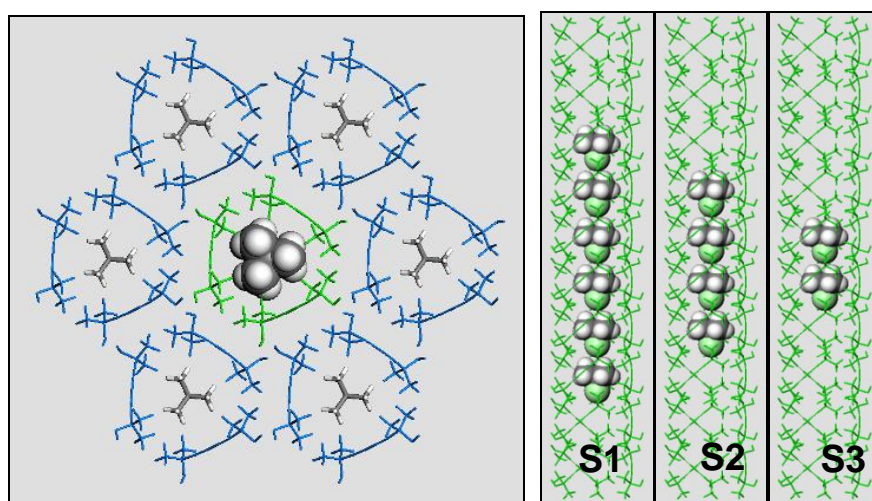


**Figure 4-10.** MM model used to investigate the polar alignment in inclusion complexes of **1**. **S1**, **S2** and **S3** represent the various simulations carried out within the central cavity.

The MM simulation shown in Figure 4-10 was carried out in two parts: one with guest molecules included in the surrounding blue channels (**GAC** – host-guest plus host-mediated guest-guest interactions) and the other with empty blue channels (**EAC** – host-guest interactions). For each part the guest in the central channel was flipped between two orientations (**A** – denotes the crystal structure orientation of the guests and **B** the opposite orientation) and their positions were allowed to optimise while the remainder of the model was fixed. The potential energies were calculated relative to **B**. All six polar guests (CMP, BMP, IMP, Cl-TMS,

TCAN and BTCM) were employed in these calculations and their relative energies were compared.

It was first investigated whether an increase in the number of guest molecules would have a cumulative effect on the energy, which would illustrate whether the model can be extrapolated to more guest molecules. The average percentage relative stabilisation was calculated for **S1**, **S2** and **S3** (6, 4 and 2 guest molecules, see Figure 4-10) for both simulations, i.e. with and without the guest molecules in the surrounding channels. If the models were correctly chosen the percentage relative stabilisation energy of **S1**, **S2** and **S3** should be consistent for both simulations despite the number of guest molecules used.

**Table 4-3.** Percentage relative stabilisation of **S1**, **S2** and **S3** for all guests considered. A negative percentage is in favour of **A** (guest orientation in crystal structure) since the  $\Delta E$  values were calculated relative to **B**.

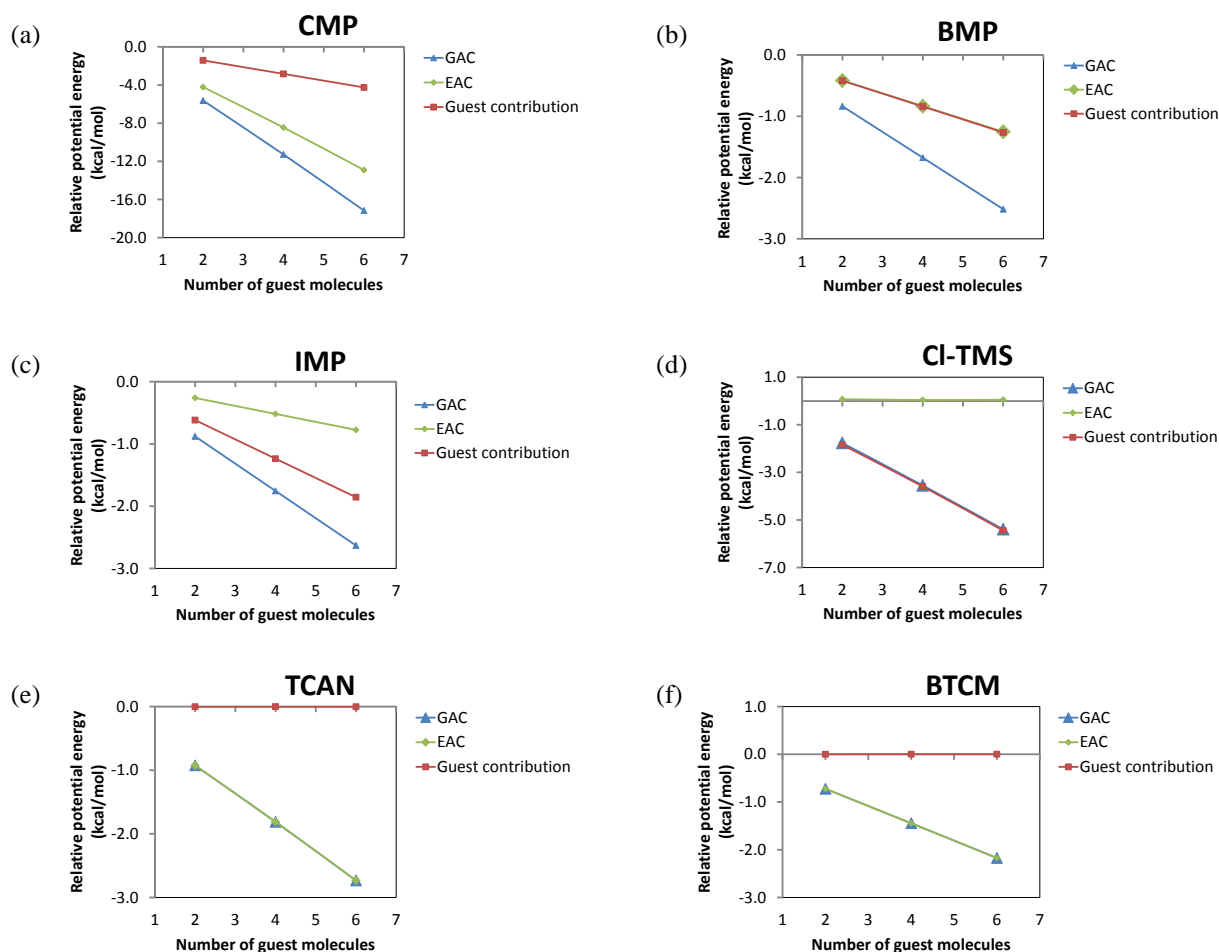
Guest filled adjacent channels (%) (GAC)						
	CMP	BMP	IMP	Cl-TMS	TCAN	BTCM
<b>6</b>	-3.98	-1.230	-0.781	-1.59	-1.94	-3.18
<b>4</b>	-3.94	-1.225	-0.777	-1.58	-1.94	-3.19
<b>2</b>	-3.95	-1.223	-0.776	-1.60	-1.94	-3.23
<b>Average</b>	-3.96	-1.226	-0.778	-1.59	-1.941	-3.20
<b>STDEV</b>	0.02	0.003	0.002	0.01	0.002	0.02

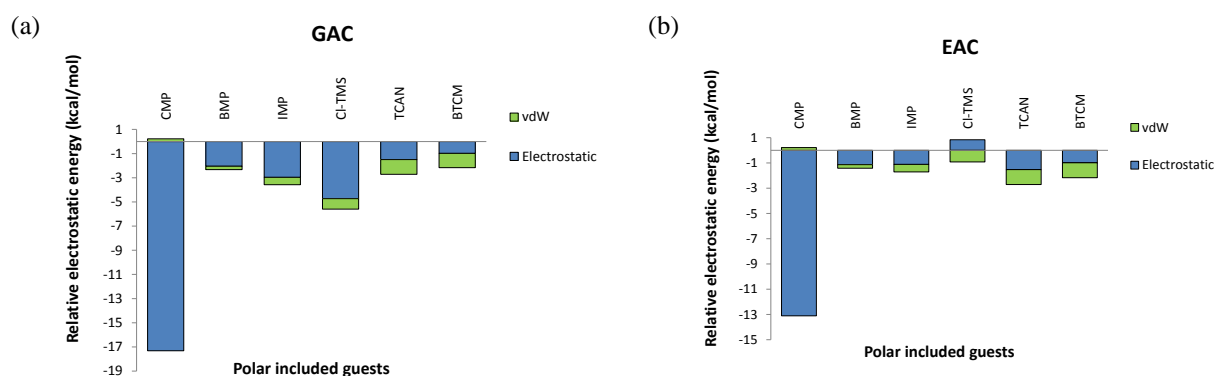
Empty adjacent channels (%) (EAC)						
	CMP	BMP	IMP	Cl-TMS	TCAN	BTCM
<b>6</b>	-3.00	-0.307	-0.233	0.07	-1.95	-3.20
<b>4</b>	-2.95	-0.306	-0.230	0.07	-1.95	-3.20
<b>2</b>	-2.96	-0.305	-0.229	0.05	-1.94	-3.25
<b>Average</b>	-2.97	0.306	-0.230	0.06	-1.947	-3.22
<b>STDEV</b>	0.02	0.001	0.002	0.01	0.003	0.02

Table 4-3 illustrates the consistency (standard deviation of < 0.02%) of both the **GAC** and **EAC** models, irrespective of the number of guest molecules used in the central channel. This shows that the model can be extrapolated to contain more guest molecules with correspondingly larger relative energies, which otherwise would have been too small for sensible analysis. The potential energy components, electrostatic and vdW, were analysed to determine which contributes the most towards the polar alignment of the guest molecules. It is important to notice that the relative energies of all the guests used are negative (in favour of **A**) except for Cl-TMS

**EAC**. However, the stabilisation energy of **Cl-TMS EAC** is negligible ( $< 0.15$  kcal/mol). This implies that both the host and guest favour the polar-ordered model (**A**).



**Figure 4-11.** Potential energy of **A** relative to **B** (**A** - congruent with crystal structure; and **B**  $180^\circ$  relative to crystal structure) obtained from the MM calculations based on the model in **Figure 4-10** for all guests studied. Negative values indicate that orientation **A** is more stable than **B**. The guest contribution was calculated as the difference between **GAC** and **EAC**.



**Figure 4-12.** Relative vdW and electrostatic energies for the 6-guest-molecule model relative to orientation **B** (negative values indicate that **A** is favoured). a) With guests in surrounding channels. b) Absence of surrounding guests.

The stabilisation of **A** relative to **B** decreases significantly from **CMP** to **BMP** and **IMP** for both **GAC** and **EAC** models (see **Figure 4-11** (a), (b) and (c)) as a result of greater electrostatic

interactions. The stronger interactions with CMP can be ascribed to CMP's large dipole-moment and the smaller size of chlorine the atom, which allows for a better fit of the chlorine atom in the channel constriction. Relative to the host-guest interactions (**EAC**) the guest contribution is smaller for CMP, similar for BMP and stronger for IMP. This implies that in the polar alignment of CMP the host plays the most important role, while in BMP the host and surrounding guest molecules have equal contributions and in IMP the host-mediated guest-guest interactions are more important than the host-guest interactions.

For Cl-TMS the relative potential energy plot (Figure 4-11(d)) shows that the host-guest stabilisation is the same for both orientations of the guests (**EAC**). However, the **GAC** plot (Figure 4-11(d)) shows stabilisation in favour of **A**, indicating that only host mediated guest-guest interactions are important in the alignment of Cl-TMS since it is unaffected by the host (**EAC** plot). From Figure 4-12 the **GAC** bar for Cl-TMS shows that the electrostatic energy is the main contributor to the stabilisation between guest molecules in adjacent channels. Even though Section 3.3.2 showed no interactions at this channel distance (12.381 Å) in the absence of the host, this model illustrates that host-mediated guest-guest interactions are significant enough to stabilise and drive the polar alignment of guest molecules (especially Cl-TMS).

TCAN and BTCM produce similar **GAC** and **EAC** relative potential energy values for all models (Figure 4-11 (e) and (f)). In addition, the vdW and electrostatic components are also equivalent for both **GAC** and **EAC** (Figure 4-12). This means that the guest molecules in the surrounding channels do not contribute towards the stabilisation of the alignment of the guests in the central channel, thus suggesting that TCAN and BTCM are only stabilised by host-guest interactions. The vdW stabilisation can be ascribed to the asymmetry in the shape of the cavity, while the electrostatic stabilisation could be due to the resulting net dipole (along the *c* axis) induced by the asymmetric features of the host. These results show that TCAN and BTCM are only affected by the slight asymmetric features of the host.

#### 4.4 SUMMARY

In addition to the three guest polar-ordered inclusion complexes of **1** already known (TCAN, BTCM and Cl-TMS clathrates), three further polar-ordered inclusion complexes (CMP, BMP and IMP) have been identified in this study.

The O...O hydrogen bond distances in the two unique H-bonded hydroxyl spirals holding the crystal together are distinctly different, which leads to asymmetry along the polar *c* axis. The deviations are relatively small but are consistent for all crystal structures. Furthermore, the two



types of H-bonded spirals could also result in a net dipole along the *c* axis, thus inducing the alignment of the guest molecules.

The potential energy changes that occur as a guest is moved through the cavity of **1** appear to be the same, independently of the orientation of the guest molecule. It was further shown that polar alignment only occurs at the growth interface between the (001) face of the crystal and the mother liquor from which it is grown. If a crystal grows in both directions along *c*, the asymmetry of a cavity at the two growth interfaces ((001) and (00-1)) would be in opposite directions, thus producing a crystal with two opposite polar domains (i.e. a bipolar crystal). For this model to work the crystal would have to grow in only one direction to achieve polar ordering.

It was also shown that the intra-channel alignment of the guest is largely driven by dipole-dipole electrostatic interactions between guest molecules within a particular channel. The calculated Boltzmann distributions showed that the parallel alignment is favoured by over 90% in the presence of the host. This illustrates that a guest molecule entering a channel can easily adopt the orientation of the other guests within that particular channel.

Larger MM simulations indicated that for CMP, BMP and IMP both the hosts and the guests in the surrounding channels contribute to the overall polar alignment of the system. This means that these guests will align in the correct orientation in the absence of the surrounding guests, but will be further stabilised by their presence. The importance of the host-guest interactions decreases from CMP to BMP to IMP, which could be a result of the decreasing electronegativity of the halogens in the same order.

Cl-TMS only interacts with the surrounding guest molecules, indicating that its alignment will be set by the seed crystal *via* host-mediated guest-guest interactions. The major contributor to the potential energy for Cl-TMS, CMP, BMP and IMP is the electrostatic component due to interactions with the hydroxyl spirals and/or the guest molecules in neighbouring channels.

The polar alignment of TCAN and BTCM is only dictated by host-guest interactions. This means that the slight asymmetric features of the host cavity are enough to induce these guests to align accordingly. They both experience equal amounts of electrostatic and vdW stabilisation where the electrostatic stabilisation is due to interactions with the hydroxyl spirals and the vdW stabilisation to steric interferences caused by the asymmetric cavity.

With the aid of DFT and MM simulations the polar-ordering of inclusion complex **1** has been explained, and the important interactions identified. These simulations predict polar-ordering for all the guests used in this study, even though different mechanisms according to

which they can be grouped are involved. It has also been shown that similar guests follow the same mechanisms and interactions to form guest polar-ordered inclusion structures.



# **CHAPTER 5**

## **POLAR-ORDERED GUESTS IN 1,2,4,5,7,8-HEXAOXONANES**

## 5.1 INTRODUCTION

1,2,4,5,7,8-Hexaoxonanes (cyclic nine-membered triperoxides) have various applications, such as in the thermolytic synthesis of macrocyclic ketones and lactones, also known as the Story reaction.<sup>71</sup> Certain low-molecular weight triperoxides (e.g. acetone derivatives) are also employed in polymer synthesis as initiators in free radical polymerisation reactions.<sup>72</sup> Triperoxides have also been found to be of interest in the design of antimalarial drugs and have shown high antimalarial activity.<sup>73</sup> The greatest area of interest regarding triperoxides is the synthesis and detection of triperoxide-based explosives, which are very sensitive and yield an explosive power rivalling that of trinitrotoluene.<sup>74</sup> For this reason, synthesis of 1,2,4,5,7,8-Hexaoxonanes should be carried out with extreme caution.<sup>39, 75</sup>

Terent'ev *et al.*<sup>39</sup> have synthesised and characterised a series of triperoxides. However, their cyclohexanone derivative (1,4,7-cyclohexane-1,2,4,5,7,8-hexaoxonane - **2**) is of particular interest because it forms a guest polar-ordered inclusion complex with chloroform. The crystal structure shows that the polar-ordered chloroform is trapped in the cavities and aligned along the crystallographic *c* axis. As mentioned in Chapter 3, this triperoxide was the only structure in the CSD with this property, with the article merely reporting the structure of the host-guest inclusion complex with CF (**2-1**: refcode - LIRREK) and not mentioning the polar-ordering of the guest molecules.

In addition to confirming the formation of the polar-ordered chloroform inclusion complex, other possible inclusion complexes, as well as other 1,2,4,5,7,8-hexaoxonane derivatives were also investigated. However, the investigation into other 1,2,4,5,7,8-hexaoxonane derivatives (cyclohexyl and cyclopentyl derivatives) was unsuccessful. In this chapter we describe the crystal structure of **2** with a number of guests (Section 5.2), as well as DFT, MM and MD (MQD) calculations that were used to suggest a mechanism for the polar-ordering of these crystals (Section 5.3). It was hoped that this would shed some light on the requirements for this family of molecules (1,2,4,5,7,8-hexaoxonanes) to form polar-ordered inclusion complexes.

## 5.2 1,4,7-CYCLOHEXANE-1,2,4,5,7,8-HEXAOXONANE (**2**)

Compound **2** was crystallised from solutions of various polar solvents in an attempt to form new polar-ordered inclusion complexes. Since **2** is poorly soluble in most solvents only those in Table 5-1 were used.

---

**Table 5-1.** Crystallisations with 1,4,7-cyclohexane-1,2,4,5,7,8-hexaoxonane (**2**) and various polar solvents:

Solvent	Inclusion	Polar-ordered	Space Group
CF	Yes	Yes	<i>R3c</i>
BF	Yes	Yes	<i>R3c</i>
CHI <sub>3</sub> /Toluene	No	No	<i>Pbca</i>
Benzene	Yes	No	<i>P1̄</i>
ACN	No	No	<i>Pbca</i>
BTCM	No	No	<i>Pbca</i>
CMP	?	-	-
BMP	?	-	-
IMP	?	-	-

Compound **2** only formed inclusion complexes with CF, BF and benzene. ACN and BTCM did not include within the host structure, which formed the close-packed polymorph instead. The last three solvents listed in Table 5-1 did not produce crystals of sufficient quality for single-crystal analysis, but they instead formed precipitates or very small crystals. In some cases benzene (a ratio of 1:10 benzene:polar solvent) was used in mixtures with the bottom five solvents (Table 5-1) for crystallisation. The unit cell parameters of crystals obtained from these mixtures indicated that they were the same as those of the benzene included structure. Crystals of sufficient quality for single-crystal analysis were isolated from CF, BF and benzene solutions.

### 5.2.1 Crystal structures

Table 5-2 contains the unit cell parameters of inclusion complexes of **2** with CF, BF and benzene. The chloroform included structure agrees with that published by Terent'ev *et al.*, confirming the polar-ordering of CF. The crystal structures of **2-1** and **2-2** are isoskeletal (the only difference being that the chlorine atoms are replaced by bromine atoms at similar positions). As expected, **2-3** crystallises in a non-polar space group since it has benzene as a guest. As such, **2-3** will not be discussed in this work. The close-packed structure (**2**) reported in the literature by Denekamp *et al.* (refcode - QQQEDD01)<sup>76</sup> is also included in Table 5-2 for comparison. Since

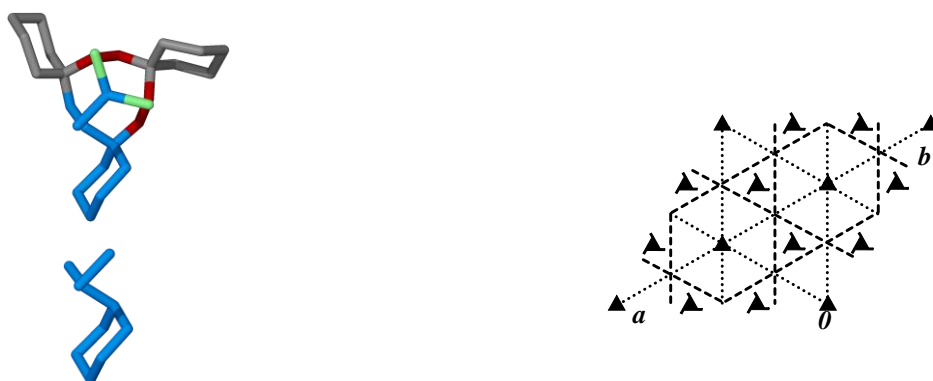
**2-1** and **2-2** are isostructural, only **2-1** will be discussed further.

**Table 5-2.** Unit cell parameters of **2** to **2-3**.

Compound	Space group	$a$ (Å)	$b$ (Å)	$c$ (Å)	$\alpha$ (°)	$\beta$ (°)	$\gamma$ (°)	Volume (Å <sup>3</sup> )
<b>2</b>	<i>Pbca</i>	11.739(1)	9.940(1)	31.993(1)	90	90	90	3733 (3)
<b>2-1</b>	<i>R3c</i>	14.203(2)	14.203(2)	18.219(1)	90	90	120	3182.5(7)
<b>2-2</b>	<i>R3c</i>	14.448(6)	14.448(6)	18.428(8)	90	90	120	3331(2)
<b>2-3</b>	<i>P</i> $\bar{1}$	10.002(2)	10.535(2)	10.906(1)	76.72(1)	88.21(1)	81.54(1)	1105.58(18)

### 5.2.2 (1,4,7-Cyclohexane-1,2,4,5,7,8-hexaoxonane)·CHCl<sub>3</sub>

(a)



(b)

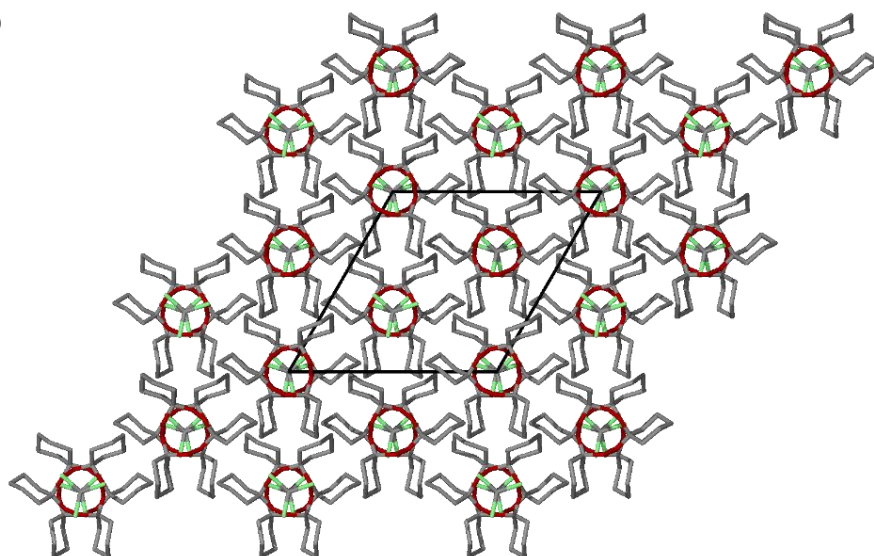


**Figure 5-1.** (a) A single molecule of **2** and CF with the asymmetric unit highlighted in blue. (b) **2-1** viewed down the crystallographic  $c$  axis. The hydrogen atoms have been omitted for clarity.

The asymmetric unit consists of a third of each of the host and guest molecules in the trigonal polar space group *R3c*. The rest of the molecules are generated by 3-fold axes passing through

the centres of the molecules (Figure 5-1 (a)). The packing is generated *via*  $3_1$  screw axes parallel to the  $c$  axis (Figure 5-1 (b)).

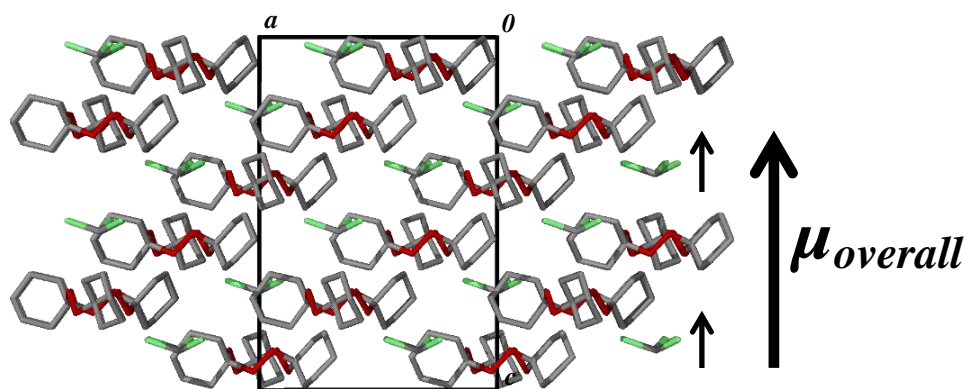


**Figure 5-2.** Inclusion complex **2-1** viewed down the crystallographic  $b$ -axis. The arrows indicate the alignment of the chloroform molecules (along the crystallographic  $c$  axis) and overall dipole moment vector.

Viewing the structure down the  $b$  axis shows the alignment of the guest molecules which are undoubtedly polar ordered along the  $c$  axis, indicated by the arrows in Figure 5-2. To investigate the structural properties more carefully, a single cavity was constructed to better identify any structural features that could influence the packing and alignment of the guest molecules.

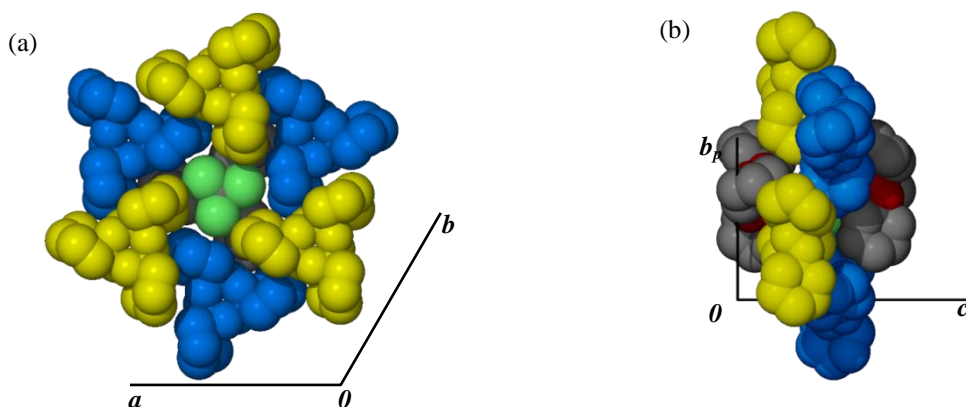


**Figure 5-3.** Space filled representation of a single cavity of **2-1**. (a) View down (001). (b) View down (100). The two different host orientations, with respect to the cavity, are shown in blue and yellow. The hydrogen atoms have been omitted for clarity.

From Figure 5-3 it is clear that the side wall is comprised of two layers that are orientated differently with respect to the cavity or guest. The cyclohexane groups of the blue molecules are orientated with their open faces toward the cavity, while for the yellow molecules the cyclohexane groups point towards the cavity causing a slight constriction. From Figure 5-3(b) we see that the cavity is asymmetric along the  $c$  axis, since its side wall consists of both blue and yellow host molecules. This packing feature probably leads to the polar-ordering of CF along the  $c$  axis.

### 5.3 COMPUTATIONAL SECTION

#### 5.3.1 Potential energy profile of a guest moving inside the cavity of compound **2**

It appears from the crystal structures that the cavities of **2** are asymmetric along the polar  $c$  axis. To confirm this, molecular mechanics calculations performed with the Forcite Plus module of Materials Studio using the cvff force field were employed to determine the energy profile of a guest moving through a cavity (CF was chosen to mimic the crystal structure as closely as possible). With a fairly short perpendicular distance of 8.2 Å between two cavities, and close contact distances of 5.04 Å between the guests in neighbouring cavities (see Table 3-2), guest-guest interactions cannot be ruled out and have to be included in the calculations as described in (Section 3.3.2). In addition, the calculations were carried out in the presence and absence of the surrounding guest molecules to establish whether they influence the alignment of the central guest.

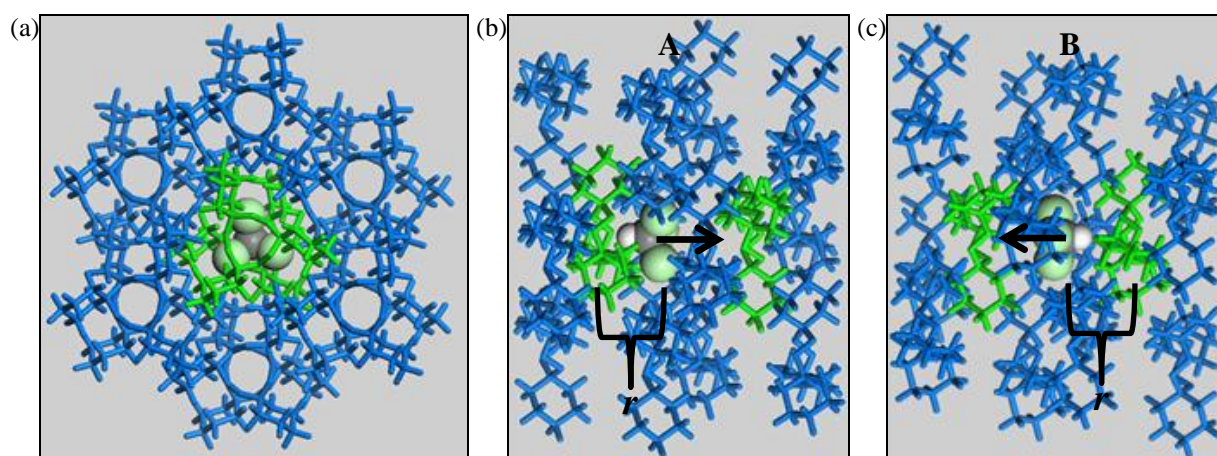


**Figure 5-4.** (a) Model used to determine the potential energy profile of CF moving in a cavity of **2**. The blue molecules form the side wall of the cavity with the green molecules on the ends. (b) Simulation **A** with CF orientation opposite to that in the crystal structure. (c) Simulation **B** with CF orientation the same as in the crystal structure; CF is translated in the direction of the arrows.  $r$  is the distance from the chlorine atoms to the peroxide ring (green host molecules).

The model consists of a single cavity with a wide spread of surrounding host molecules to account for any long range interactions that might be present. The green host molecules in the centre have their peroxide rings exposed to the cavity while the cyclohexane groups of the blue host molecules form the side walls of the cavity. Simulations **A** and **B** assume opposite CF orientations, with **B** congruent with the CF direction in the crystal structure. The starting positions were chosen in order to obtain enough data points on both sides of the minima, but data points were excluded where excessive bond and angle deformations of the guest were found. The guest was translated in the directions of the arrows (Figure 5-4 (b) and (c)) along the  $c$  axis in increments of 0.1 Å and allowed to optimise at each point. For a cavity to be

symmetrical the same potential energy scan should be obtained, regardless of the guest orientation. The two data sets (A and B) were overlaid by matching the CF-peroxide ring (green host molecules) distance ( $r$ ), measured as indicated in Figure 5-4 (b) and (c).

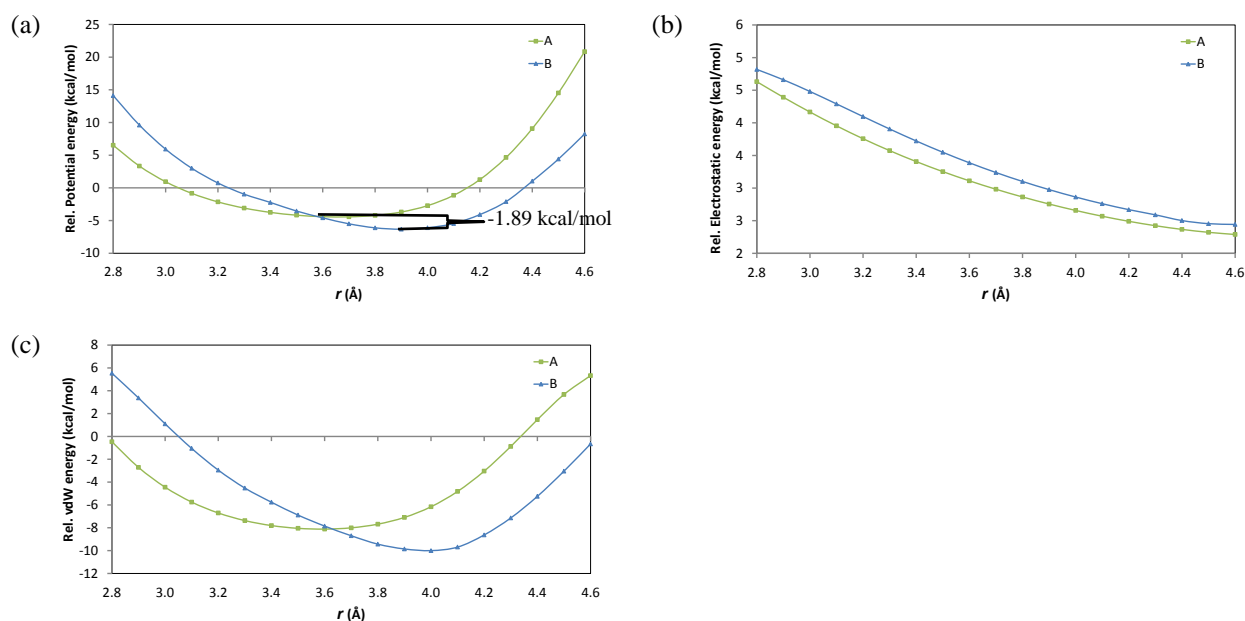


**Figure 5-5.** (a) Total relative potential energy plot. (b) Electrostatic energy component of the total potential energy. (c) vdW energy component of the total potential energy.  $r$  is the distance from the chlorine atoms to the peroxide ring as shown in **Figure 5-4**.

According to the molecular mechanics calculations, simulation **B** corresponds to the more stable conformation at 1.89 kcal/mol (see Figure 5-5). The 4.6 Å mark coincides with the centre of the cavity along the  $c$  axis (decreasing values of  $r$  move CF closer to the peroxide rings). This means that CF, in **A** and **B**, is positioned closer to one side of the cavity (with its  $\delta^+$  side facing towards the peroxide ring). In **A** (3.6 Å) the minimum energy conformation of CF is much closer to the peroxide ring than for **B** (4.0 Å), resulting in the minimum in **B** being more stable than that of **A**. This is as a result of the asymmetric features of the side wall of the cavity (Figure 5-3).

In order to obtain more accurate values for the relative energies, we performed DFT calculations for the minima of the two simulations. The structures of the global minima obtained from the MM results for **A** and **B** were optimised and the energy calculated at the MPW1PW91/6-311++(d,p) level of theory. Only the molecules necessary to construct the cavity were used in these calculations in order to minimise calculation time while still achieving sensible results.

**Table 5-3.** DFT energies with calculated Boltzmann distribution.

Energy (Hartree)	Energy (kcal/mol)	Relative energy (kcal/mol)	Boltzmann distribution (%)
------------------	-------------------	----------------------------	----------------------------



A	-2574.15762	-1615308	2.905369	0.73
B	-2574.16225	-1615311	0	99.27

According to the results shown in Table 5-3, **B** is 2.9 kcal/mol more stable than **A**; thus if a polar molecule such as CF is trapped in a cavity of **2**, it has a 99.3% probability of aligning in accordance with **B** which is the orientation confirmed by single-crystal X-ray diffraction. This is therefore further evidence that the orientation of the guest in the cavity found in the crystal structure is energetically favoured.

### 5.3.2 Molecular mechanics simulations of guest orientation changes within the cavity

It was established in Section 5.3.1 that the side wall of the cavity can induce directionality in the guest molecules. What therefore still remains is to describe a suitable mechanism for the polar ordering of **2-1**. To investigate this, the model in Figure 5-6 was constructed with the aim of simulating the behaviour of a guest molecule as it approaches the cavity from either side of the polar *c* axis, along *+c* and *-c*.

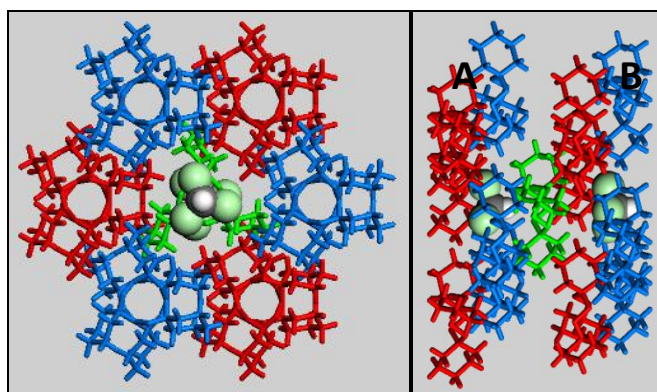


**Figure 5-6.** Open cavity model used to investigate the polar ordering. Red – host with cyclohexane group pointing towards the inside of the cavity. Blue – host with cyclohexane groups facing the cavity. Green - faces its peroxide ring towards the cavity. The calculation was divided into two: sides **A** and **B** as indicated and calculated one guest at a time.

The orientation of the guest in the crystal structure is defined as  $0^\circ$ ; the opposite orientation as  $180^\circ$ . The guest molecule orientations on sides **A** and **B** (Figure 5-6) were changed between  $0^\circ$  and  $180^\circ$  and optimised in each state while the host positions were kept fixed. The Boltzmann distribution (298.0 K) was calculated for both scenarios to determine the preferred orientations, while the potential energy was partitioned into its components and compared to determine the driving force responsible for the observed alignment in the crystal structure.



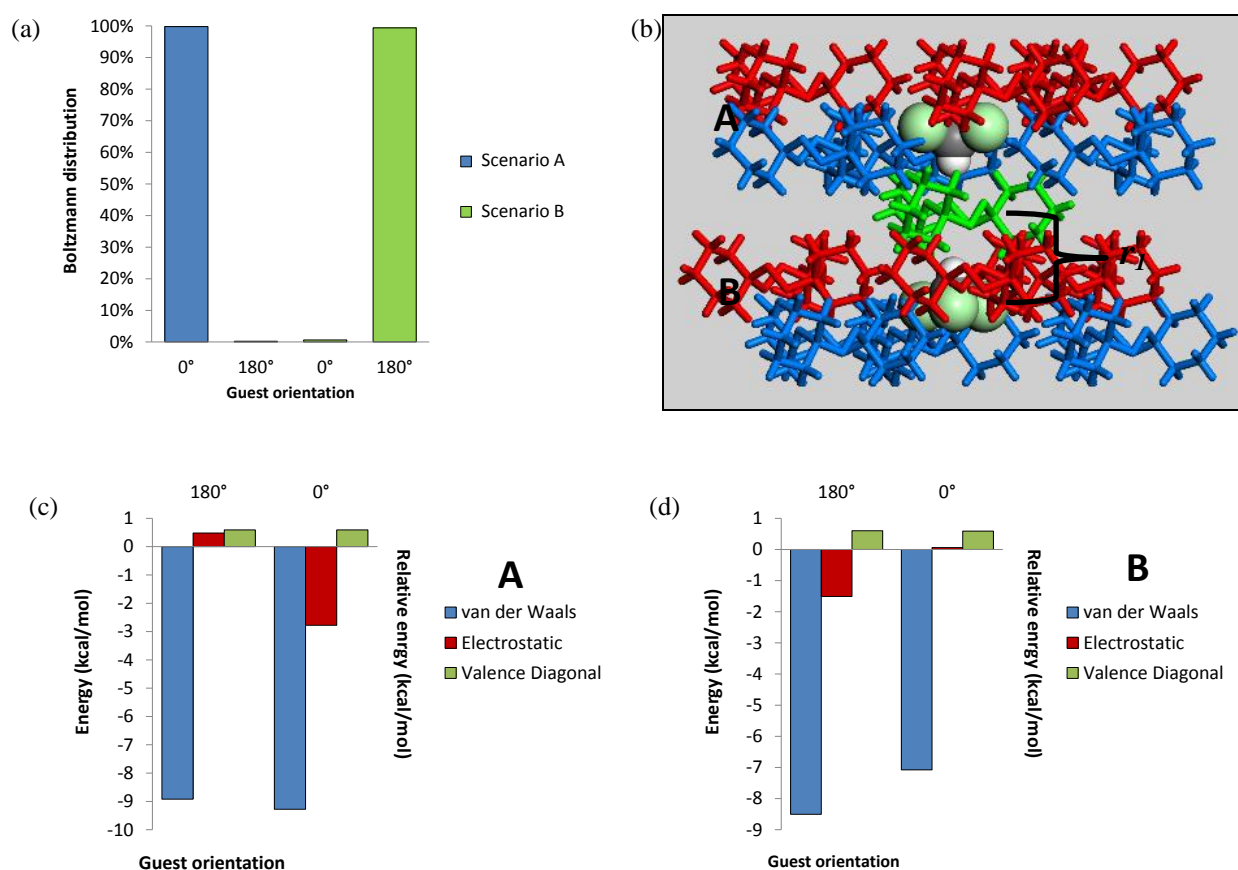


**Figure 5-7.** Results from the molecular mechanics calculations of the model in **Figure 5-6**. (a) Boltzmann distribution calculated at 298.0 K. (b) Scenario produced by simulation results. (c) **A**: total potential energy divided into its components. (d) **B**: total potential energy divided into its components. 0° denotes the orientation that is congruent with the crystal structure and 180° the opposite orientation.

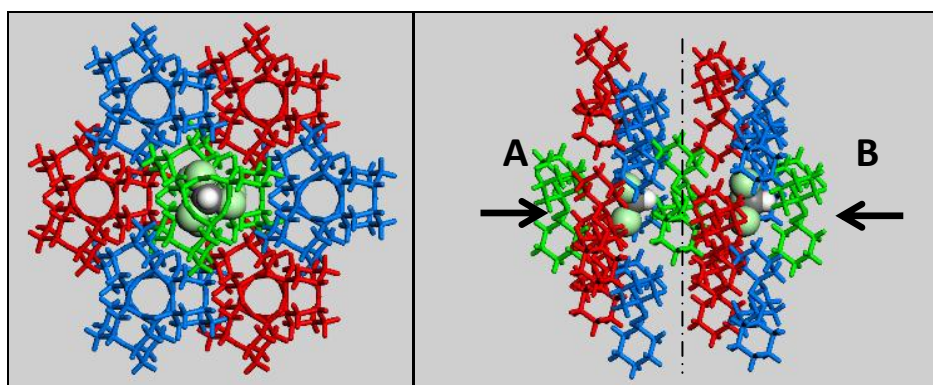
It is clear from Figure 5-6 that the side wall of the cavity is asymmetric along the *c* axis and can induce alignment in one direction; however this is not what is found from the molecular mechanics results. As seen in Figure 5-7 the guest on side **A** is orientated such that it is consistent with the crystal structure, while on side **B** it has the opposite orientation. From the components comprising the potential energy, it can be seen that the alignment for both models is driven largely by the electrostatic interactions. The electrostatic stabilisation of the 0° conformation in **A** and 180° conformation in **B** (Figure 5-7(d)) results from the dipole-dipole interactions of CF with the peroxide ring of the green host molecules. This is made clear by the loss of the electrostatic interaction when CF is inverted (**A** (0° to 180°) and **B** (180° to 0°)) as shown in Figure 5-7(c) and (d). There is also a loss of vdW stabilisation (dispersive interactions with the surrounding host molecules) on both sides (**A** and **B**). The larger difference in vdW stabilisation between the 0° and 180° conformations of CF in **B**, compared to those of **A**, results from the 0°-CF having to move ca. 0.4 Å towards the outside of the cavity relative to 180°-CF, due to special requirements. This results in the loss of vdW interactions.

Figure 5-7(b) shows the outcome of these simulations, illustrating that the outward growth of the crystal from the initial host “seed” would involve alignment of the CF molecules in the  $0^\circ$  conformation on the one side, and the  $180^\circ$  conformation on the other side, resulting in two polar domains (i.e. the crystal should be bipolar).<sup>37, 77</sup> The crystals that were used for SCD analysis were not cut and would have resulted in the guest molecules appearing to be disordered over the  $0^\circ$  and  $180^\circ$  conformations if the crystal had consisted of opposite polar domains. The fact that this is not the case implies that there is another factor playing a role in the orientation of the guests. Hence it was decided to perform molecular quench dynamics simulations, which are described in the next section.

### 5.3.3 Molecular quench dynamics simulations

The MQD simulations were run at 298.0 K to assess the behaviour of the guest in the cavity during the encapsulation process. A 0.5 ns quench dynamics calculation at  $298.0 \pm 2$  K (see The Smart algorithm is a cascade of the steepest descent, ABNR (Adjusted basis set Newton-Raphson), and quasi-Newton methods.

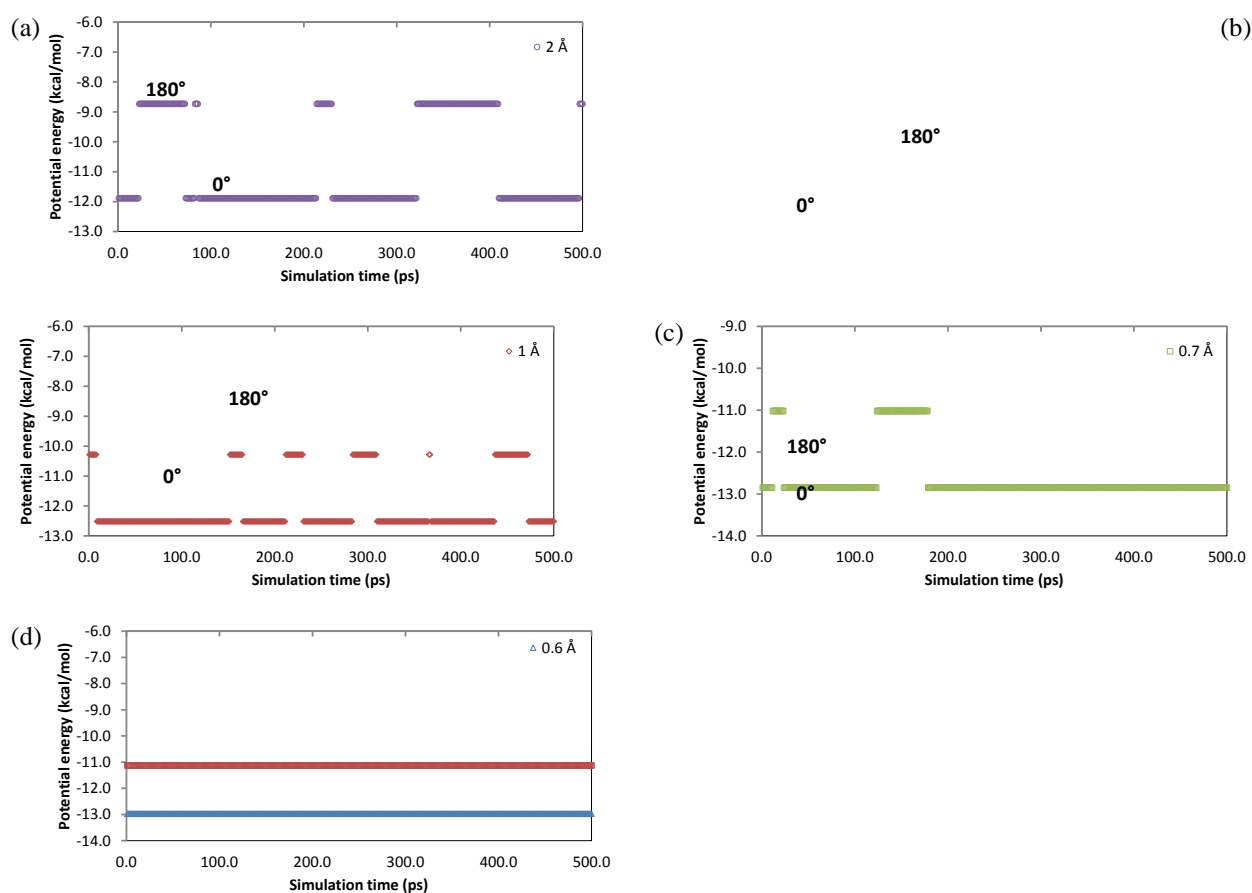
Table 2-2 for MQD parameters) was performed using the model in Figure 5-8. This could indicate whether the guest can change orientation after being confined in the cavity (assuming the  $0^\circ$  conformation) and if not, at what stage during the encapsulation process the alignment occurs. MQD calculations were used to search the conformational space of a system to find all possible conformation of CF within the model used (see Figure 5-8). Producing all the conformations from the same model allows for better comparison and more accurate Boltzmann probability distribution statistics.



**Figure 5-8.** Left - closed cavity model used to determine polarity formation as viewed along an axis coinciding with the crystallographic *c* axis. Right – The simulation was divided into sides, **A** and **B** divided by the line dotted line. The green molecules on either end were translated in the direction of the arrows from an offset of 2 Å. Red – host with cyclohexane group pointing towards the inside of the cavity. Blue – host with cyclohexane groups facing the cavity. Green - faces its peroxide ring towards the cavity.

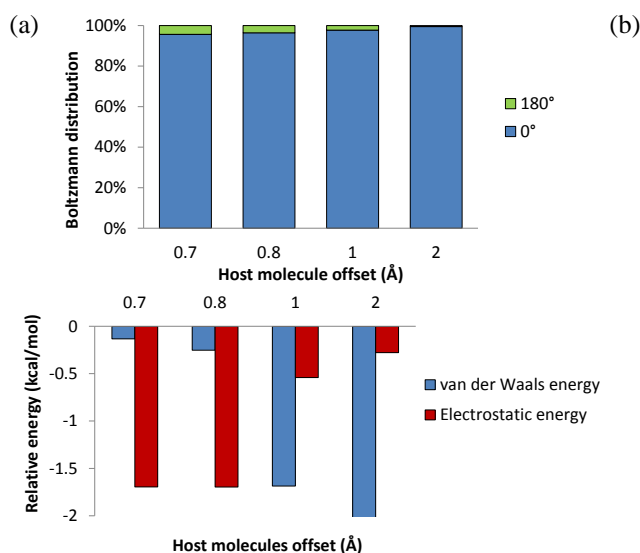
All the atomic positions in the model were fixed with the exception of the two CF molecules being studied in the respective simulations (**A** and **B**). Calculations for each side, **A** and **B**, were carried out separately to simplify the interpretation of the resulting data. In both simulations (**A** and **B**) the outer green host molecules were manually translated from an offset of 2 Å from the crystal structure position in the direction of the arrows to a 0.5 Å offset; 0.5, 0.6, 0.7, 0.8, 0.9, 1.0 and 2 Å offsets were used for the simulation of both sides. During simulation **A**, the green host molecule on side **B** was kept fixed, while during simulation **B** the green host molecule on side **A** was fixed. This kept the two simulations separate but still within the same model. The quench dynamics simulation involved the CF molecule being studied receiving an initial velocity, allowing it to move around the cavity dynamically. The model was then optimised at set intervals (every 1 ps for 500 ps) during the dynamics simulation in an effort to find all the possible minimum energy conformations.

Figure 5-9 (a), (b) and (c) show that both conformations can occur at offsets between 2.0 – 0.7 Å; however, the 0° conformation is favoured over the 180° conformation at these host offsets. The difference in energies between the 0° and 180° conformations decreases from 2.0 to 0.7 Å (3.2, 2.2 and 1.8 kcal/mol). By 0.6 Å the guest can no longer change its orientation, yielding only one conformation, which depends on the guest conformation (0° or 180°) attained just prior to 0.6 Å. Figure 5-9 (d) shows the results for both conformations, which were calculated separately, and indicates that the orientation at the start of the simulation is maintained throughout. Thus, even though the 0° conformation is clearly 2.0 kcal/mol lower in energy at this offset, CF in the 180° conformation is unable to reorient to the more favourable 0° conformation (Figure 5-9(d)). At distances greater than 0.6 Å the guest is able to reorient to the preferred 0° conformation, which it maintains as it moves closer to its final position in the crystal, due to steric and electrostatic reasons, as seen in Figure 5-10.



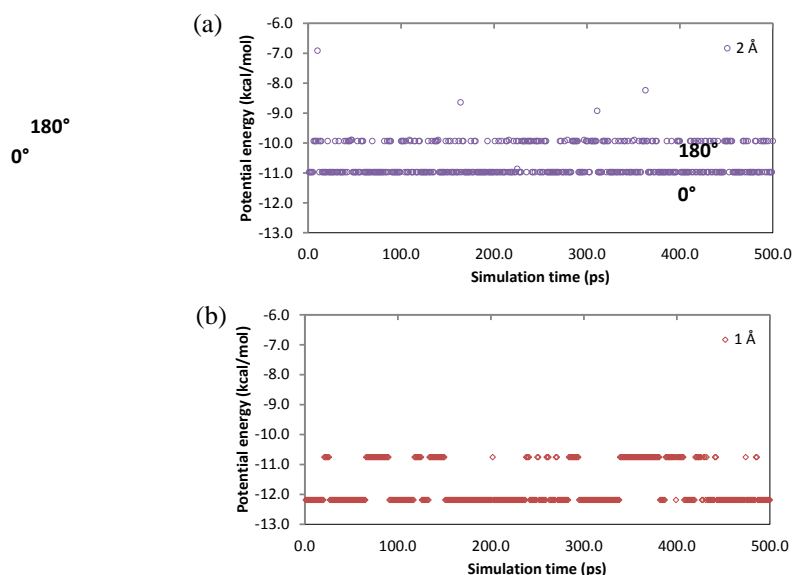
**Figure 5-9.** Potential energy output produced by the MQD calculations for side A at different offset distances: (a) 2.0 Å, (b) 1.0 Å, (c) 0.7 Å, (d) 0.6 Å. Orientations of the conformations are indicated on each chart. **The two data sets in the 0.6 Å plot were obtained from two separate MQD calculations.**

The Boltzmann distributions in Figure 5-10(a) confirm the preference for the  $0^\circ$  conformation with percentage probabilities above 95% throughout the simulation. Figure 5-10b shows that the electrostatic energy stabilises the  $0^\circ$  conformation from a host offset of 0.8 Å and lower. However, from a host offset above 0.8 Å it is stabilised by the vdW energy (dispersive interactions). The electrostatic stabilisation could imply that the dipole-dipole interaction (stabilising) between the guest and the peroxide rings is stronger in the  $0^\circ$  than the  $180^\circ$  conformation. At larger host offsets (greater than 0.8 Å), the guest in the  $0^\circ$  conformation sits ca. 0.4 Å deeper into cavity than the guest in the  $180^\circ$  conformation. Since the guest in the  $180^\circ$  conformation sits further away from the bulk of the model (greater than 0.8 Å), it experiences a slight loss of host-guest dispersive interactions with the surrounding molecules compared to the  $0^\circ$  conformation.



**Figure 5-10.** Boltzmann distribution at 298.0 K and relative electrostatic and vdW constituents of the potential energy (relative to the 0° conformation: negative values are in favour of the 0° conformation) generated by the quench dynamics simulations. 0° conformation is consistent with guest orientation as found in the crystal structure.

Simulation **B** yields results analogous to **A**, thus indicating that the 0° conformation is the preferred conformation and thus the orientation the guest will assume before reaching an offset of 0.6 Å, after which it is unable to alter its orientation (as seen in simulation **A**). However, the difference in energies between the 0° and 180° conformations increases from 2.0 to 0.7 Å (1.0, 1.4 and 1.9 kcal/mol) compared to simulation **A** where the relative difference in energy decreases.



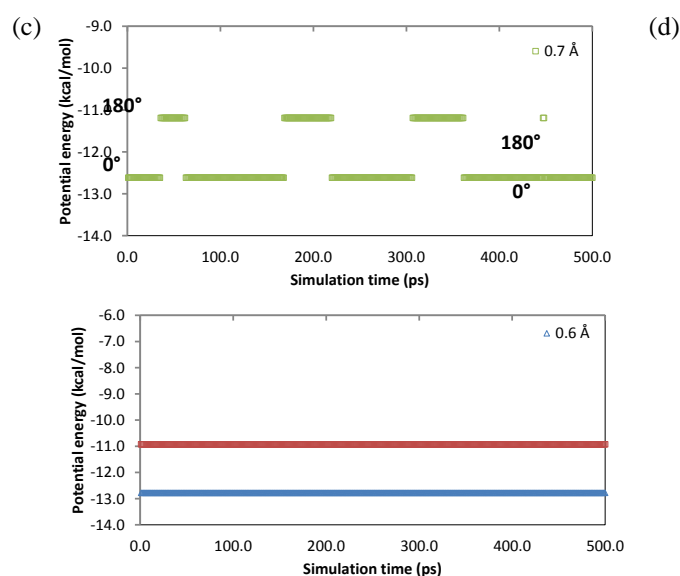


**Figure 5-11.** Potential energy output produced by the MQD calculations for side **B** at different offset distances: (a) 2.0 Å, (b) 1.0 Å, (c) 0.7 Å, (d) 0.6 Å. Orientations of the conformations are indicated on each chart. **The two data sets in the 0.6 Å plot were obtained from two separate MQD calculations.**

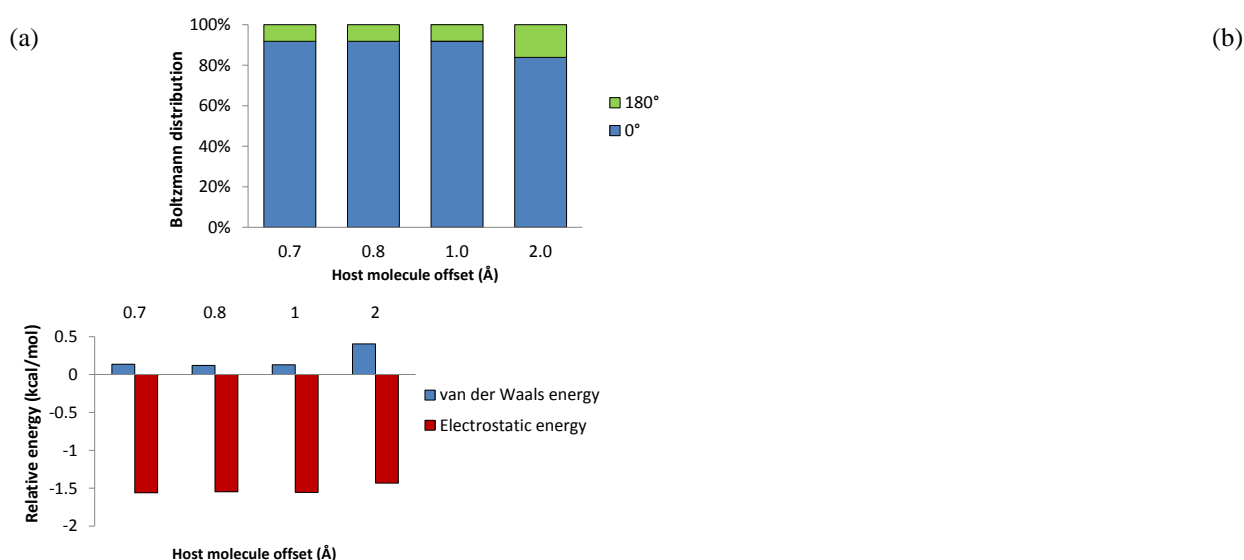


**Figure 5-12.** (a) Boltzmann distribution at 298.0 K. (b) The relative electrostatic and vdW components of the total potential energy (relative to the 0° conformation: negative values are in favour of the 0° conformation). The 0° conformation is consistent with guest orientation as found in the crystal structure.

The Boltzmann distributions shown in Figure 5-12(a) confirm the preference for the 0° conformation by more than 90% when the host offset is less than 1.0 Å. Figure 5-12b shows that the electrostatic energy stabilises the 0° conformation throughout the simulation. Even though the 0° conformation suffers a slight loss of vdW stabilisation (host-guest dispersive interactions), it compensates for the loss with the electrostatic interactions (a stabilising dipole-dipole interaction with the peroxide rings). The guest in the 180° conformation sits closer to the peroxide ring than the optimum position and is destabilised as a result. This effect could be a result of the steric influence of the asymmetric cavity side wall (see Section 5.2.1) which drives

the guest to one side of the cavity, thus positioning the Cl atoms closer to the peroxide rings, and increasing the repulsive Cl···O electrostatic interactions.

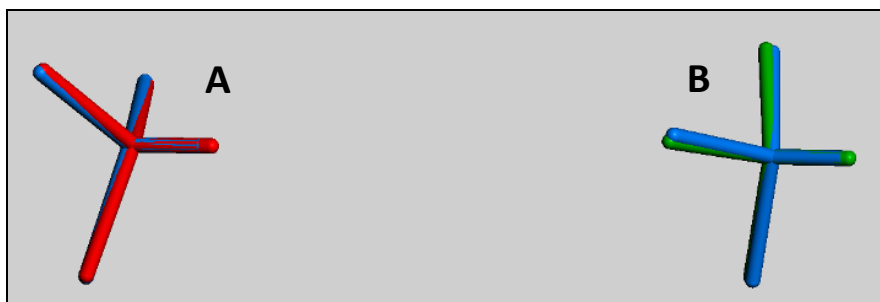


**Figure 5-13.** Overlay of the simulated CF positions at the 0.0 Å host offset of both models (**A** and **B**) on the CF position in crystal structure. The blue molecules represent the crystal structure positions, red - simulation **A** and green - simulation **B**.

From the overlay of the calculated CF orientations with the experimental one shown in Figure 5-13 it is clear that the calculated and crystal structure positions of the CF molecules compare very well, with only a slight inconsistency in the chlorine atoms positions. This illustrates that the MQD model used here was adequate for the modelling of the guest orientations in both simulations **A** and **B**, since we can accurately determine the guest position and orientation.

If the guest molecule in both **A** and **B** assumes the 0° conformation at a 0.7 Å host offset it is highly probable that it will be trapped in that orientation and unable to change its orientation. Contrary to the MM simulations, these simulations (MQD) predict a guest polar-ordered crystal. It also suggests that the orientation of the guest in **2** is as a result of the crystal growth mechanism.

## 5.4 SUMMARY

We synthesised the triperoxide **2** and produced two polar-ordered crystal structures of which one is novel (**2-2**) and the other (**2-1**) has been reported in the literature. Both inclusion complexes crystallised in the polar space group  $R3c$  with the polar axis along the crystallographic  $c$  axis.

The potential energy profile of CF moving along the  $c$  axis inside a cavity of compound **2** yielded an asymmetric energy profile, implying that the cavity has a structure-directing property. The minimum energy conformations of the two orientations (0° and 180°) were compared and yielded an energy difference of 1.89 kcal/mol in favour of the 0° conformation. Recalculation of the minima using DFT yielded a relative potential energy of 2.91 kcal/mol in favour of the 0° conformation. This corresponds to the 0° conformation being favoured with 99.3% probability at 298.0 K according to the Boltzmann distribution.

MM simulations suggested the formation of a bipolar crystal (crystal with two opposite polar domains), along the crystallographic *c* axis, with the guests in sides **A** and **B** assuming the 0° and 180° conformations, respectively. However, crystals used for structure determination were not cut and yielded the structure with CF polar ordered along the *c* axis, suggesting that a bipolar crystal is not possible, and thus invalidating the simulation (a bipolar crystal would result in the disorder of the CF guests across the two orientations).

By means of MQD simulations we investigated the orientation of the guest just prior to encapsulation by searching the conformational space of the model used. The simulation was divided into two parts, **A** and **B**, which refer to the two unique sides of the model along the *c* axis (the polar axis). Both simulations (**A** and **B**) yielded 0° as the preferred orientation, which agrees with the orientation of the guest found in the crystal structure. Analysis of the components of the total potential energy suggests that the driving force behind the polar-ordering of this system is mainly electrostatic interactions between the guest and the peroxide ring caused by the slight steric influence of the asymmetric side wall of the cavity, which affects the position of the guests relative to the peroxide rings, thus influencing the electrostatic repulsion between the guest molecules (mainly the chlorine atoms) and the peroxide rings. The 0° conformation experiences less electrostatic repulsion than the 180° conformation, which causes it to be more stable, and thus the preferred guest alignment for guest polar-ordered inclusion complexes of **2**.



# CHAPTER 6

## POLAR-ORDERED GUEST MOLECULES IN 1,3,5-TRIOXANES

## 6.1 INTRODUCTION

1,3,5-trioxanes are commonly used compounds owing to their versatility. They are used in stabilising solutions employed in colour photography, as burning regulators in fumigants, and also for the separation of aldehydes from ketones that have similar boiling points.<sup>78</sup> Although these versatile compounds have been investigated extensively, no reference is made in the literature to the polar-ordering behaviour of trioxanes. The structures of thirteen 1,3,5-trioxane structures have been deposited in the CSD, and only three of them are polar ordered: 1,3,5-trioxane, and the cyclohexyl and endolongifolyl 1,3,5-trioxane derivatives. The 2,4,6-(endolongifolyl)-1,3,5-trioxane·CDCl<sub>3</sub> (**3-1**) inclusion complex reported by Dimitrov *et al.* (CSD refcode - MUTYAB) is of particular interest since its host and guest molecules are both polar ordered (in the same direction).<sup>40</sup> The paper by Dimitrov *et al.* merely reports the structure of the host-guest inclusion complex (**3-1**) and does not mention the polar-ordering of the complex.

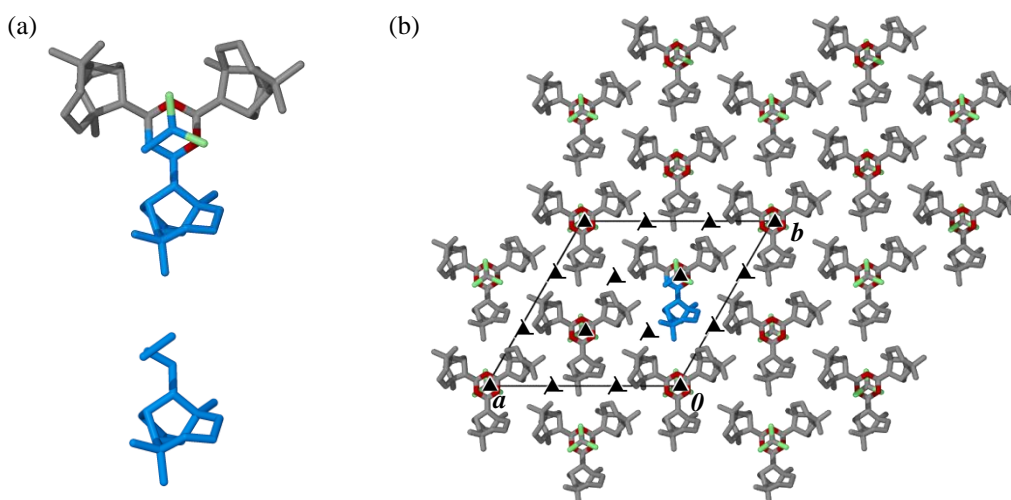
## 6.2 CRYSTAL STRUCTURES

The 1,3,5-trioxanes **4**, **5** and **6** were the only compounds successfully synthesised, however, they did not form inclusion complexes with solvents used (**3-1** requires a very intricate synthesis process). In the cases of **4** and **5**, crystals of sufficiently high quality were obtained by recrystallisation from chloroform (or toluene). However, no suitable crystals could be obtained for **6**. Using SCD to determine the structures, **4** and **5** were found to pack in a very similar manner. Unit cell data of **3-1**, **4** and **5** are reported in Table 6-1.

**Table 6-1.** Unit cell parameters of **3-1**, **4** and **5**.

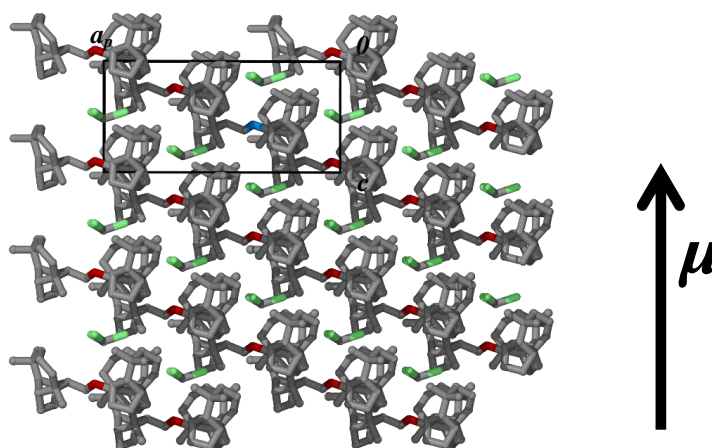
Compound	Space group	<i>a</i> (Å)	<i>b</i> (Å)	<i>c</i> (Å)	Volume (Å <sup>3</sup> )
<b>3-1</b>	<i>R</i> 3	21.063(1)	21.06 (1)	8.56 (1)	3290(2)
<b>4</b>	<i>P</i> 6 <sub>3</sub> <i>cm</i>	11.84(1)	11.84(1)	8.00(1)	969.7(1)
<b>5</b>	<i>P</i> 6 <sub>3</sub>	11.57(1)	11.57(1)	7.85(1)	909.9(1)

As shown in Table 6-1, three compounds crystallised in polar space groups. Even though **4** and **5** did not include any solvent, they produce polar crystals. We will only discuss the crystal structures of **3-1** and **4** since the crystal structure of **5** is similar to that of **4** along all projections.

6.2.1 2,4,6-(endolongifolyl)-1,3,5-trioxane·CDCl<sub>3</sub> (3-1)

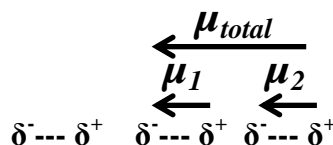
**Figure 6-1.** (a) A molecule of the host-guest complex **3-1** with the asymmetric unit shown in blue below. (b) The packing diagram of **3-1** viewed down [001]. The hydrogen atoms were omitted for clarity.

**3-1** crystallises in the polar space group *R3* with three molecules in the unit cell. The 1:1 host-guest compound is located on a crystallographic threefold axis (Figure 6-1 (a)). This results in the asymmetric unit containing one third each of the host and guest molecules. The molecules stack in columns parallel to the *c* axis.

Polar-ordering of 2,4,6-(endolongifolyl)-1,3,5-trioxane·CDCl<sub>3</sub> (3-1)

**Figure 6-2.** Polar-ordered host-guest packing arrangement of **3-1** viewed along [100].  $\mu$  is the dipole moment vector as indicated by the arrow. The hydrogen atoms are omitted for clarity.

The guest CF molecules are arranged in a polar fashion along the *c* axis and are located in the cavities formed by the host molecules. Both the host and guest molecules are aligned parallel to the *c* axis. The resulting polar-ordered structure has a net dipole which coincides with the *c* axis, as shown in Figure 6-2.



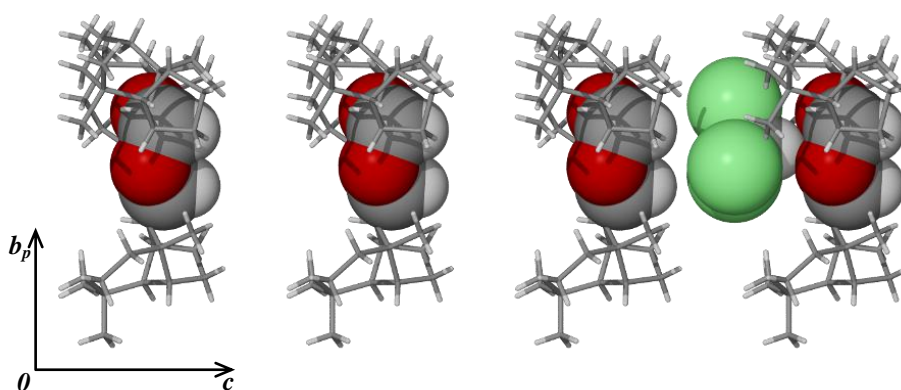


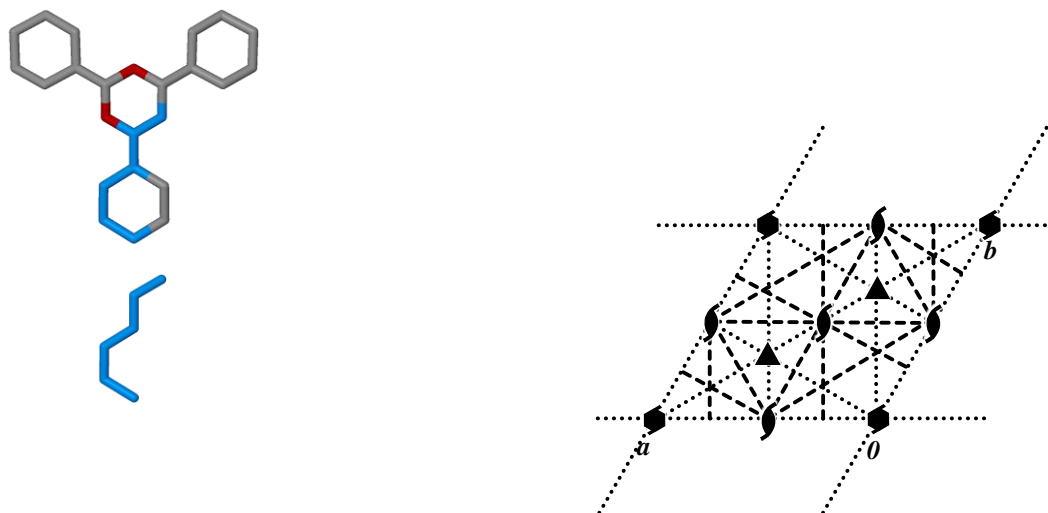
**Figure 6-3.** Compound **3-1** viewed along [100] (the trioxane ring and CF guest molecules are rendered in space fill). Partial charges are indicated in the diagram.<sup>40</sup>  $\mu_1$  and  $\mu_2$  indicate the dipole moment vectors of the host and guest, respectively ( $\mu_{\text{total}} = \mu_1 + \mu_2$ ).

As a result of the bulky endolongifolyl R groups, the trioxane rings of **3-1** are much further apart as compared to those of **4**. The increased distance between the host molecules leads to the loss of the weak C—H...O hydrogen bond interactions that are commonly observed in structures where the host molecules are more closely packed. The separation of the host molecules also allows for the inclusion of CF (Figure 6-3). The dipole moment vectors of the host ( $\mu_1$ ) and guest ( $\mu_2$ ) molecules act in concert, resulting in a larger dipole moment vector ( $\mu_{\text{total}}$ ) per complex unit.

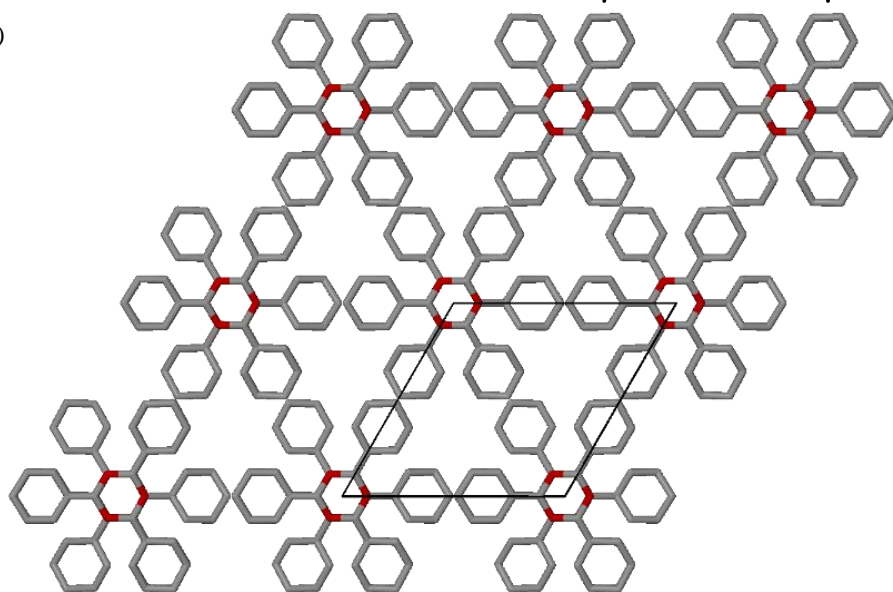
### 6.2.2 2,4,6-(cyclohexane)-1,3,5-trioxane (**4**)

**4** crystallises in the polar space group  $P6_3cm$  with two molecules in the unit cell. The asymmetric unit contains one sixth of a molecule while the rest of the molecule is generated by  $3m$  symmetry (Figure 6-4(a)). The molecules propagate by means of a  $6_3$ -screw operation along  $c$ . **4** packs in such a way that it forms layers that stack parallel to the  $b$  axis. **5** has a very similar packing arrangement with very similar crystal morphology.

(a)

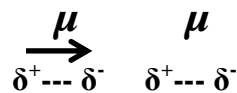


(b)



**Figure 6-4.** (a) A single molecule of **4** with the asymmetric unit highlighted in blue (below). (b) Packing arrangement of **4** viewed down [001] in space filled representation.

The molecules are linked by weak C—H...O hydrogen bonds along the [001] direction as shown in Figure 6-5(b). The weak C—H...O interactions may enable preferential crystal growth along [001]. This is supported by the needle-like morphology of the crystals of **4**, and was confirmed by face indexing of the crystals. The dipole moment vectors of the host molecules (indicated by the arrows in Figure 6-5(b)) also propagate along the *c* axis, and this is indicative of the polar ordering of the host molecules.



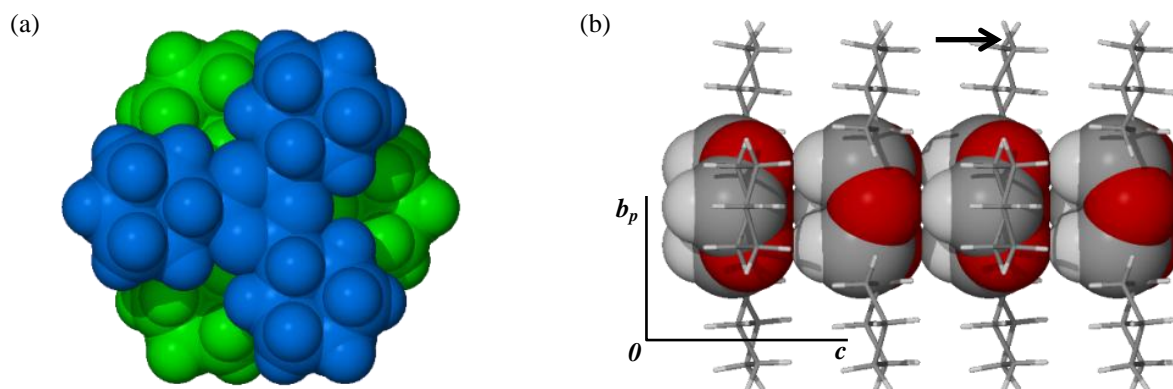


**Figure 6-5.** (a) Space filled representation of two host molecules (blue and green) of **4** viewed down [001]. b) View of **4** along [100] (the trioxane ring is rendered in space fill).  $\mu$  indicates the dipole moment vectors of the host molecules.

### 6.2.3 Brief summary

Both **3-1** (where both the host and guest are aligned in the same direction) and **4** (consisting of only the host) are polar ordered. The structural properties observed in **3-1** and **4** were investigated further using computational methods (MM, MD and MQD simulations) in order to gain insight into the mechanisms involved in inclusion and polarity formation of the 1,3,5-trioxanes. These calculations are described in Section 6.3.

## 6.3 MOLECULAR MODELLING OF 1,3,5-TRIOXANES

Using MM and MQD simulations we have attempted to establish why compound **3-1** can include a small guest such as CF and cause all other guests to align in the same direction, as compared to compound **4** which does not include a guest. We examined the structural deformation caused by the presence and/or absence of the guest and weighed it against the relative stabilisation in both cases, as an indication of whether the host would include the guest. The relative potential energy surface profile (see Sections 4.3.1 and 5.3.1) was determined for a CF molecule translated along the crystallographic  $c$  axis within the cavity of **3-1** from one side to the other. This tells us whether the cavity has guest-directing capabilities, making polar-ordered inclusion possible. Other MM and MQD calculations will be used to determine the stage of the crystal growth process at which the guest assumes the correct orientation as determined by SCD. This could shed some light on the crystal growth mechanism involved, and establish if there is an important interaction leading to a polar-ordered structure. All these calculations were conducted in an effort to establish the physical and chemical character required for the 1,3,5-trioxane family of molecules to form guest polar-ordered crystals.

### 6.3.1 Role of R groups in 1,3,5-trioxanes

To determine the role of the R groups we studied the effect (steric or otherwise) they have on the packing and stabilisation of the system. The packing of the host along the *c* axis is of greater interest since the most important interactions occur along this axis (Figure 6-5(b) and Figure 6-3). The significance of these interactions have been evaluated with regards to the ability of the host to include a guest. **3-1** and **4** were used in these calculations, which were carried out using MM geometry optimisation.

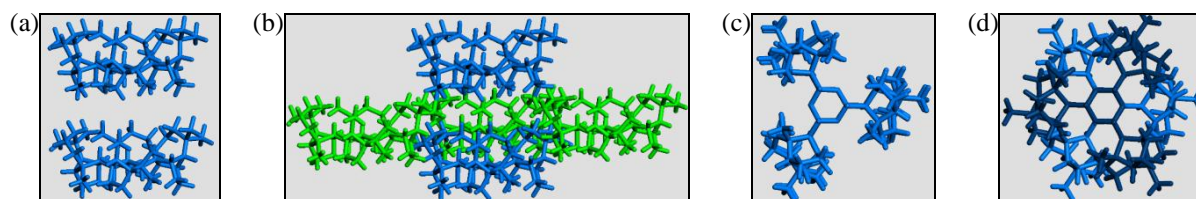


**Figure 6-6.** (a) Model without steric-interfering surrounding host (**A**). (b) Model with surrounding steric-interfering host (**B**). (c) Aligned stacking. (d) Offset stacking. One molecule is shown in dark blue to differentiate between the two molecules.

Models **A** (Figure 6-6(a)) and **B** (Figure 6-6(b)) were both calculated with the aligned and offset arrangement of the molecules (Figure 6-6(c) and (d)). These models (guest omitted for calculations) should indicate the effects of the bulky R groups of the surrounding green molecules on the stacking of the blue molecules. Both models, **A** and **B** (Figure 6-6), were optimised in both aligned and offset stacking mode with energies calculated relative to that of the aligned stacking model. In both models only the top blue molecule was allowed to optimise its position.

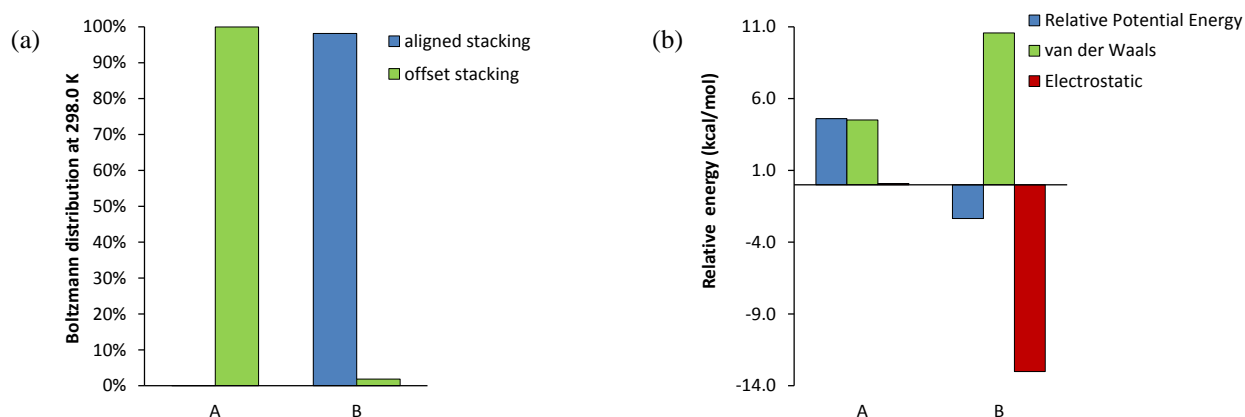


**Figure 6-7.** Results obtained from MM calculation of model described in Figure 6-6 plotted as (a) Boltzmann distribution at 298.0 K. (b) relative potential, vdW and electrostatic energy relative to the offset stacking. **A** denotes the model in Figure 6-6(a), without green molecules. **B** denotes the model in Figure 6-6b, with green molecules.

Figure 6-7a shows that offset stacking is favoured (4.6 kcal/mol lower than the aligned stacking, 99.96% probability) in the absence of the surrounding host, while the aligned stacking

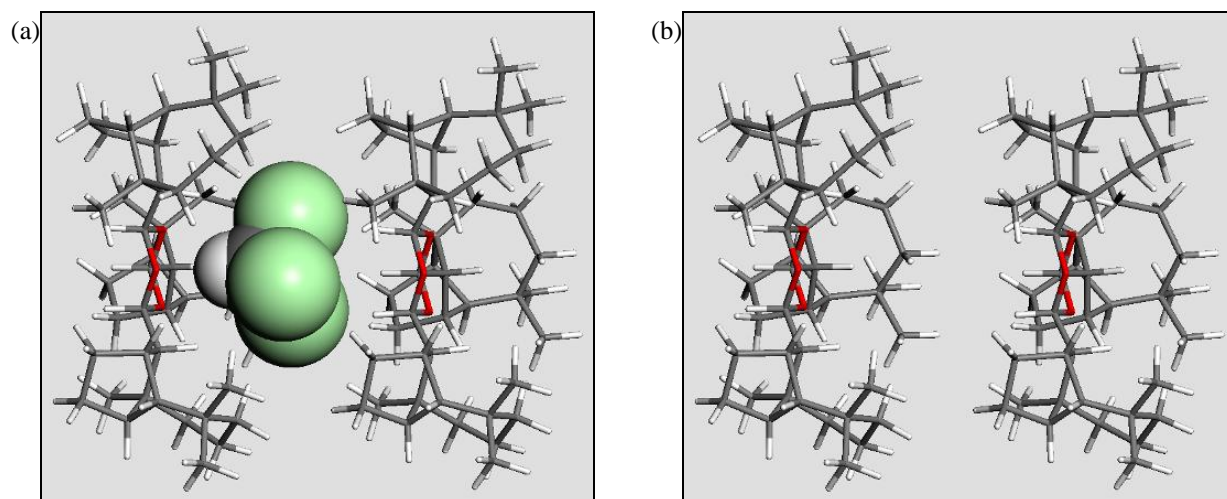


is favoured (-2.4 kcal/mol, 98.15%) in the presence of the surrounding host. The surrounding host (Figure 6-6(b)) causes just enough steric interference to destabilise the offset stacking of the blue host molecules (Figure 6-6(d)), thus increasing the distance between them.

From Figure 6-7(b) we see that the stabilisation of the offset stacking in **A** is driven by the vdW interactions as a result of the close packing of the molecules (in an attempt to eliminate all void spaces). In **B**, with the aligned stacking, the vdW component is even more destabilising due to the increased distance between the blue molecules. In this case the stabilisation of the aligned stacking comes from the electrostatic component of the energy. The absence of the electrostatic stabilisation in **A** (without green molecules) tells us that the electrostatic stabilisation in model **B** is caused by the interaction between the blue and green molecules. The enlargement of the cavity and subsequent loss of the dipole-dipole interactions between the trioxane rings could promote the inclusion of CF without overall destabilisation of the system; however, inclusion of CF would interrupt the dipole-dipole interactions between the trioxane rings.

### 6.3.2 Guest stabilisation

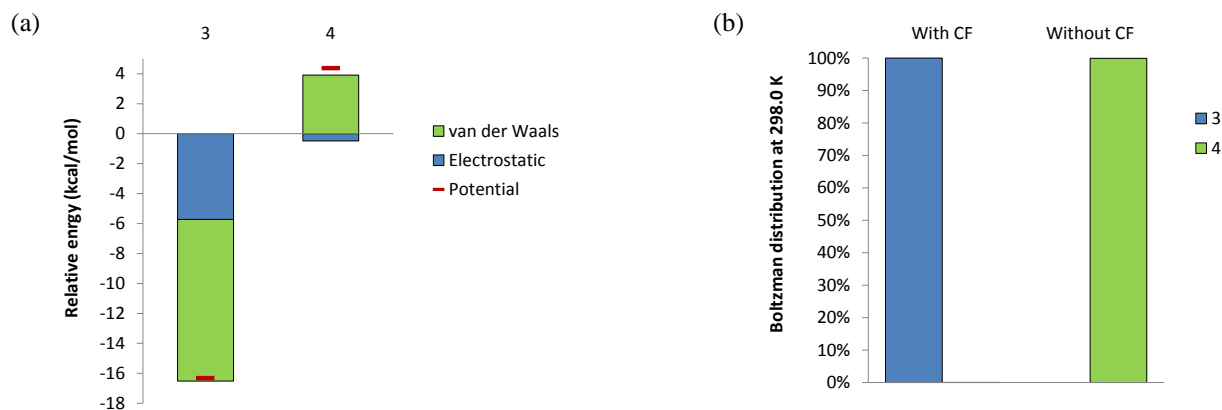
The only major difference between **3-1** and **4** is the size of the R groups which, as demonstrated above, plays a major role in the packing of these compounds. It was also shown in section 6.3.1 above that the endolongifolyl groups are responsible for separating the trioxane rings of the molecules stacked along the *c* axis, thereby diminishing the dipole-dipole interactions between the trioxane rings. Here we determine the effect of CF inclusion on the stacking of the host molecules (**3** and **4**) and, more specifically, whether CF inclusion would stabilise or destabilise the packing. This could provide some insight into why **3** includes CF while **4** does not.





**Figure 6-8.** Models used to determine the guest stabilisation of both **3** and **4**, demonstrated by the model of **3**. (a) Guest (CF) included. (b) Guest-omitted model. The same model was applied to the cyclohexyl derivative.

The simplified models shown in Figure 6-8 were optimised with and without CF for both **3** and **4** (only **3** is shown). All the molecules in the model were allowed to optimise to investigate the impact of the guest on the position of the two host molecules and to compare the resulting structures. The total potential energy and all its tensors were obtained and analysed to determine the main contributors to the stabilisation of the guest in **3-1** compared to **4**.



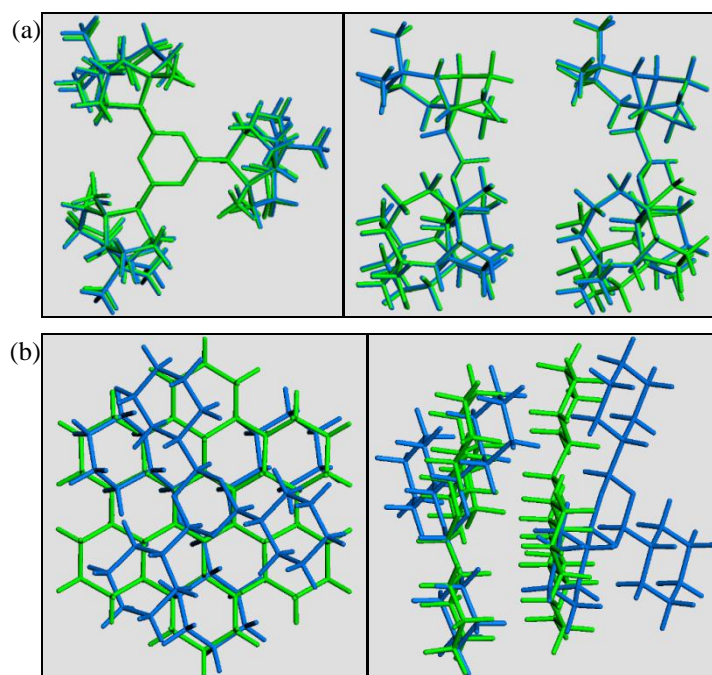
**Figure 6-9.** (a) Relative total potential energy of CF included models of **3** and **4** with their electrostatic and vdW components relative to the guest-free models. A negative value favours CF guest inclusion and a positive value favours the guest-free structure. (b) Boltzmann distribution calculated from the relative total potential energies in (a).

Figure 6-9(a) shows that **3-1** favours the CF inclusion by 16.3 kcal/mol, thus demonstrating the high stability of the CF inclusion complex, translating to a 100.0% probability according to the Boltzmann distribution (Figure 6-9(b)). The large vdW stabilisation (10.8 kcal/mol) results from the inclusion of CF, showing that inclusion is favoured provided the guest is a good fit for the cavity. The electrostatic stabilisation in **3-1** that exists in the presence of CF can be ascribed to the dipole-dipole interactions between CF and the trioxane rings of the two host molecules. Other than the effect of inclusion evident in the stabilisation of the vdW energy, the electrostatic interactions further stabilise the inclusion of CF in **3**.

**4** favours the close-packed arrangement, based on the positive relative potential energy of 4.4 kcal/mol (Figure 6-9(a)) translating to a 99.94% probability according to the Boltzmann distribution (Figure 6-9(b)). The inclusion of CF causes a loss of vdW stabilisation by 3.9 kcal/mol indicating an increased distance between the host molecules (loss of the dispersion interaction). The slight electrostatic stabilisation can be explained by the electrostatic interactions between CF and the trioxane rings which are almost balanced by the loss of the dipole-dipole interaction between the trioxane rings upon inclusion of CF, leaving a small net overall stabilisation. The inclusion of CF in **4** makes up for the loss in electrostatic energy but not for the vdW energy which destabilises the system, upon CF inclusion, shifting the structure

towards the close-packed system as opposed to **3** where the electrostatic interactions play a larger role.

For a better visual representation of what is occurring in the simulation of the CF inclusion, the two structures were overlaid for both compounds (**3-1** and **4**), to show any deformations caused by the inclusion of CF (Figure 6-10 below).



**Figure 6-10.** Overlays of (a) **3** and (b) **4**, CF included (blue molecules) and guest-free models (green molecules), after the geometry optimisation (for clarity, only the host molecules are shown).

From **Figure 6-10(a)** it is clear that there is no significant difference between the host positions of the two models (with and without CF) as shown by the overlay of the blue and green molecules. Apart from stabilising the system, CF does not drive the host molecules in **3** apart (which would cause a loss of vdW stabilisation). These effects and the good fit of CF within the cavity is the probable reason for the inclusion of CF in **3**.

Conversely, the inclusion of CF in **4** greatly changes the host packing of the simulated model (Figure 6-10(b)). The hosts are pushed apart (blue molecules) by the CF molecule, causing a loss of vdW stabilisation. The electrostatic stabilisation from the CF dipole-dipole interactions does not sufficiently compensate for the loss of vdW stabilisation driving **4** to a close-packed system.

Larger R groups such as endolongifolyl on the 1,3,5-trioxanes would naturally drive the host molecules apart, thus weakening the dipole-dipole stabilisation of the trioxane rings, and allowing the trioxanes to include smaller solvents such as CF. **4** and **5**, which have smaller R groups, prefer a close-packing arrangement, as they would need to undergo significant changes in packing to accommodate a guest (**Figure 6-10(b)**), while **3** does not (Figure 6-10(a)). The R

groups of the 1,3,5-trioxanes are therefore a design feature that can be modified to yield new trioxanes for inclusion of guests such as CF.

### 6.3.3 Potential energy profile of guest moving inside cavity of **3-1**

With a perpendicular distance (relative to the  $c$  axis) of 12.161 Å between the cavities, guest-guest interactions can be ruled out as significant contributors towards the polar alignment of the guests (see section 3.3.2). However, as mentioned in Section 6.2 (Figure 6-5), the cavity of **3-1** appears to be asymmetric along the crystallographic  $c$  axis, which happens to be the polar axis as well. This means that the host can induce directionality along this axis to yield a polar-ordered structure. Molecular mechanics was employed to determine the energy profile and relative stabilisation of the guests within these cavities, in order to determine the most stable guest alignment direction and the driving force behind this.

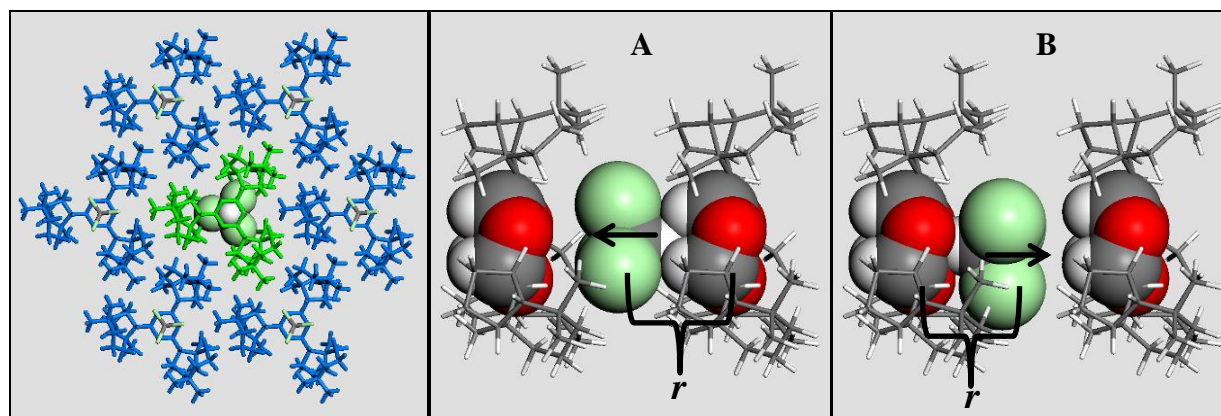


**Figure 6-11.** Model used for the potential energy profile of CF moving inside a cavity of **3-1**. Only the central host (green) and guest molecules are shown in models **A** and **B** with the surrounding blue host molecules omitted for clarity. The guest (CF) was translated in the direction of the arrow, as indicated.  $r$  is the distance between the CF and the trioxane rings.

It was decided to use the guest that includes in **3** (CF) to determine what interactions (electrostatic, vdW or steric) CF might have with the walls of the cavity in these calculations. The surrounding blue host molecules account for any long range dispersion interactions which will show in the vdW energy. Models **A** and **B** assume opposite CF orientations, with **B** congruent with the CF direction in the crystal structure. The starting position was chosen in order to obtain enough data points on both sides of the minima. Some data points were excluded due to excessive bond and angle deformation of the guest in the calculation. The guest was translated in the direction of the arrows (Figure 6-11 **A** and **B**) along the  $c$  axis in increments of 0.1 Å and allowed to optimise at each point. For a cavity to be symmetrical it should produce the same potential energy scan regardless of the guest orientation and direction of translation. The

two data sets (**A** and **B**) were overlaid, matching the CF-trioxane distance ( $r$ ), measured as indicated in Figure 6-11.

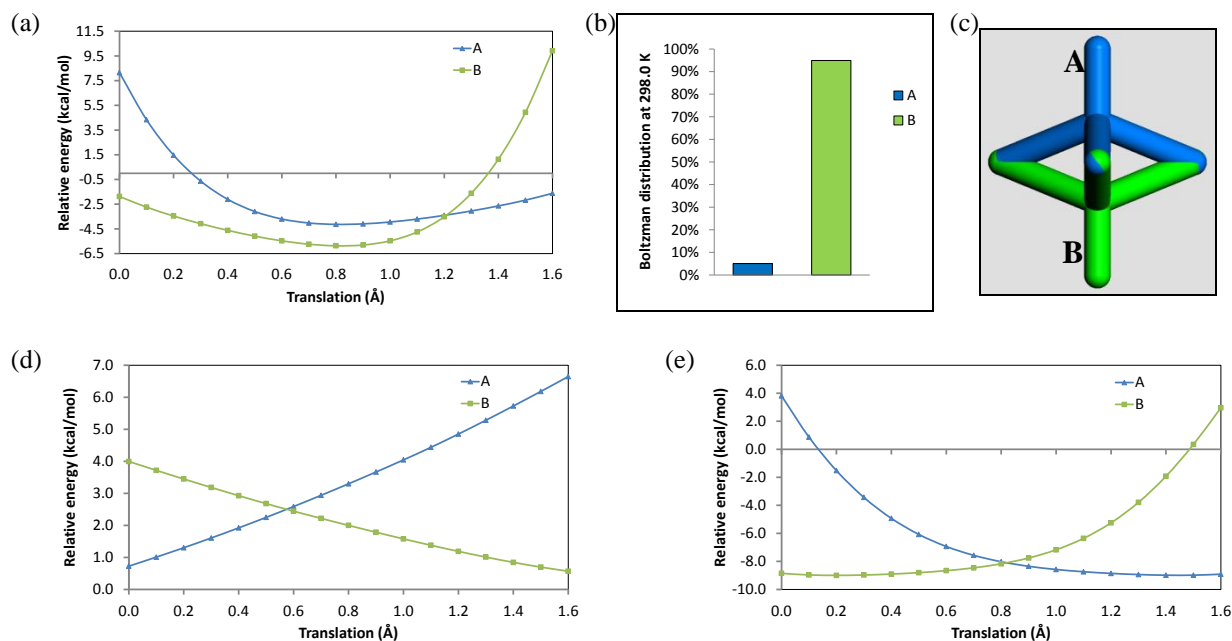


**Figure 6-12.** (a) Total relative potential energy plot. (b) The Boltzmann distribution calculated for the minima of **A** and **B** at 298.0 K. (c) Overlay of the CF molecules at the minima in **A** and **B**. (d) Electrostatic energy component of the total potential energy. (e) vdW energy component of the total potential energy.

Figure 6-12(a) shows that the two potential energy profiles do not match, indicating an asymmetrical cavity along the  $c$  axis. From Figure 6-12(a) it can be seen that **B** is more stable than **A** by 1.7 kcal/mol, which translates to a Boltzmann distribution (Figure 6-12(b)) of 94.9% in favour of **B**. The corresponding guest positions for the minima in each model can be overlaid, showing a good match for the chlorine positions (Figure 6-12(c)). This suggests a strong electrostatic interaction between the chlorine atoms and the trioxane oxygen atoms, thus driving the chlorine atoms to the positions found in the crystal structure regardless of the guest orientation. The difference in the two orientations arises from the dipole-dipole interactions present in **B** (not **A**, Figure 6-3) that stabilise the model, driving the guest towards **B**. Model **B** has a lower electrostatic energy than **A** at the minimum (at 0.8 Å translation) but no difference in vdW energy (Figure 6-12(d) and (e)). The lower electrostatic energy of **B** is due to the increase in the dipole-dipole interactions between CF and the trioxane rings on both sides of the guest which stabilises the guest, and thus imposes directionality on the guest. This shows that the polar-ordering of CF in **3-1** is driven by the dipole-dipole interactions between the guests and the trioxane rings enclosing them. For the sake of completeness, the simulation was also carried out in the absence of the surrounding guests, yielding indistinguishable results.

### 6.3.4 Investigation of polar alignment by means of MQD simulations

We know from Section 6.3.3 that CF has a preferred orientation inside the cavity of **3** that is consistent with the crystal structure. The bulky R group in **5** is responsible for relieving the dipole-dipole interaction between the trioxane rings, but the system regains stabilisation *from* dipole-dipole interactions with the included CF guests. Here we attempted to gain some insight into the encapsulation process of CF in **3-1** and the significance thereof on the crystal growth mechanism. Similar to Section 5.3.3, MQD simulations will be used to evaluate the guest alignment inside the host cavity during different stages of encapsulation. Since we are only interested in the minimum conformations of the guests inside the cavity, the quench dynamics task in the Forcite Plus module of Materials Studio is ideal for this simulation (Section 2.5.7).

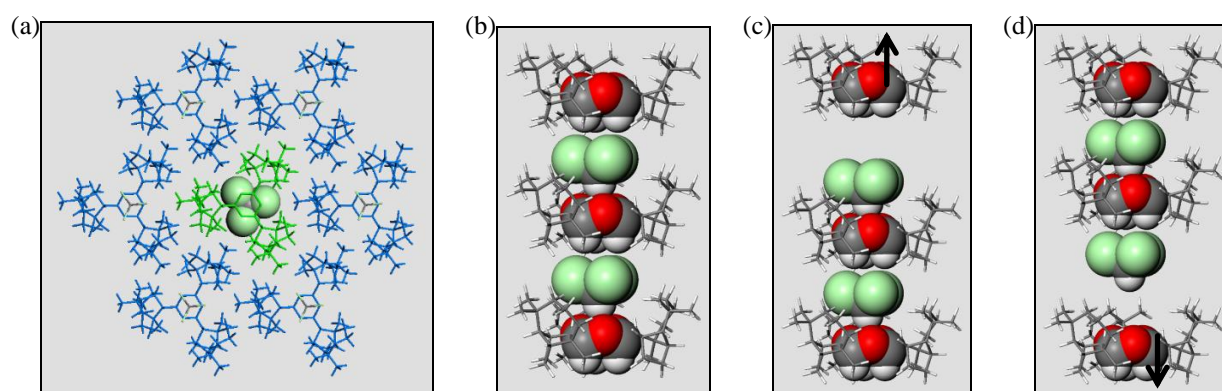


**Figure 6-13.** (a) Model used for MQD simulations of **3-1**. (b), (c) and (d) shows only the central green column with the guests and trioxane rings in space filled representation. (b) Crystal structure positions. (c) The top host molecule was translated away as indicated by the arrow - simulation **A**. (d) The bottom host molecule was translated away as indicated by the arrow - simulation **B**.

The model was chosen with sufficient surrounding host (blue) and guest molecules (Figure 6-13(a)) to account for any long-range dispersive (vdW) interactions. Only the central CF molecules (shown in space filled representation) were allowed to move in the dynamics calculations. Both the top (Figure 6-13(c)) and bottom (Figure 6-13(d)) had to be simulated since the alignment of the two outer host molecules is different relative to the central host molecule. In each of the two simulations one of the host molecules, as indicated by Figure 6-13(c) and (d), was manually translated to offsets of 3 and 4 Å from the crystal structure positions (Figure 6-13(b)) in the direction of the arrow. The model depicted in Figure 6-13(b) is the starting position for both simulations and represents the crystal structure positions of the molecules. The MQD calculation was run for simulations **A** (Figure 6-13 (b), (c) at 3 and 4 Å) and **B** (Figure 6-13 (b), (d) at 3 and 4 Å), respectively, to evaluate the effect of moving each of the two CF molecules of interest separately.



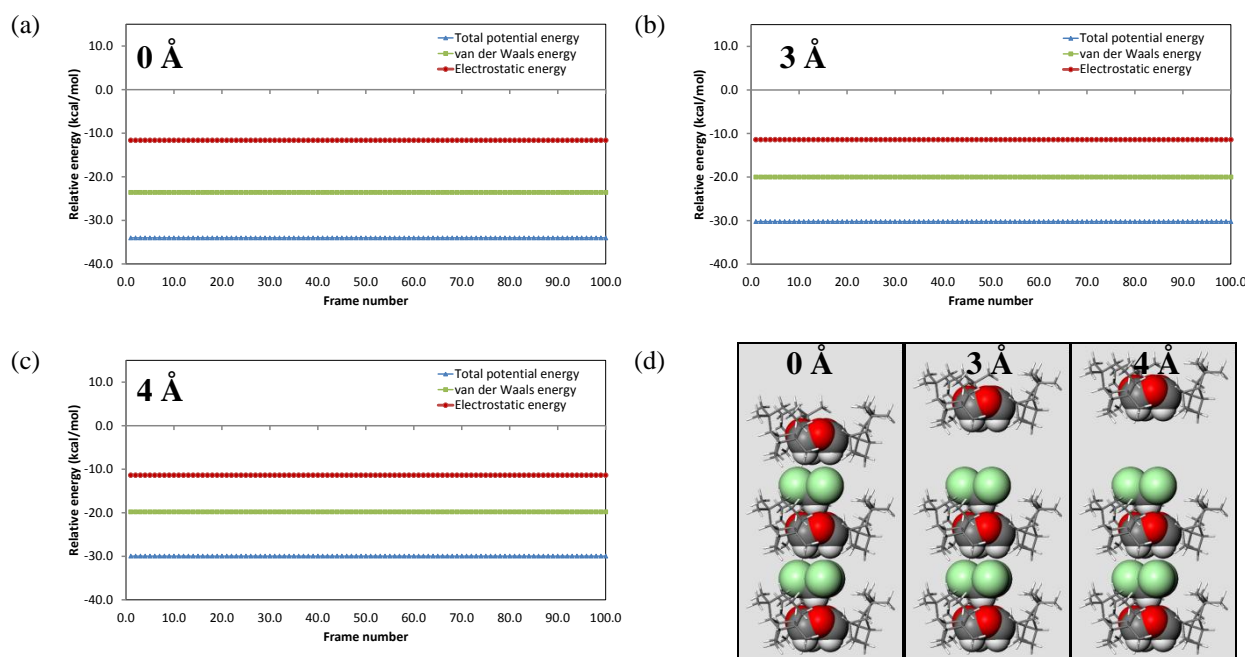


**Figure 6-14.** Simulation A results. (a), (b) and (c) are the energy profiles at 0, 3 and 4 Å translation respectively, which includes the total potential energy and its **vdW** and **electrostatic** constituents. (d) Structures of the minimum energy conformations. The surrounding molecules of the model were omitted for clarity in this figure.

Simulation A only yielded one conformation consistent with the crystal structure (Figure 6-14(a), (b) and (c)). An increase in total potential energy (blue line) is noticeable as the host offset is increased to 4 Å. The components of the potential energy revealed the increase to be due to the vdW energy (green line), while the electrostatic energy remained essentially unchanged. This destabilisation of the vdW energy results from the top host molecule moving away from the rest in the model. This reduces the dispersive interactions (expressed as the vdW energy). The guest position and orientation are unaffected (Figure 6-14(d)) by the movement of the host, demonstrating the stability of this conformation (orientation) in this simulation.

Also notable is the consistency of the electrostatic energy even with the loss of the host on top (chlorine side of the guest). This means that the electrostatic stabilisation of the guest is due to the dipole-dipole interactions between CF and the oxygen side of the trioxane ring (on the hydrogen side of the top CF; Figure 6-14(d)).

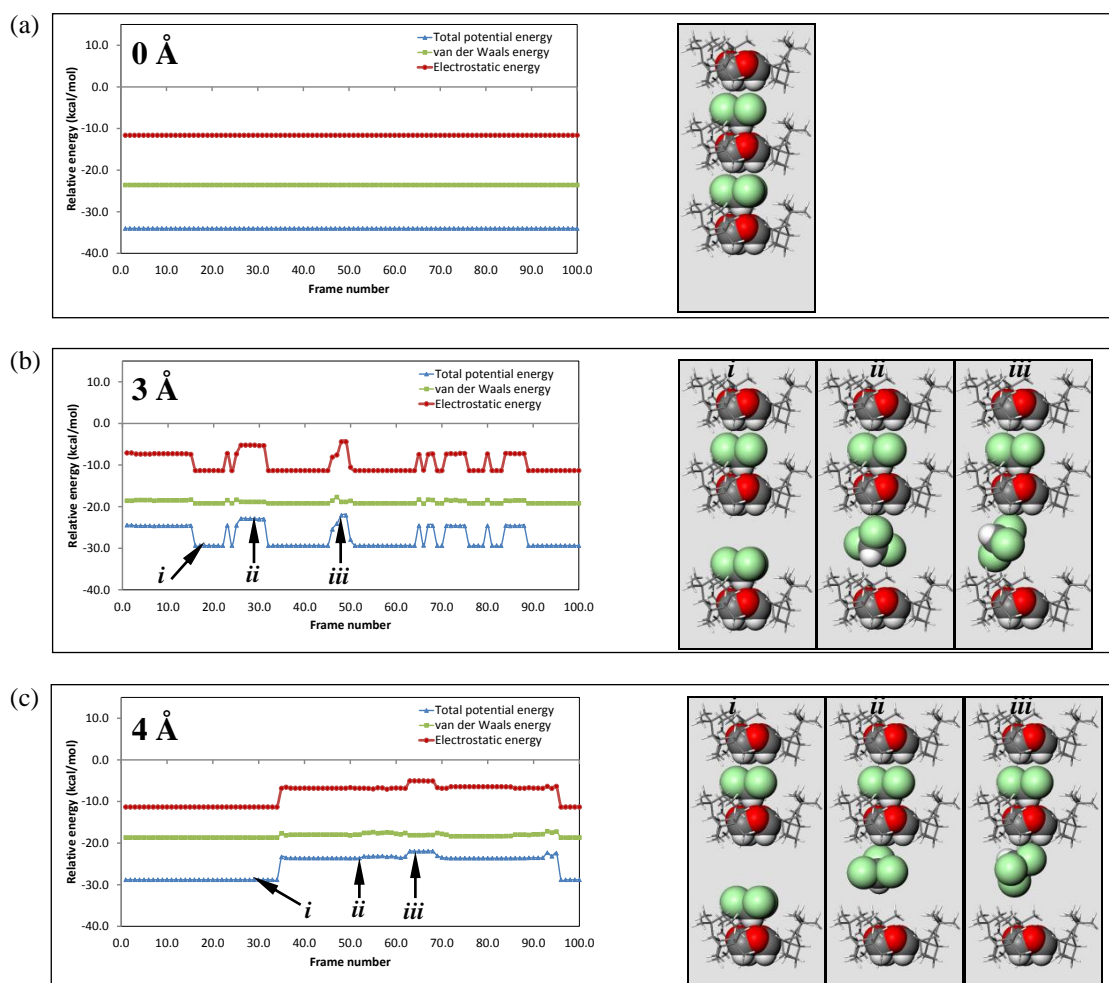


**Figure 6-15.** Simulation **B** results. Left - energy profiles at (a) 0, (b) 3 and (c) 4 Å translations, respectively, which includes the total potential energy and its **vdW** and **electrostatic** constituents. Right - the structures of the conformations with labels corresponding to that of the energy profiles.

Figure 6-14(a) shows that the 0 Å offset model produces the most stable result with only one conformation. This shows that CF is caught in a particular orientation once it is trapped in the cavity. Simulation **B** yields 3 conformations (*i*, *ii* and *iii*) of the guest for the 3 and 4 Å offset models (Figure 6-14(b) and (c)). Conformation *i* is the most stable in both models with the CF orientation congruent with the guest on top. As seen in simulation **A** before, CF prefers to coordinate to the oxygen side (partially negative -  $\delta^-$ ) of the trioxane ring. The other conformations are too high in energy (3 Å - 4.8 (*ii*), 6.5 (*iii*) kcal/mol and 4 Å - 5.5 (*ii*), 6.9 (*iii*) kcal/mol higher), thus favouring conformation (*i*) by nearly 100% probability according to the Boltzmann distribution at 298.0 K.

When looking at the total potential energy tensors, we see that the vdW component increases the energy of the system by 3.8 kcal/mol from a 0 to 4 Å offset. This effect is due to the bottom host molecules being translated away from the rest in the model (Figure 6-15(b) and (c)) causing a loss in dispersive (vdW) interactions between the molecules in the system, as would be expected for both simulation **A** and **B**.

It is clear from Figure 6-15(a) and (b) that the difference in stabilisation between the conformations is due to the electrostatic component of the total potential energy. This shows that the displacement of CF only affects the electrostatic energy component. More specifically, the dipole-dipole interaction (electrostatic) between CF and the partially negative oxygen side of the trioxane rings is responsible for stabilising conformations *i* of both the 3 and 4 Å models. In the cases of *ii* and *iii*, the interaction of CF with the partially positive hydrogen side of the trioxane ring does not compensate for the loss of the interaction with the oxygen side of the ring. This implies that these dipole-dipole interactions are very important in the crystal growth mechanism of these polar-ordered crystals. Unlike the 1,2,4,5,7,8-hexaoxonanes (Chapter 5), where the alignment of the guest is driven by steric effects (vdW) of the host, the 1,3,5-trioxanes use dipole-dipole electrostatic interactions to align the guests accordingly.

These results show that CF coordinates much more strongly to the  $\delta^-$  oxygen side than the  $\delta^+$  hydrogen side of the trioxane rings, resulting in a preference that impacts on the crystal growth mechanism promoting the polar-ordered growth. We therefore postulate the following two growth mechanisms that are consistent with these observations:

1. As the guest is trapped in the cavity it aligns to interact with the partially negative ( $\delta^-$ ) side of the trioxane ring, stabilising the system *via* dipole-dipole electrostatic interactions. This requires the host to grow in the same alignment, thus producing a guest polar-ordered crystal.
2. The CF guest coordinates to the trioxane ring first and crystallises as a unit producing a guest polar-ordered system. However, the NMR measurements carried out by Dimitrov *et al.*<sup>40</sup> did not show any peak shifts for the CF hydrogen, which would be observed if coordination occurred in solution. This suggests that the coordination or interaction within the host-guest unit rather occurs as part of the crystallisation mechanism.

## 6.4 SUMMARY

The crystal structure of the endolongifolyl derivative of 1,3,5-trioxane (**3-1**) was identified from the CSD as containing polar-ordered CF molecules in its cavities. To investigate this observation we aimed to synthesise a series of 1,3,5-trioxanes with a range of R groups and crystallise them from different polar solvents. However, we were only able to synthesise three 1,3,5-trioxanes (**3**, **4** and **5**) which did not include any solvents. The crystal structure of **4** corresponds to the structure that has already been reported in the literature. **5** yielded a crystal structure that packs similarly to **4** along all projections.



In order to explain the polar-ordering of **3-1** we used the structural data deposited in the CSD, for MM, MD and MQD simulations. We investigated the effect of the R groups on the packing and interactions of the system (MM) and the stabilisation of the guests within the cavities by identifying the major interactions (MM). We also determined the guest potential energy profile of a **3-1** cavity to determine whether the cavity is asymmetrical, thus inducing an alignment in a specific direction (MM). Lastly, we investigated the possible process/mechanism of the polar alignment (MM and MQD).

These calculations revealed that the R groups play a significant role in the inclusion of guests (in this case CF). Large R groups such as endolongifolyl can create enough space for a small polar guest, such as CF, to include. The amount of electrostatic and vdW energy lost when larger R groups are used is balanced by the inclusion of a guest (such as CF) that fits tightly into the cavity. The inclusion of CF stabilises the system *via* vdW (particularly dispersive interactions) and electrostatic (dipole-dipole interactions with  $\delta^-$  side of the trioxane rings) interactions. The trioxanes with smaller R groups do not include any solvents and prefer to close pack, since the trioxane rings can interact *via* stronger dipole-dipole interactions, thus stabilising the system.

The potential energy profile of the guest moving through the cavity is asymmetrical implying that the host can induce directionality in the guest trapped in the cavity. The difference in energy between the two minimum energy conformations is 1.7 kcal/mol, which translates to a Boltzmann distribution of 94.9% probability in favour of the guest being oriented as found in the crystal structure. This difference arises from the electrostatic component of the total potential energy caused by dipole-dipole interactions between the hosts and guest. However, MD calculations of CF in a complete cavity at 298.0 K revealed that CF cannot change its orientation once it is trapped, indicating that its alignment is imposed prior to this.

The MQD simulations also show that CF cannot change its orientation once it is trapped inside the cavity. The vdW energy component is a dispersive interaction caused by close packing of the system and inclusion of CF and does not contribute to the alignment of the guest. Conformation *i* (which maximises the dipole-dipole  $\delta^+_{\text{CF}} - \delta^-_{\text{trioxane ring}}$  interactions) was revealed to be the most stable in both simulations **A** and **B** (both sides of the central host). In simulation **B** the one host molecules and CF molecule are translated away from the bulk of the model to form conformation *i*, thus suffering a loss of vdW stabilisation, but gaining a much greater electrostatic stabilisation.

We have proposed that the  $\delta^+_{\text{CF}} - \delta^-_{\text{trioxane ring}}$  dipole-dipole interactions could lead to a CF-trioxane complex forming during the crystallisation process just before the guest is trapped.

These CF-trioxane also units would be polar and could stack on top of one another *via* dipole-dipole electrostatic interactions along the crystallographic *c* axis. Another growth mechanism proposed involves the guest optimizing its orientation during the process of encapsulation, which would also result in a guest-polar-ordered crystal. Ultimately the polar-ordering ability is an inherent property of the host and its crystal growth mechanism.

# **CHAPTER 7**

## **CONCLUSION**

## 7.1 CONCLUDING REMARKS

The aims of this study were to identify compounds that form guest polar-ordered inclusion complexes with simple polar guests such as CF, BF, TCAN, etc. and to elucidate their polar-ordering ability with respect to specific design features of the host compound. This involved identifying suitable compounds from the CSD, in an attempt to extend the number of known structures of guest polar-ordered inclusion complexes. Following on these results we aimed to employ computational methods, using the crystal structure data to construct the models, in order to explain the polar alignment of the guests.

The CSD survey identified ten inclusion complexes where the guests were polar-ordered. These were compared to identify similarities concerning their polar-ordering ability. These structures share commonalities in their space groups (*R3c*, *R3* (5 compounds) and *Cc* (3 compounds)) as well as included guests (CF (6 crystal structures) and ACN (4 crystal structures)). It was also revealed that the lateral guest-guest distances were longer than 8.2 Å. A computational study using DFT (in the absence of the host) showed a strong intra-channel association between the guest molecules. The lateral guest-guest interactions (interactions between guests in neighbouring channels) showed a cut-off at 9.1 Å, indicating that the lateral guest-guest interactions become insignificant at these distances for the identified polar-ordered crystal structures (in the absence of the host). However, host-mediated guest-guest interactions were not excluded.

On the basis of the CSD study three types of compounds (2,7-dimethylocta-3,5-diyne-2,7-diol (**1**), 1,4,7-cyclohexane-1,2,4,5,7,8-hexaoxonane (**2**) and the 1,3,5-trioxanes (**3** - **5**)) were studied in this work for two main reasons: their ability to form polar-ordered inclusion complexes with various small guest molecules and their relatively simple syntheses and Since the compounds investigated have vastly different molecular structures, they were investigated separately by means of visual analysis of the crystal structures and computational modelling techniques.

Compound **1** proved to be the most versatile compound, forming seven polar-ordered crystals. The crystal structures were carefully examined and we identified a common asymmetric feature in the hydrogen-bonded spirals holding the structures together. The modelling of a guest moving through the cavities of **1** indicated a symmetrical potential energy profile, which suggests that the cavities of **1** were symmetrical. However, calculations conducted for a larger model with six of the solvents that led to polar-ordered inclusion

complexes indicated that host-guest interactions (Cl-TMS), host mediated guest-guest interactions (TCAN and BTCM) or a combination thereof (CMP, BMP and IMP), were responsible for the polar-ordering of these guests in **1**.

Two polar-ordered crystal structures of **2** were obtained, of which one was novel (**2**·CHBr<sub>3</sub>) while the other (**2**·CHCl<sub>3</sub>) had been previously reported. Both inclusion complexes crystallise in the polar space group *R3c* with the polar axis along [001]. The side walls of the cavity of **2** exhibits asymmetric features along the polar *c* axis, which, through the appropriate computational modelling, was shown to induce directionality of the included guests (an asymmetric potential energy profile in favour of the crystal structure guest-orientation (0° conformation)). The relative energies of the two orientations calculated *via* DFT modelling (2.9 kcal/mol in favour of the 0° conformation) revealed a 99.3% probability of obtaining the 0° conformation at 298.0 K, according to the Boltzmann distribution.

MD calculations illustrated that the guest molecules cannot change their orientation once they are trapped within a cavity, suggesting that the alignment of the guest molecules has to occur upon or prior to encapsulation. Further investigation involved using MQD to evaluate the conformational space of the molecular models, simulating the period just prior to encapsulation of the guest. These simulations yielded the crystal structure alignment of the guest molecules as the preferred orientation. Analysis of the components of the total potential energy suggested that the driving force behind the polar-ordering of the guest molecules was primarily electrostatic interactions between the guest molecules and one of the peroxide rings, facilitated by the slight steric influence of the asymmetric side wall of the cavity.

Three 1,3,5-trioxanes (**3**, **4** and **5**) were synthesised with the aim of obtaining polar-ordered inclusion complexes. However, this proved to be unsuccessful. Nevertheless, the trioxanes synthesised still formed polar-ordered crystals due to the strong electrostatic interactions between the trioxane rings. This suggests that the polar inclusion of CF in **3** might only be enhancing the already existing polarity of **3-1** rather than causing it. **3-1** and **4** were used to investigate the polar-ordering of the trioxanes by means of visual inspection of their crystal structures and computational modelling. A computational comparison of the effect of the different 1,3,5-trioxane R groups confirmed their importance in the packing arrangement of the host molecules and inclusion of guests (in this case CF). The modelling of a guest moving through the cavity suggested an asymmetric cavity, implying that the host can impose directionality on the guest molecules trapped within the cavity. Further modelling indicated that the guest molecules cannot change their orientation once they are trapped, implying that the alignment of the guest molecules has to occur as part of the crystallisation mechanism. This was

---

illustrated by a series of MQD simulations involving both sides of the trioxane rings, which showed that a polar-ordered system was obtained. It was also shown that the most important interactions between the host and guest, as far as the polar alignment of the guest is concerned, are of an electrostatic nature (dipole-dipole electrostatic interactions).

The aims for this study were thus achieved for compounds **1** and **2** since novel guest polar-ordered inclusion complexes were obtained and their polar-ordering ability was explained. Even though polar-ordered inclusion complexes of the synthesised trioxanes were not realised, these compounds nevertheless pack in a polar fashion, which was shown to play a role in the polar-ordering of the guests and could also yield interesting properties.

## 7.2 FUTURE WORK

The inclusion compounds of **1** provide a useful series of polar-ordered inclusion complexes with a wide range of guests with different dipole moments. Further crystallisation can be performed with mixed solvent systems (e.g. TCAN and BTCM) in an effort to tune the polarity of the resulting inclusion complex to be intermediate between that of the individual guests by varying the ratio of the two solvents used. **2** can be grown from SiHCl<sub>3</sub>, which is similar to CHCl<sub>3</sub> and CHBr<sub>3</sub> and should be a good fit the cavity. This would increase the number of known guest polar-ordered inclusion complexes of **2**, allowing more detailed analysis of the properties and behaviour of the guest polar-ordered inclusion complexes of **2**. The same can be applied to the 1,3,5-trioxanes, which also have not been studied for their polar-ordering abilities.

These polar crystals can be studied further for their physical properties, especially their non-linear optical susceptibility. Analysis of these crystals by scanning pyroelectric microscopy (SPEM) and phase sensitive second harmonic microscopy (PS-SHM) can contribute a great deal to the characterisation of the polarity of these crystals. These methods provide a way to map the polarity of a crystal, and therefore also the polar domains of the crystal.<sup>37, 79</sup> These techniques would also be applied to crystals obtained *via* systematic crystal growth experiments employing different polar and non-polar crystals as seeds in an effort to further elucidate the polar ordering mechanisms. PS-SHM and SPEM experiments can also reveal bipolar states in a crystal,<sup>37</sup> which could be compared to the results from the computational models described in this study.

Quantitative non-linear optical conversion efficiency measurement can be determined by using a powder technique developed by Kurtz and Perry.<sup>80</sup> This method utilizes crystals ground into a fine powder and sandwiched between two glass slides which serve as the sample cell. Irradiation of the samples with a Q-switched Nd-YAG laser, with the first harmonic output of

1064 nm,<sup>81</sup> would produce an SHG signal depending on the SHG susceptibility and efficiency of the material, relative to KDP or urea crystals.<sup>82</sup>

Possible electrical and magnetic properties could also be evaluated by investigating how these materials would interact with an electric current (variable voltage and current) as well as electromagnetic fields. Furthermore, the characterisation of these properties would be the first step toward establishing possible applications for these materials.

**REFERENCES**

1. Kabe R.; Nakanotani H.; Sakanoue T.; Yahiro M.; Adachi C., Effect of molecular morphology on amplified spontaneous emission of bis-styrylbenzene derivatives. *Adv. Mater.* **2009**, *21*, 4034-4038.
2. Srinivasan K.; Kanimozhi S., Effect of different solvents on the habit of meta-nitroaniline single crystals. *Cryst. Res. Technol.* **2010**, *45*, 611-618.
3. (a) Wong K. T.; Chien Y. Y.; Chen R. T.; Wang C. F.; Lin Y. T.; Chiang H. H.; Hsieh P. Y.; Wu C. C.; Chou C. H.; Su Y. O.; Lee G. H.; Peng S. M., Ter(9,9-diarylfluorene)s: Highly efficient blue emitter with promising electrochemical and thermal stability. *J. Am. Chem. Soc.* **2002**, *124*, 11576-11577; (b) Glaser R.; Knotts N.; Yu P.; Li L. H.; Chandrasekhar M.; Martin C.; Barnes C. L., Perfect polar stacking of parallel beloamphiphile layers. Synthesis, structure and solid-state optical properties of the unsymmetrical acetophenone azine DCA. *Dalton Trans.* **2006**, 2891-2899.
4. Holman K. T.; Pivovar A. M.; Ward M. D., Engineering crystal symmetry and polar order in molecular host frameworks. *Science* **2001**, *294*, 1907-1911.
5. Lloyd G. O. Crystal engineering of porosity. MsC thesis. University of Stellenbosch, Stellenbosch, 2006.
6. Seddon K.R.; Zaworotko M., Crystal engineering: the design and application of functional solids. *Series C: Math. and Phys. Sci.* **1996**, *539*, 155-160.
7. Lehn J. M., Supramolecular chemistry: concepts and perspectives, Weinheim: VCH. **1995**.
8. Lehn J. M., Supramolecular chemistry: concepts and perspectives, Nauka, Novosibirsk. **1998**, 334-336.
9. Lehn J. M., Supramolecular chemistry - scope and perspectives molecules, supermolecules, and molecular devices. *Angew. Chem. Int. Ed.* **1988**, *27*, 88-112.
10. Lehn J. M., Perspectives in supramolecular chemistry - from molecular recognition towards molecular information-processing and self-organization. *Angew. Chem. Int. Ed.* **1990**, *29*, 1304-1319.
11. Desiraju G. R., Designer crystals: intermolecular interactions, network structures and supramolecular synthons. *Chem. Commun.* **1997**, 1475-1482.
12. Fischer E., Einfluss der configuration auf die wirkung der enzyme. *Ber. Deutsch. Chem. Ges.* **1894**, *27*, 2985-2993.
13. Lehn J. M., Supramolecular chemistry scope and perspectives - molecules supermolecules molecular devices. *J. Incl. Phenom.* **1988**, *6*, 351-396.
14. Aakeröy C. B., Crystal engineering: Strategies and architectures. *Acta Crystallogr., Sect. B: Struct. Sci.* **1997**, *53*, 569-586.
15. Kitaigorodsky A. I., Molecular Crystals [in Russian]. Nauka, Moscow: 1971; p 424.
16. Desiraju G. R., Supramolecular synthons in crystal engineering - a new organic-synthesis. *Angew. Chem. Int. Ed.* **1995**, *34*, 2311-2327.
17. Etter M. C., Encoding and decoding hydrogen-bond patterns of organic-compounds. *Acc. Chem. Res.* **1990**, *23*, 120-126.



## References

- 
18. (a) Su D.; Wang X.; Simard M.; Wuest J. D., Molecular tectonics. *Supramol. Chem.* **1995**, *6*, 171-178; (b) Grosshans P.; Jouaiti A.; Bulach V.; Planeix J.; Hosseini M. W.; Nicoud J., Molecular tectonics: from enantiomerically pure sugars to enantiomerically pure triple stranded helical coordination network. *Chem. Commun.* **2003**, 1336-1337.
  19. Iyere P. A.; Boadi W. Y.; Atwood D.; Parkin S., Supramolecular aggregation in 4,4'-bipyridin-11'-ium dichloride, 4,4'-bipyridin-1,1'-ium dinitrate and 4,4'-bipyridin-1-ium bromide. *Acta Crystallogr. Sect. B-Struct. Sci.* **2003**, *59*, 664-669.
  20. Jeffrey G. A., An introduction to hydrogen bonding. Oxford University Press, Oxford: 1997.
  21. Aakeröy C. B., C. B.; Seddon, K. R., The hydrogen bond and crystal engineering. *Chem. Soc. Rev.* **1993**, *22*, 397-407.
  22. Pauling L., The nature of the chemical bond. *Cornell University Press, Ithaca, New York* **1960**.
  23. Pimentel G. C.; McClellan A. L., The hydrogen bond. W. H. Freeman and Co., San Fransisco: 1960.
  24. (a) Cappella B.; Dietler G., Force-distance curves by atomic force microscopy. *Surf. Sci. Rep.* **1999**, *34*, 1-104; (b) Accelrys *Materials Studio*, 4.3; Accelrys Software, Inc: 2008.
  25. (a) Yu N.; Polycarpou, A. A., Adhesive contact based on the Lennard-Jones potential: a correction to the value of the equilibrium distance as used in the potential. *J. Colloid Interface Sci.* **2004**, *278*, 428-435; (b) Raff L. M., Principles of physical chemistry. 1 ed.; Prentice-Hall, Inc: New Jersey, 2001; p 22 - 25.
  26. Sauers R. R., Steric Attraction: The Far Side. *J. Chem. Educ.* **1996**, *73*, 114-116.
  27. (a) Couderc G.; Hulliger J., Channel forming organic crystals: guest alignment and properties. *Chem. Soc. Rev.* **2010**, *39*, 1545-1554; (b) Tsuwi J.; Berger R.; Labat G.; Couderc G.; Behrnd N. R.; Ottiger P.; Cucinotta F.; Schurmann K.; Bertoni M.; Viani L.; Gierschner J.; Cornil J.; Prodi-Schwab A.; De Cola L.; Wubbenhorst M.; Hulliger J., Alignment and relaxation dynamics of dye molecules in host-guest inclusion compounds as probed by dielectric spectroscopy. *J. Phys. Chem. A* **2010**, *114*, 6956-6963; (c) Glaser R.; Knotts N.; Wu Z. Y.; Barnes C. L., Dipole parallel alignment in the crystal structure of a polar biphenyl: 4'-acetyl-4-methoxybiphenyl (AMB). *Cryst. Growth Des.* **2006**, *6*, 235-240.
  28. (a) McArdle C. B., Side chain liquid crystal polymers. Chapman and Hall: New York, 1989; (b) Williams D. J., Non-linear optical properties of organic materials. *Thin Solid Films* **1992**, *216*, 117-122.
  29. Glaser R.; Kaszynski P., Anisotropic organic materials - approaches to polar order, ed. ACS Symp. Ser, American Chemical Society, Washington, DC, : 2001; Vol. 798.
  30. (a) Etter M. C.; Huang K. S., Induction of noncentrosymmetry by polar hydrogen-bonded chains in nitroaniline crystals. *Chem. Mater.* **1992**, *4*, 824-827; (b) Wong M. S.; Gramlich V.; Bosshard C.; Gunter P., Hydrogen bonded lambda-shaped packing motif based on 4-nitrophenylhydrazones: a promising design tool for engineering acentric crystals. *J. Mater. Chem.* **1997**, *7*, 2021-2026.
  31. (a) Lin W. B.; Evans O. R.; Xiong R. G.; Wang Z. Y., Supramolecular engineering of chiral and acentric 2D networks. Synthesis, structures, and second-order nonlinear optical properties of bis(nicotinato)zinc and bis{3-2-(4-pyridyl)ethenyl benzoato}cadmium. *J. Am. Chem. Soc.* **1998**, *120*, 13272-13273; (b) Marder S. R.; Tiemann B. G.; Perry J. W.; Cheng L. T.; Tam W.; Schaefer W. P.; Marsh R. E., Organic and organometallic compounds - 2nd-order molecular and macroscopic optical nonlinearities. *J. Nonlinear Opt. Phys. Mater.* **1991**, *455*, 187-199.
  32. (a) Marder S. R.; Perry J. W.; Tiemann B. G.; Schaefer W. P., Organometallic salts with large 2nd-harmonic-generation powder efficiencies - (e)-1-ferrocenyl-2-(1-methyl-4-pyridiniumyl)ethylene salts. *Organometallics* **1991**, *10*, 1896-1901; (b) Marder S. R.; Perry J. W.; Schaefer W. P., 4-n-methylstilbazolium toluene-para-sulfonate salts with large 2nd-order optical nonlinearities. *J. Mater. Chem.* **1992**, *2*, 985-986.
-

## References

- 
33. (a) Hertzsch T.; Kluge S.; Weber E.; Budde F.; Hulliger J., Surface recognition of dipolar molecules entering channels of the organic zeolite tris(o-phenylenedioxy)cyclotriphosphazene. *Adv. Mater.* **2001**, *13*, 1864-1867; (b) König O.; Burgi H. B.; Armbruster T.; Hulliger J.; Weber T., A study in crystal engineering: Structure, crystal growth, and physical properties of a polar perhydrotriphenylene inclusion compound. *J. Am. Chem. Soc.* **1997**, *119*, 10632-10640.
34. Sim G. A., The crystal structure of 11-amino-undecanoic acid hydrobromide hemihydrate. *Acta Crystallogr.* **1955**, *8*, 833-840.
35. (a) Hoss R.; König O.; V., K.-H.; Berger U.; Rogin P.; Hulliger J., Crystallization of supramolecular materials: Perhydrotriphenylene (PHTP) inclusion compounds with nonlinear optical properties. *Angew. Chem. Int. Ed. Engl.* **1996**, *35*, 1664-1666; (b) Farina M.; di Silvestro G.; Sozzani P., Comprehensive supramolecular chemistry, ed. . D. D. MacNicol, F. Toda and R. Bishop, Pergamon, Oxford, : 1996; Vol. 6; (c) Hulliger J., Markov-type evolution of materials into a polar state. *Chem. Eur. J.* **2002**, *8*, 4578-4586.
36. (a) Hertzsch T.; Budde F.; Weber E.; Hulliger J., Supramolecular-wire confinement of I-2 molecules in channels of the organic zeolite tris(o-phenylenedioxy)cyclotriphosphazene. *Angew. Chem. Int. Ed.* **2002**, *41*, 2281-2284; (b) Hertzsch T.; Gervais C.; Hulliger J.; Jaeckel B.; Guentay S.; Bruchertseifer H.; Neels A., Open-pore organic material for retaining radioactive I-2 and CH<sub>3</sub>I. *Adv. Funct. Mater.* **2006**, *16*, 268-272; (c) Sozzani P.; Comotti A.; Bracco S.; Simonutti R., Cooperation of multiple CH center dot center dot center dot pi interactions to stabilize polymers in aromatic nanochannels as indicated by 2D solid state NMR. *Chem. Commun.* **2004**, 768769; (d) Comotti A.; Bracco S.; Feretti L.; Mauri M.; Simonutti R.; P., S., A single-crystal imprints macroscopic orientation on xenon atoms. *Chem. Commun.* **2007**, 350352.
37. Behrnd N. R.; Couderc G.; Wubbenhorst M.; Hulliger J., Scanning pyroelectric microscopy revealing the spatial polarity distribution in topologically centric crystals of trans-4-chloro-4'-nitrostilbene. *Phys. Chem. Chem. Phys.* **2006**, *8*, 4132-4137.
38. Rech M.; Batagiannis A.; Hulliger J., Polarity formation by a higher order interaction Markov-like chain. *J. Math. Chem.* **2009**, *46*, 1181-1187.
39. Terent'ev A. O.; Platonov M. M.; Sonneveld E. J.; Peschar R.; Chernyshev V. V.; Starikova Z. A.; Nikishin G. I., New preparation of 1,2,4,5,7,8-hexaoxonanes. *J. Org. Chem.* **2007**, *72*, 7237-7243.
40. Dimitrov V.; Rentsch G.; Linden A.; Hesse M., The ozonolysis of longifolene: A tool for the preparation of useful chiral compounds. Configuration determination of new stereogenic centers by NMR spectroscopy and X-ray crystallography. *Helv. Chim. Acta* **2003**, *86*, 106-121.
41. (a) Kohn W.; Sham L. J., Self-consistent equations including exchange and correlation effects. *Phys. Rev.* **1965**, *140*, A1133-A1138; (b) Hohenberg P.; Kohn W., Inhomogeneous electron gas. *Phys. Rev.* **1964**, *136*, B864-B871.
42. (a) Kohn W.; Becke A. D.; Parr R. G., Density functional theory of electronic structure. *J. Phys. Chem.* **1996**, *100*, 12974-12980; (b) Eberhard K.U.G.; Reiner M. D., Density Functional Theory. Plenum Press, New York: 1995; Vol. 337.
43. (a) Møller C.; Plesset M. S., Note on an approximation treatment for many-electron systems. *Phys. Rev.* **1934**, *46*, 618-622; (b) Pople J. A.; Head-Gordon M.; Raghavachari K., Quadratic configuration interaction. A general technique for determining electron correlation energies. *J. Chem. Phys.* **1987**, *87*, 5968-5975; (c) Boese A. D.; Oren M.; Atasoylu O.; Martin J. M. L.; Ka'Illy M.; Gauss J., W3 theory: Robust computational thermochemistry in the kJ/mol accuracy range. *J. Chem. Phys. Rev.* **2004**, *120*, 4129-4141.
44. Sholl D. S.; Steckel J. A., Density Functional Theory: A Practical Introduction. John Wiley & Sons, Inc: 2009.
45. Kohn W.; Sham. L. J., Self-consistent equations including exchange and correlation effects. *Phys. Rev.* **1965**, *140*, A1133-A1138.
-

## References

- 
46. Dreuw A.; Head-Gordon M., Single-reference ab initio methods for the calculation of excited states of large molecules. *Chem. Rev.* **2005**, *105*, 4009-4037.
47. Friesner R. A.; Guallar V., Ab initio quantum chemical and mixed quantum mechanics/molecular mechanics (QM/MM) methods for studying enzymatic catalysis. *Annu. Rev. Phys. Chem.* **2005**, *56*, 389-427.
48. Frisch M. J., Trucks G. W., Schlegel H. B., Scuseria G. E., Robb M. A., Cheeseman J. R., Montgomery J. A., Vreven T., Kudin K. N., Burant J. C., Millam J. M., Iyengar S. S., Tomasi J., Barone V., Mennucci B., Cossi M., Scalmani G., Rega N., Petersson G. A., Nakatsuji H., Hada M., Ehara M., Toyota K., Fukuda R., Hasegawa J., Ishida M., Nakajima T., Honda Y., Kitao O., Nakai H., Klene M., Li X., Knox J. E., Hratchian H. P., Cross J. B., Bakken V., Adamo C., Jaramillo J., Gomperts R., Yazayev O., Austin A. J., Cammi R., Pomelli C., Ochterski J. W., Ayala P. Y., Morokuma K., Voth G. A., Salvador P., Dannenberg J. J., Zakrzewski V. G., Dapprich S., Daniels A. D., Strain M. C., Farkas O., Malick D. K., Ortiz J. V., Cui Q., Baboul A. G., Clifford S., Cioslowski J., Stefanov B. B., Liu G., Liashenko A., Piskorz P., Komaromi I., Martin R. L., Fox D. J., Keith T., Al-Laham M. A., Peng C. Y., Nanayakkara A., Challacombe M., Gill P. M. W., Johnson B., Chen W., Wong M. W., Gonzalez C., Pople J. A., *Gaussian 03*, Revision C.02; Gaussian, Inc.: Wallingford CT, 2004.
49. Tirado-Rives J.; Jorgensen W. L., Performance of b3lyp density functional methods for a large set of organic molecules. *J. Chem. Theory Comput.* **2008**, *4*, 297-306.
50. Leach A. R., *Molecular Modeling: principles and applications*. 2nd ed.; 2001; p 165.
51. Keserü G. M.; Kolossváry I., *Molecular mechanics and conformational analysis in drug design*. Blackwell Science Ltd.: 1999; p 8.
52. Hinchliffe A., *Modelling Molecular Structures*. 2nd ed.; WILEY Publishers: 2000; p 24-25.
53. Rappé A. K.; Casewit C. J., *Molecular mechanics across chemistry*. University Science Books: Sausalito, CA, 1997.
54. Wei K. C.; Zhou H.; Wen H.; Xu W.; Xu Z. H., Molecular mechanics and dynamics simulations of various disperse models on the water surface (001). *J. Mol. Model.* **2003**, *9*, 142-152.
55. Boeyens J. C. A.; Comba P., Molecular mechanics: theoretical basis, rules, scope and limits. *Coord. Chem. Rev.* **2001**, *212*, 3-10.
56. Andersen H. C., Molecular dynamics simulations at constant pressure and/or temperature. *J. Chem. Phys.* **1980**, *72*, 2384-2393.
57. Leach A. R., *Molecular Modeling: principles and applications*. 2nd ed.; 2001; p 382-385.
58. Duan Y.; Kollman P. A., Pathways to a protein folding intermediate observed in a 1-microsecond simulation in aqueous solution. *Science* **1998**, *282*, 740-744.
59. Nangia A., Database research in crystal engineering. *CrystEngComm.* **2002**, 1-9.
60. *APEX2*, 2.1; Bruker AXS Inc: MADISON, 2004
61. *M86-Exx078 APEX2 User Manual*, Bruker AXS Inc.: 2006.
62. (a) Atwood J. L.; Barbour L. J., Molecular graphics: From science to art. *Cryst. Growth Des.* **2003**, *3*, 3-8; (b) Barbour L. J., X-Seed -- A Software Tool for Supramolecular Crystallography. *J. Supramol. Chem.* **2001**, *1*, 189-191.
63. *POV-Ray for Windows*, 3.6.1a.icl8.win32; Persistence of Vision Raytracer, Persistence of Vision Pty. Ltd. : Williamstown, Victoria, Australia, 2004.
-

## References

- 
64. Sheldrick G. M. *SHELX Manual*, <http://shelx.uni-ac.gwdg.de/SHELX/shelx.pdf>.
65. Sheldrick G. M., A short history of SHELX. *Acta Crystallogr., Sect. A: Found. Crystallogr.* **2008**, *64*, 112-122.
66. Schaftenaar G.; Noordik J.H., Molden: a pre- and post-processing program for molecular and electronic structures. *J. Comput.-Aided Mol. Design* **2000**, *14*, 123-134.
67. (a) Adamo C.; Barone V., Exchange functionals with improved long-range behavior and adiabatic connection methods without adjustable parameters: The mPW and mPW1PW models. *J. Chem. Phys. Rev.* **1998**, *108*, 664-675; (b) Perdew J.P.; Ziesche P.; Eschrig H., Electronic structure of solids. 91 ed.; Akademie Verlag, Berlin: 1991; Vol. 11; (c) Perdew J. P.; Burke K.; Wang Y., Generalized gradient approximation for the exchange-correlation hole of a many-electron system. *Phys Rev B* **1996**, *54*, 16533-16539; (d) Perdew J. P.; Chevary J. A.; Vosko S. H.; Jackson K. A.; Pederson M. R.; Singh D. J.; Fiolhais C., Erratum: Atoms, molecules, solids, and surfaces - Applications of the generalized gradient approximation for exchange and correlation. *Phys Rev B* **1993**, *48*, 4978-4978; (e) Perdew J. P.; Chevary J. A.; Vosko S. H.; Jackson K. A.; Pederson M. R.; Singh D. J.; Fiolhais C., Atoms, molecules, solids, and surfaces: Applications of the generalized gradient approximation for exchange and correlation. *Phys Rev B* **1992**, *46*, 6671-6687; (f) Petersson G. A.; Irikura K. K.; Frurip D. J., Computational Thermochemistry: Prediction and Estimation of Molecular Thermodynamics. ACS: Washington, D.C., 1998; Vol. 677, p 237.
68. Vogel A.J., Vogel's textbook of practical organic chemistry. 5th ed.; Longman Group UK Ltd.: New York 1989; p 5.
69. Elamparuthi E.; Ramesh E.; Raghunathan R., InCl<sub>3</sub> as an efficient catalyst for cyclotrimerization of aldehydes: Synthesis of 1,3,5-trioxane under solvent-free conditions. *Synth. Commun.* **2005**, *35*, 2801-2804.
70. (a) Norikane Y.; Kitamoto K.; Tamaoki N., Novel crystal structure, Cis-Trans isomerization, and host property of meta-substituted macrocyclic azobenzenes with the shortest linkers. *J. Org. Chem.* **2003**, *68*, 8291-8304; (b) Lin I. J. B.; Lai J. S.; Liu L. K.; Wen Y. S., Phase-transfer catalyzed base hydrolysis of  $\text{Pt}(\text{ph}_2\text{pch}_2\text{pph}_2)\text{Cl}_2$  - synthesis and crystal-structure of the trinuclear compound  $\text{Pt}^3(\mu\text{-}3\text{-o})(\mu\text{-}\eta\text{-}2\text{-pph}_2\text{O})_3(\text{pph}_2\text{me})_3 \text{pf}_6.\text{chCl}_3$ . *J. Organomet. Chem.* **1990**, *399*, 361-364; (c) Mahadevan I. B.; Russell R. A.; Tiekink E. R. T.; Warrenner R. N., Crystal structure of (1  $\alpha$ ,2  $\beta$ ,3  $\alpha$ ,4  $\alpha$ ,5  $\alpha$ ,6  $\alpha$ ,7  $\beta$ ,8  $\alpha$ )-4,5-dichloro-tetracyclo-6.2.1.0(2,7).0(3,6) undec-9-ene-3,6-diyl bismethanol chloroform solvate, C<sub>13</sub>H<sub>16</sub>Cl<sub>2</sub>O<sub>2</sub> center dot 1/3 CHCl<sub>3</sub>. *Zeitschrift Fur Kristallographie*: 1996; Vol. 211, p 645-646; (d) Karmazin L.; Mazzanti M.; Bezombes J. P.; Gateau C.; Pecaut J., Comparative structural studies of iodide complexes of uranium(III) and lanthanide(III) with hexadentate tetrapodal neutral N-donor ligands. *Inorg. Chem.* **2004**, *43*, 5147-5158; (e) Davies C. J.; Solan G. A.; Fawcett J., Synthesis and structural characterisation of cobalt(II) and iron(II) chloride complexes containing bis(2-pyridylmethyl)amine and tris(2-pyridylmethyl)amine ligands. *Polyhedron* **2004**, *23*, 3105-3114; (f) Thuery P.; Asfari Z.; Nierlich M.; Vicens J., Two triethylammonium ion complexes of monoanionic calix 4 arene. *Acta Crystallogr., Sect. C: Cryst. Struct. Commun.* **2002**, *58*, O223-O225; (g) Eujen R.; Petrauskas E.; Roth A.; Brauer D. J., The structures of 1-chlorogermatrane and of 1-fluorogermatrane, revisited. *J. Organomet. Chem.* **2000**, *613*, 86-92.
71. Story P. R.; Denson D. D.; Bishop C. E.; Clark B. C.; Farine J. C., A new general synthesis of macrocyclic compounds. *J. Am. Chem. Soc.* **1968**, *90*, 817-818.
72. Morales G.; Eyler G. N.; Cerna J. R.; Canizo A. I., Use of cyclic di- and triperoxides as initiators of styrene polymerization at high temperature with a view to their use in industrial applications. *Molecules* **2000**, *5*, 549-550.
73. (a) Dong Y. X.; Creek D.; Chollet J.; Matile H.; Charman S. A.; Wittlin S.; Wood J. K.; Vennerstrom J. L., Comparative antimalarial activities of six pairs of 1,2,4,5-tetraoxanes (peroxide dimers) and 1,2,4,5,7,8-hexaoxanes (peroxide trimers). *Antimicrob. Agents Chemother.* **2007**, *51*, 3033-3035; (b) Dong Y. X.; Vennerstrom J. L., NMR studies and antimalarial evaluation of ketone diperoxides (1,2,4,5-tetraoxanes) and ketone triperoxides (1,2,4,5,7,8-hexaoxanes): A pairwise comparison. *Abstr. Pap. Am. Chem. Soc.* **1999**, *217*, 353-ORGN.
-

## References

- 
74. Bauer C.; Willer U.; Schade W., Use of quantum cascade lasers for detection of explosives: progress and challenges. *Opt. Eng.* **2010**, *49*, 111126-111127.
  75. Terent'ev A.; Platonov M.; Krylov I.; Nikishin G., Synthesis of 1,2,4,5,7,8-hexaoxonanes by iodine-catalyzed reactions of bis(1-hydroperoxycycloalkyl) peroxides with ketals. *Russ. Chem. Bull.* **2009**, *58*, 335-338.
  76. Denekamp C.; Gottlieb L.; Tamiri T.; Tsoglin A.; Shilav R.; Kapon M., Two separable conformers of tatp and analogues exist at room temperature. *Org. Lett.* **2005**, *7*, 2461-2464.
  77. Batagiannis A.; Wust T.; Hulliger J., Universality behaviour for polarity formation in channel-type inclusion compounds. *J. Math. Chem.* **2009**, *45*, 869-881.
  78. Camarena R.; Cano A. C.; Delgado F.; Zúñiga N.; Alvarez C.; García O., Synthesis of 1,3,5-trioxanes: A new, simple method using a bentonitic earth as catalyst. *Tetrahedron Lett.* **1993**, *34*, 6857-6858.
  79. Labat G.; Behrnd N. R.; Couderc G.; Bonin M.; Tsuwi J.; Batagiannis A.; Berger R.; Bertoni M.; Prodi-Schwab A.; Hulliger J., Polymorphism, polar morphology and absolute structure determination of 4-iodo-4'-nitrobiphenyl (INBP). *CrystEngComm.* **2010**, *12*, 1252-1262.
  80. (a) Wang Y. J.; Pan S. L.; Hou X. L.; Liu G.; Wang J. D.; Jia D. Z., Non-centrosymmetric sodium borate: Crystal growth, characterization and properties on  $\text{Na}_2\text{B}_4\text{O}_{12}\text{H}_{10}$ . *Solid State Sci.* **2010**, *12*, 1726-1730; (b) Dhanaraj P. V.; Rajesh N. P., Studies on the growth and characterization of tris (glycine) calcium(II) dichloride-a nonlinear optical crystal. *Physica B* **2011**, *406*, 12-18.
  81. Kurtz S. K.; Perry T. T., A powder technique for the evaluation of nonlinear optical materials. *J. Appl. Phys.* **1968**, *39*, 3798-3813.
  82. Yen C. C.; Araoka F.; Tokita M.; Kawauchi S.; Park B.; Takezoe H.; Watanabe J., Hyperpolarizability components for alpha- and omega-helical polypeptides in polar crystals determined from second-harmonic generation measurements. *JPN. J. APPL. PHYS. Part 1-Reg. Papers Short Notes & Rev. Papers* **2004**, *43*, 7026-7031.

## APPENDICES

The supplementary CD attached contains:

- NMR spectra for **2** and **4 – 6**
- .CIF files for **1-4 – 1-6, 2-1 – 2-3, 4** and **5**
- .XYZ coordinate files for all the models presented here